EFFECT OF WORKING FLUID AND FLUID LOADING ON THE PERFORMANCE OF ROTATING HEAT PIPES

EFFECT OF WORKING FLUID AND FLUID LOADING ON THE PERFORMANCE OF ROTATING HEAT PIPES

By

DEEPAYAN HOME, B.E

A Thesis

Submitted to the School of Graduate Studies

in Partial Fulfillment of the Requirements

for the Degree

Master of Applied Science

McMaster University

MASTER OF APPLIED SCIENCE (2004) McMaster University

(Mechanical Engineering) Hamilton, Ontario

TITLE: Effect of Working Fluid and Fluid Loading on the Performance of Rotating Heat Pipes

AUTHOR: Deepayan Home,
B.E (Punjab Engineering College, Chandigarh, India)

SUPERVISOR: Dr. C.Y. Ching
Department of Mechanical Engineering
Dr. D.Ewing
Department of Mechanical Engineering

NUMBER OF PAGES: xix, 102

ABSTRACT

The steady state heat transfer performance of axially rotating heat pipes with methanol, ethanol and water as working fluid was measured for rotational speeds up to 4000 RPM, or centrifugal acceleration up to 150g, and heat transfer rates up to 0.7 kW. The measurements were used to characterize the effect of working fluid and fluid loading on the heat transfer performance of the rotating heat pipes with 1^0 internal condenser taper and straight adiabatic and evaporator sections. The effect of working fluid was examined for heat pipes where the liquid occupied approximately 19% of the pipe interior volume. In the heat pipes with ethanol and methanol as the working fluid, the thermal resistance of the heat pipes decreased as the heat flux increased before reaching a constant value. However, in the case of heat pipe with water, the thermal resistance increased with the increase in heat flux before appearing to reach a constant value. It was found that the thermal resistance of methanol and ethanol heat pipes were 50% to 80% larger than the thermal resistance of the water heat pipe.

The effect of fluid loading was examined for three heat pipes using water as the working fluid where the liquid occupied approximately 6%, 7% and 19% of the pipe interior volume. It was found that the heat pipe with the lowest amount of water failed to operate. In this case, the thermal resistance was dramatically larger than the other heat pipes even at low heat fluxes. The heat pipe with 7% of water operated normally and had

a thermal resistance smaller than the heat pipe with 19% of water.

The experimental results were compared to predictions from an existing analytical model for high speed rotating heat pipes that accounts for natural convection heat transfer within the liquid film at the evaporator at high accelerations. The predictions from the model were in reasonable agreement with the experimental results for the heat pipes with water as the working fluid. The model over predicted the thermal resistance for the heat pipes with methanol and ethanol as the working fluids by 50% to 80%.

ACKNOWLEDGEMENTS

I would like to dedicate this work to the loving memory of my father. I would like to thank my mom for her invaluable love, support and encouragement that has always enabled me to overcome difficult situations in life.

The author would like to thank the following people for their contributions to this work:

Drs. C.Y.Ching and D.Ewing for their continuous guidance, support and encouragement throughout the course of the master's work.

Dr. Tony Robinson for his advice and suggestions during the initial phase of this program. Andrew Buyers, Ron Lodewyks, Joe Verhaege and Dave Shick for their technical guidance and help.

Pratt & Whitney Canada (P&WC) for funding the present work. Joseph Brand and Mike Dowhan of Pratt & Whitney Canada (P&WC) for valuable suggestions.

Acrolab for their assistance in making the heat pipes.

Friends and colleagues of the Thermal Management Research Laboratory (TMRL) for their support and friendship.

TABLE OF CONTENTS

LIST OF FIGURES

NOMENCLATURE

g	acceleration due to gravity	m/s^2
a	centrifugal acceleration	m/s^2
R	non-dimensional number, $R = \frac{\Delta P_v}{\rho_l \omega^2 r \sin \alpha L}$	
ΔP_v	vapor pressure drop	N/m^2
q_c	average condenser heat flux	W/m^2
ω	angular velocity	rad/s
r	mean radius of condenser section	m
α	internal condenser taper angle	degree
ΔT_{fc}	temperature drop across condensate film	°C
L	length of the heat pipe	m
L_c	length of the condenser section	m
L_e	length of the evaporator section	m
ρ_l	liquid density	kg/m^3
k_l	liquid conductivity	W/mK
μ_l	liquid dynamic viscosity	Ns/m^2

h_{fg}	latent heat of vaporization	J/kg
R_{th_c}	condenser thermal resistance	K/W
M	liquid transport factor	$(W/m^2)^4 s^2/K^3$
Q_{cond}	condenser heat transfer rate	kW
$\dot{m}_{cond}$	mass flow rate of water in the condenser water jacket	kg/s
c_p	specific heat of water	kJ/kg°C
$T_{cond,i}$	inlet temperature of water at the condenser water jacket	°C
$T_{cond,o}$	outlet temperature of water at the condenser water jacket	°C
Q_{evap}	power in to the evaporator	kW
Q_{elec}	electrical power	kW
Q_{IC}	power removed by the induction cooling loop	kW
$\dot{m}_{IC}$	mass flow rate of water in the induction cooling loop	kg/s
$T_{IC,i}$	water temperature at the inlet of the induction heating system	°C
$T_{IC,o}$	water temperature at the outlet of the induction heating system	°C
Q_{loss}	total heat loss to the ambient	kW
Q_{conv}	heat loss by convection	kW
Q_{rad}	heat loss by radiation	kW

$T_{evap,w}$	evaporator wall temperature	°C
$T_{cond,w}$	condenser wall temperature	°C
T_{∞}	ambient temperature	°C
A	outer surface area of heat pipe	m^2
D	outer diameter of the heat pipe	m
h	heat transfer coefficient	W/m^2K
Nu_D	Nusselt number of a rotating horizontal cylinder in air, $Nu_D = \frac{hD}{k_{air}}$	
k_{air}	thermal conductivity of air	W/mK
Re_{ω}	rotational Reynolds number, $\mathrm{Re}_{\omega} = \pi\rho\omega D^2 / \mu$	
Gr_D	rotating pipe Grashof number, $Gr_D = \omega^2 D\beta\Delta T D^3 / 2\nu^2$	
Pr	Prandtl number of air, $\mathrm{Pr} = \nu / \alpha$	
ε	emissivity	
σ	Stefan-Boltzman constant	W/m^2K^4
N	rotational speed	RPM
b	motor controller setting	
T_{RTD}	temperature measured by RTD	°C
ΔT_{cond}	temperature rise across the condenser water jacket	°C
x	local position on the heat pipe wall	m

R_{th}	thermal resistance of the heat pipe	K/W
Gr	Centrifugal Grashof number, $Gr = \omega^2 r \cos\alpha\beta\Delta T\delta^3 / \nu^2_l$	
Re	liquid film Reynolds number, $\mathrm{Re} = 4u_l\delta / \nu_l$	
δ	liquid film thickness	m
γ	fluid loading ratio, $\gamma = \frac{actual\ mass\ of\ fluid}{\min imum\ mass\ of\ fluid}$	

Chapter 1 Introduction

There is increasing demand for efficient thermal management techniques in numerous practical heating and cooling applications. For example, the miniaturization of electronic components in electronics, automotive, and space applications has resulted in an increase in the power densities and cooling requirements of 40 to100 W/cm^2. This has necessitated the need for more efficient cooling mechanisms (Peterson, 1994). A comparison of the typical heat transfer that can be provided by different cooling techniques is shown in Figure 1.1 (Lin et al., 2002). The highest heat transfer rates are achieved in cooling techniques that include the phase change. These can typically provide an order of magnitude higher heat transfer rates than even forced single phase cooling systems.

The two-phase heat transfer systems are normally more complicated and expensive than single-phase cooling systems. One relatively simple design of two-phase heat transfer systems are heat pipes. Heat pipes are closed two-phase heat transfer devices that transport heat by evaporating a working fluid in the high temperature evaporator section and condensing the working fluid in the lower temperature condenser section. The fluid flow in the heat pipe is typically driven by gravity or surface tension forces developed in an internal wick or grove structure. Thus, heat pipes are passive devices that can provide an internal two-phase heat transfer mechanism with a thermal resistance an order of magnitude smaller than other passive devices.

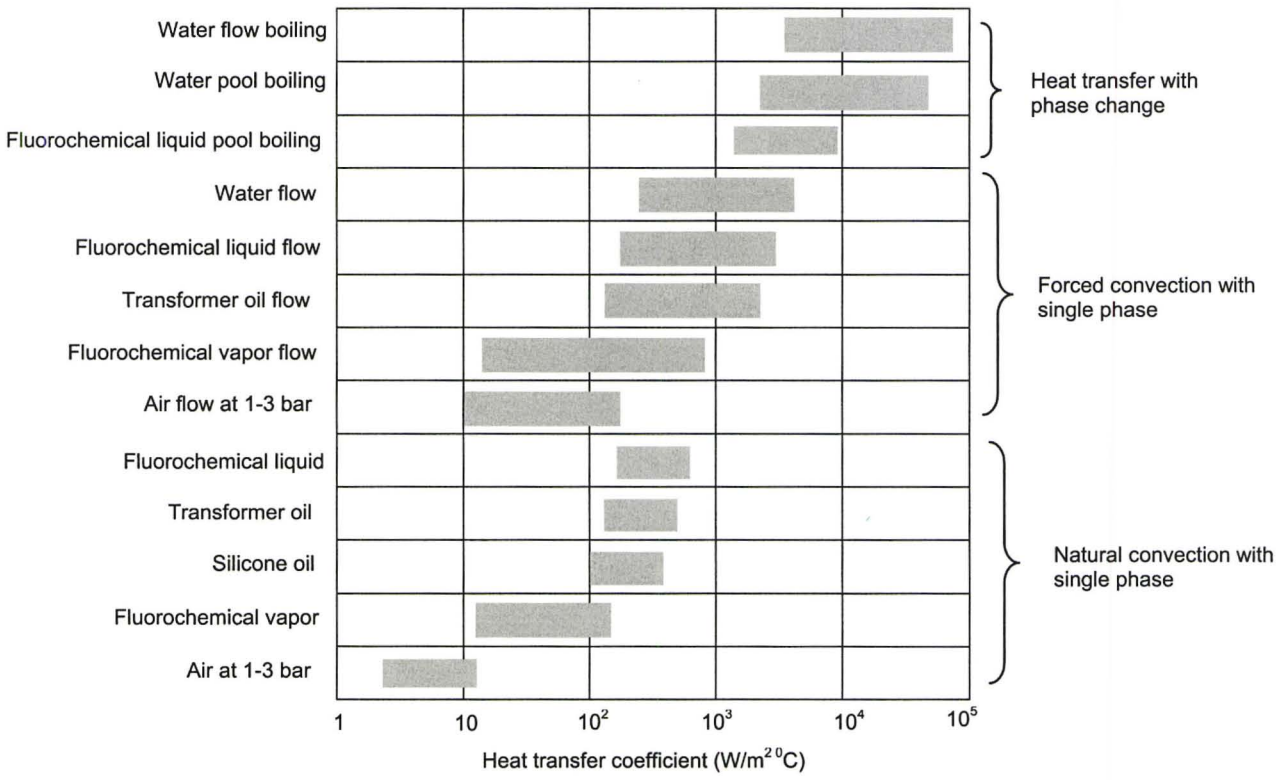

Figure 1.1 Comparison of heat transfer coefficients for single-phase natural convection, forced convection, heat transfer with a phase change (Lin et al., 2002).

There has been considerable interest in using heat pipe for thermal management in gas turbine aero engines. Most of these investigations have focussed on using rotating or revolving heat pipes. In these heat pipes, the centrifugal force developed by the rotation of shaft is used to drive the working fluid in the heat pipe. For example, Ponnappan et al. (1997) considered using high speed rotating heat pipes to cool the electrical generators used in aero engines, while Ling et al. (2000) considered using high temperature revolving heat pipes to cool the turbine blades. In these cases, including heat pipes in the aero engine would reduce the use of bleed air from the compressor thereby increasing the engine efficiency and likely simplifying the design of the cooling system in the aero engine.

This investigation was part of a project to evaluate the use of rotating heat pipes for anti-icing the nose cone of small scale aero engines. It has been proposed to use a rotating heat pipe to transport waste heat from the engine gearbox to the nose cone in order to prevent the formation of ice droplets. The rotating heat pipes for this application would have to function to -60 ^{0}C so it was necessary to evaluate the performance of heat pipes with working fluids that would not freeze at this temperature. The effect of working fluid on the performance of the condenser region of rotating heat pipe was considered previously by Daniels and Al-Jumaily (1975) but this focussed primarily on the condenser section. Song et al. (2004) found, however, that the thermal resistance of the evaporator section could be significant in high speed rotating heat pipes. Vasiliev and Khrolenok (1990) also considered the effect of working fluid on the performance of rotating heat pipes, but in this case they examined heat pipes with a large step in radius

between the evaporator and the condenser sections. In this case, the liquid would pool in the evaporator rather than flowing along the heat pipe. As a result, the operation of the evaporator and condenser sections are somewhat independent of each other. The objective of this investigation was to characterize the effect of working fluid on the overall thermal performance of high speed rotating heat pipes without a step in the radius of the wall.

Song et al. (2004) and others have found that the evaporator of the heat pipe seems to dry out when there was too little working fluid in the heat pipe. This would be unacceptable in anti-icing applications. Song et al. (2004) showed that the heat pipe had a lower thermal resistance when there was less working fluid in the heat pipes. The apparent dry out only occurred at a single operating condition. Thus, a second objective was to further characterize the apparent failure of the heat pipe when there was too little working fluid in the heat pipe.

Experiments were performed to characterize the performance of heat pipes with similar volumes of water, methanol and ethanol as the working fluid. Experiments were also performed with rotating heat pipes with three different amounts of water as the working fluid. The experimental results were also compared to the predictions from an analytical model developed for the rotating heat pipe by Song et al. (2003).

This thesis consists of six chapters. Investigations of rotating heat pipes and their practical applications are reviewed in Chapter 2. The experimental methodology used in this investigation is presented in Chapter 3. The results are discussed in Chapter 4 and finally the conclusions and recommendations for future work are presented in Chapter 5

and Chapter 6 respectively.

Chapter 2 Literature Review

Rotating heat pipes are a closed two-phase heat transfer device that consists of a closed hollow rotating shaft filled with a working fluid, such that the liquid occupies a fraction of the internal volume and vapor occupies the remainder. The concept of rotating heat pipes was first proposed by Gray (1969), who determined that rotating heat pipes were capable of transferring more heat than a stationary heat pipe. Unlike conventional heat pipes, rotating heat pipes normally do not include a wick structure. The flow in rotating heat pipes is driven by the centrifugal force generated by the shaft rotation. The rotating heat pipes normally consist of three types of sections, an evaporator section or sections where the working fluid is evaporated, an adiabatic section or sections where there is little heat transfer, and a condenser section where the fluid is condensed and the heat removed.

The operation of the rotating heat pipe depends on the location of the evaporator and condenser section relative to the axis of rotation. In an axially rotating heat pipe shown in Figure 2.1 the vapor and liquid flow is nominally parallel to the axis of rotation. In this case, the flow is driven by a hydrostatic pressure developed in the film or by a small component of the centrifugal force in the flow direction if a small internal taper is included in the heat pipe. In a radially rotating heat pipe or a revolving heat pipe shown in Figure 2.2, the liquid and vapor flow in the radial direction perpendicular to the axis of rotation and the liquid flow is directly driven by the centrifugal force. The excess liquid

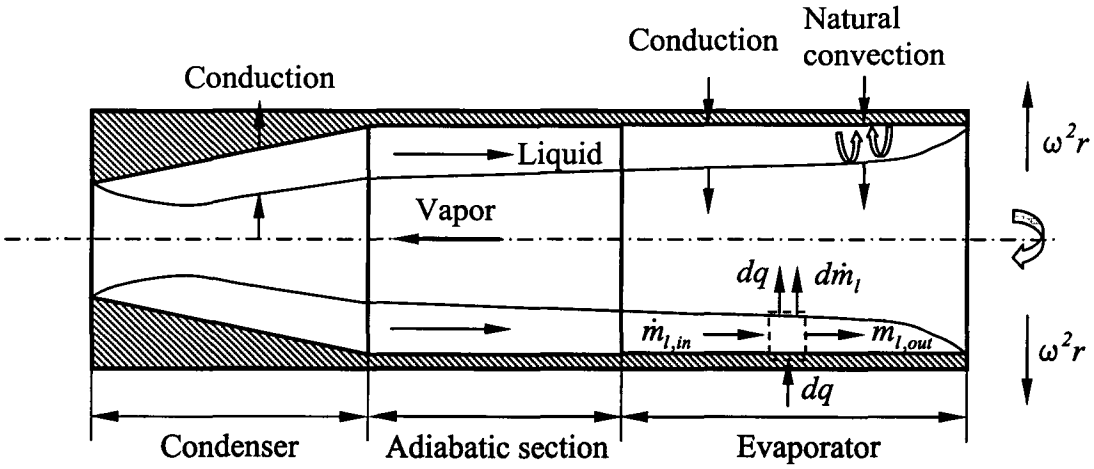

Figure 2.1 Schematic of flow pattern and heat transfer in an axially rotating heat pipe.

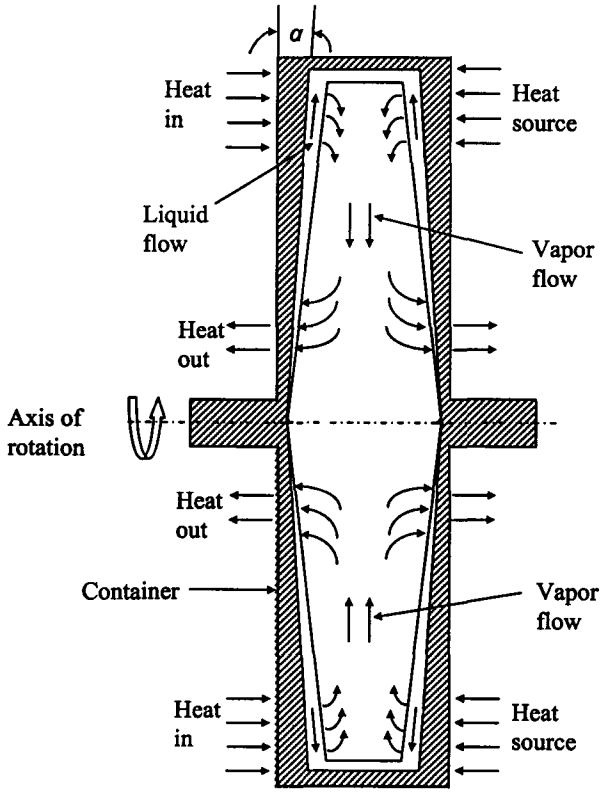

Figure 2.2 Schematic of flow pattern and heat transfer in a radially rotating heat pipe.

in the high speed revolving heat pipe pools near the outside wall so they operate similar to thermo syphons. There are also number of potential applications where the heat pipe is oriented at an angle relative to the axis of rotation (Chen and Tu, 1987) or where the pipe was off the axis of rotation as shown in Figures 2.3 and 2.4 respectively.

The liquid flow in the axial rotating heat pipes of interest here, is important in determining the performance of the device. There are a number of different designs for the internal geometry of rotating heat pipe that affect the liquid flow. The simplest design, in terms of manufacturing and cost, is the cylindrical heat pipe where the internal radius of the heat pipe is constant throughout. The fluid flow in the cylindrical heat pipe is driven by a hydrostatic pressure gradient that develops due to a variation in the film thickness from condenser to the evaporator. In this case, the film thickness is largest in the condenser and the conduction of heat through this film is a major part of the thermal resistance of the device (Song et al., 2003). In order to reduce the thickness of the film in the condenser, the condenser section is often tapered. In this case, a component of the centrifugal force along the taper drives the liquid flow in the condenser. This significantly reduces the thickness of condensate film in the condenser section and reduces the thermal resistance (Marto, 1984). The heat pipe can be tapered throughout as considered by Li et al. (1993). The heat pipe can also be designed with a step change in the radius between the adiabatic section and the evaporator (Vasiliev and Khrolenok, 1990). These changes in the radius also act to reduce the thickness of the film in the condenser by reducing the length that the liquid must be driven from the condenser by the hydrostatic force. In most designs there is a trade off because adding a taper in the heat pipe or a step change in the

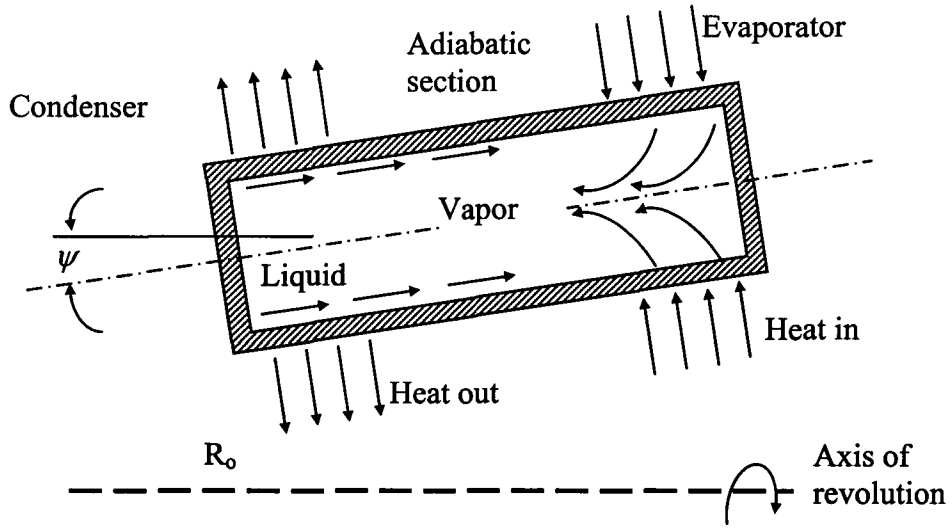

Figure 2.3 Schematic of a revolving heat pipe with heat pipe axis inclined to axis of revolution.

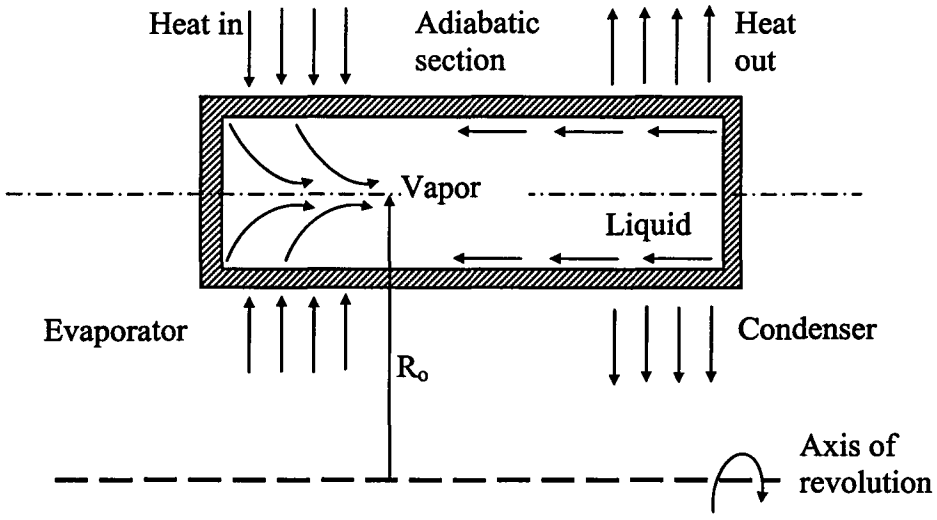

Figure 2.4 Schematic of a revolving heat pipe with the heat pipe axis parallel to axis of revolution.

radius reduces the internal area for heat transfer in the condenser section (Song et al., 2002). Marto and Weigel (1981) also considered modifying the condenser section with spiral fins to drive the fluid out of the condenser.

There have been a number of investigations that have considered incorporating rotating heat pipe in practical applications. Gray (1969), who originally proposed the rotating heat pipe, noted that they could be used in a number of applications including cooling the tips of high speed drills. Fries (1970), Oslejsek and Polasek (1976), Groll et al. (1978) and others considered using rotating heat pipes in electrical motors to create a more uniform temperature between the rotor and stator, and to cool the motors in order to increase the load capacity of a given motor and reduce the motor size. Maezawa et al. (1981) considered using rotating heat pipes to cool the brakes in heavy vehicles. They found the temperature of the brake housing was considerably reduced when rotating heat pipes were incorporated. Rotating heat pipes have also been used as heat recovery systems in various rotary processes including drum dryers and milk pasteurization systems (Marto, 1984). There is currently considerable interest in incorporating rotating heat pipe in aero engine applications as summarized in Table 2.1. For example, Ponnappan et al. (1997) and Ponnappan and Leland (1994, 1995) considered using rotating heat pipes to cool the rotors in high speed and high power electrical machines, such as switched reluctance and permanent magnet generators, that are the power units for the U.S. Air Force More Electric Airplane. These generators are to be directly coupled to turbine engine shaft and thus run at 60000 RPM or higher. As a result, it was found that the generators have large losses that accumulate in the rotors as waste heat. It

Investigators	Approach	Rotational speed; (Centrifugal acceleration)	Working fluid	Findings
Ponnappan and Leland (1994)	Experimental	500–3500 RPM (2g–100g)	Water	The condenser cooling method and rotational speed had a significant effect on the operating temperature of the heat pipe.
Ponnappan and Leland (1995)	Experimental	3500–7000 RPM (100g-400g)	Water	The rotational speed and condenser cooling method affect the heat transport capacity of the heat pipe.
Streby at al. (1996)	Design/ Experimental	Analysis on resonance rotational speed was performed.	Water, Methanol	The dynamics of the heat pipe design is important in high speed applications.
Ponnappan and Leland (1998)	Experimental	3500-13500 RPM (100g-1488g)	Methanol	Permanent magnet alternator with rotating heat pipe rotor functioned at lower operating temperatures and provided a sizeable thermal advantage over the baseline rotor.
Ponnappan and Leland (1998)	Experimental	5000-30000 RPM (204g-7350g)	Water, Methanol	The heat transported by the water heat pipe was approximately two times the methanol heat pipe.
Leland et al. (1999)	Experimental	No rotation.	Methanol	Residual gas analysis was studied.Non condensable gases were generated in a 4130 steel thermosyphon due to chemical reaction or contamination inside the thermosyphon.
Ling et al. (2000)	Experimental	$470 \leq a/g \leq 1881$	Sodium	The radially rotating miniature heat pipe has a thermal conductance of 60 to 100 times higher than cylindrical copper rod and can potentially be used for turbine blade cooling.

Table 2.1 Summary of investigation on high-speed rotating heat pipes for aero engine applications.

was proposed that high speed rotating heat pipe could be retrofitted in to the shaft to remove the waste heat generated within the rotor. Ponnappan et al. (1998) investigated the performance of 25.4 mm diameter high speed methanol and water rotating heat pipes at speeds up to 30000 RPM. The highest heat rates transported were 1033 W and 644 W for water and methanol high speed rotating heat pipes, respectively. Ling et al. (2000) also proposed that miniature radially rotating heat pipes could be used for cooling of high temperature gas turbine blades in the aero engines.

2.1 Flow pattern and heat transfer characteristics

The flow pattern inside the rotating heat pipe has a significant effect on the heat transfer performance of the heat pipe. The flow pattern in the rotating heat pipe depends on the amount of working fluid in the heat pipe and centrifugal acceleration applied to the heat pipe. The liquid flow inside a horizontal cylindrical rotating heat pipe is generally classified into three types of flow patterns as shown in Figure 2.5 (Nakayama et al., 1984). At low rotational speeds, gravity is important and most of the liquid collects in a pool along the bottom of the heat pipe. In this case, there is a thin film wetting the upper surface of the heat pipe so the heat transfer in this film regime tends to be large. As rotational speed increases, both gravitational and centrifugal accelerations become important. As a result, the film on the upper wall becomes thicker and the heat transfer performance of the rotating heat pipe decreases due to thickening of the liquid film. As the rotational speed is increased further, the centrifugal acceleration dominates and the flow becomes essentially fully annular. The heat transfer for the annular flow regime

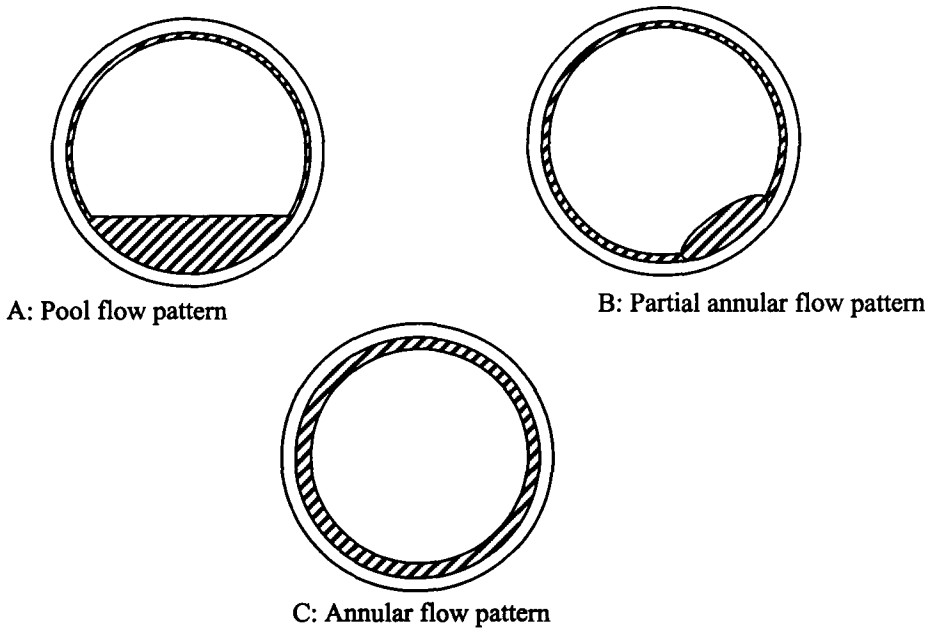

Figure 2.5 Schematic diagram of condensate flow pattern inside a horizontal cylindrical rotating heat pipe (Nakayama et al., 1984).

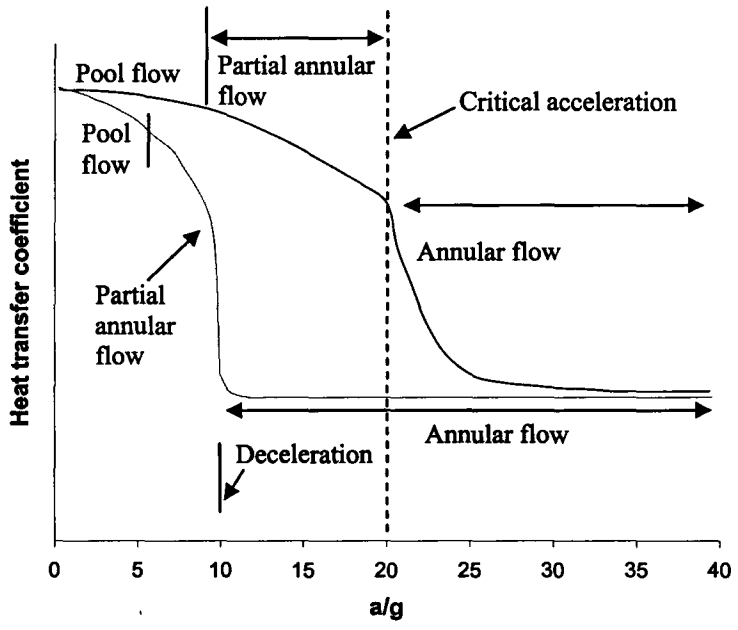

Figure 2.6 Effect of rotational speed on the evaporation and condensation coefficient in horizontal rotating heat pipes (Peterson, 1994).

tends to be the poorest because the heat must be conducted across this thick film in the condenser section.

The critical speed for transition to fully annular flow occurs when the acceleration is approximately 20g, though the critical speed depends on the fluid loading in the heat pipe (Katsuta et al., 1984; Nakayama et al., 1984). The collapse of the annular flow when the rotational speed is decreased is lower than the critical speed and occurs at approximately 10g (Peterson, 1994) so there is a hysteresis in the flow pattern. This results in a hysterisis in the heat transfer performance. The typical change in the heat transfer coefficient with rotational acceleration is shown in Figure 2.6 (Peterson, 1994). These results indicate that the heat transfer performance is significantly affected by the rotational acceleration in the range up to approximately 40 g.

For a 10-40 mm diameter heat pipe, the transition to fully annular flow would occur at a speed of approximately 1000 RPM. Thus, in moderate size heat pipe it is expected that the flow would be fully annular in most aero engine applications where the rotational speed is typically 10,000 RPM or higher. Thus, the literature review will focus on the investigations of heat pipes where the flow should be annular.

2.2 Investigations on the performance of rotating heat pipes

The film condensation inside a rotating truncated cone was first studied by Ballback (1969). Ballback used a Nusselt-type analysis to model the condensation on the inside of a taper cone following the approach used previously by Sparrow and Hartnett (1961) to model the condensation on the outside of rotating cones. The effect of gravity

and interfacial shear stress of the vapor were neglected in this formulation. Daley (1970) later modified Ballback's model to include the thermal resistance of the condenser wall and the thermal resistance of the cooling outside the cone that would more closely match the tapered condenser in a heat pipe. In both cases, the analysis neglected the hydrostatic forces in the film so they could only be used for cones with large angles. Marto (1973) later included hydrostatic pressure variation within the condensate film in the condensation model so that it could be used for condensers with small angles. Marto found that the effect of the hydrostatic force was small even at very small half cone angles when the rotational speed was sufficiently high.

Daniels and Al-Jumaily (1975) later included the effect of shear stress from the counter flow vapor and the effect of gravity in the model for the condenser. They noted that vapor exerts a drag force on the liquid interface and a momentum drag due to the condensation of vapor on the slower moving liquid film. Daniels and Al-Jumaily (1975) approximated the vapor shear force using a conventional correlation developed for axisymmetric flow in smooth pipes. The model predicted that the vapor drag would increase the thickness of the film thereby increasing its thermal resistance, but its effect was only significant at low speeds and higher heat transfer rates. Daniels and Al-Jumaily (1975) compared the predictions from their model to measurements for a 55 mm diameter copper heat pipe with an internal taper angle of 2^0 charged with Arcton 113, Arcton 21 and water at speeds of 600 to 1200 RPM or a/g up to 44. The measurements were in reasonable agreement with the predictions from the model for Arcton 113 and the Arcton 21. The measurements for the water heat pipe did not agree with the model because this

heat pipe did not seem to have sufficient amount of working fluid to operate properly. In particular, the temperature difference across the liquid condensate was much higher than predicted by the model.

In most of the investigations, the effects of the vapor flow in the rotating heat pipe are neglected, or modelled using a simple flow in a pipe. The effect of the axial vapor pressure drop on the heat transfer performance of the rotating heat pipe was considered in more detail by Marto (1976) using a 1-D aproximation. Marto proposed that the importance of the vapor pressure drop could be estimated by

$$R = \frac{\Delta P_v}{\rho_l \omega^2 r \sin \alpha L} \tag{2.1}$$

where ΔP_v is the vapor pressure gradient from the evaporator to the condenser. The model predicted that the vapor pressure drop was important only at low rotational speeds. In these cases, the vapor pressure drop reduced the heat transfer rate because it opposes the liquid film motion and thus would tend to thicken the liquid film in the condenser. The criterion was not verified for small diameter rotating heat pipes under large heat loads, where the vapor and liquid velocities would be large. Tien and Chung (1979) noted that in these cases that the interfacial shear stress becomes large and liquid droplets may also be entrained into the vapor. Tien and Chung argued that when the relative velocity between the liquid and vapor is sufficiently large the interface becomes unstable and enhanced wave formation is generated which together with the large interfacial shear force leads to the entrainment of the liquid in the vapor.

The aforementioned analyses consider the performance of the condenser section

of the rotating heat pipe for isothermal wall that often does not occur in practical applications. Daniels and Al-Baharnah (1978) considered the effect that different condenser wall materials, external heat transfer coefficients, and the presence of non-condensable gases would have on the performance of the condenser using the model proposed by Daniels and Al-Jumaily (1975). The model predicted that the condenser end wall temperature was directly proportional to the heat transfer rate and inversely proportional to the cooling external heat transfer coefficient. For heat pipes with highly conductive walls, the heat transfer along the heat pipe wall increased, decreasing the condenser end temperature. The presence of non-condensable gas lowered the condenser end temperature and raised the operating temperature of the rotating heat pipe. This effect was found to be more prominent for non-condensable gases with lower molecular weight.

Salinas and Marto (1991) investigated the performance of a tapered condenser with fins using a modified Nusselt condensation analysis for the flow in the troughs and conjugate heat transfer in the wall. The effect that the number of fins, wall thermal conductivity, rotational speed, and the magnitude of the outside heat transfer coefficient had on the performance of the rotating heat pipes with water and Freon-113 as working fluids were studied for rotation speeds of 1000-15000 RPM. The model predicted that heat transfer rate could be significantly increased by placing fins on the inner wall. The increase was largest at the lower speeds and approximately 100 fins. They compared the local heat flux distributions in half of a fin-trough cell for stainless steel and copper. The isotherms in the stainless steel fins were more 2-D flow path of heat than the copper fins. The heat transfer increased when the speed of the device was increased.

Marto and Wagenseil (1979) compared the performance of copper heat pipes with smooth walled cylindrical condenser, taper heat pipes, and internally finned cylindrical condensers. They found that the tapered condenser had half the thermal resistance of the smooth walled cylinder. They also found that internally finned cylindrical condenser had 100 to 200% better heat transfer coefficient than the smooth walled cylindrical condenser and was similar to the tapered heat pipe. Marto and Weigel (1981) later examined the performance of copper cylinder heat pipe with straight axial fins, spiralled fins, and helical corrugations that used distilled water, ethyl alcohol and Freon-113 as the working fluids. The internally finned condenser with spiralled fins provided the best heat transfer coefficient that was several times higher than the coefficient for the cylindrical heat pipe. The spiralled fins would tend to act as a pump forcing the condensate back to the evaporator section. The heat transfer improvement was largest for the organic working fluids that otherwise provide poor performance because the thermal resistance would primarily occur on the inside of the heat pipe in these cases. The axially grooved condenser section was not effective for heat transfer enhancement in the rotating heat pipe. In this case, the condensate would likely accumulate in the trough and could not be returned easily to the evaporator. The results for the spirally convoluted surface were quite different from the other surfaces. At high rotational speeds and small temperature differences, this surface behaved worse than the smooth-walled cylinder for ethyl alcohol and water, but improved the performance for Freon-113. This was attributed to the fact that for both water and ethanol there was insufficient vapor formed to overcome the wall resistance caused by the whirling action of the deeply convoluted surface at low heat

loads. Marto and Weigel also suggested that the presence of convolutions on both sides of the convoluted surface, have a detrimental effect on the outside performance at low temperature differences and high speeds. At higher heat loads, more vapor is formed to overcome the wall resistance that leads to performance enhancement. Further work needs to be done with this surface to understand the heat transfer mechanism that occurs.

The heat transfer in the evaporator of a rotating heat pipe is a complicated process. In particular, the phase transformation mechanism in the evaporator can be either nucleate boiling in thick liquid layers or evaporation from thin liquid films (Marto, 1984). Most analytical investigations on rotating heat pipes have considered low and moderate rotation rates (<3000 RPM) with typical centrifugal accelerations less than 200 g. Under these conditions, it is thought that nucleate boiling occurs in the evaporator resulting in a very low thermal resistance in the evaporator section (Marto, 1984). Thus, it is normally argued that the thermal resistance in the evaporator is much less important than the thermal resistance of the condenser. Daniels and Al-Jumaily (1975) also found that the predictions deduced from only considering the condenser were in reasonable agreement with the experimental results at very low speeds. Daniels and Williams (1978) performed visual observations inside a 76 mm diameter copper heat pipe to examine the heat transfer mechanism inside the evaporator. They found that at low speed (600 RPM) the boiling action in the evaporator was violent with large vapor bubbles and frothy liquid-vapor interface. With an increase in speed to 800 RPM or $a/g \approx 28$ however, the bubble evolution in the evaporator was reduced due to the increased centrifugal acceleration. It is well known that nucleate boiling in pool is suppressed as centrifugal acceleration

increases (Merte and Clark, 1961; Judd and Merte, 1972; Ulucakli and Merte, 1990). Under these conditions, the phase transformation in the evaporator may occur by film evaporation at the liquid surface (Marto, 1984) and can be treated in a similar way to laminar film condensation. Vasiliev and Khrolenok (1990) proposed a model for a stepped heat pipe and measured the performance of these devices at high centrifugal accelerations. In the stepped heat pipe, the liquid pooled in the evaporator increased the liquid pressure at the wall thereby suppressing nucleate boiling at high accelerations. In these cases, the heat appeared to be transferred across the evaporator by natural convection inside the liquid film.

Li et al. (1993) later developed a model for a fully tapered heat pipe. In this case, there is a constant flow along the wall so the liquid does not pool in the evaporator like the stepped heat pipe. Li et al. (1993) proposed a film evaporation model for the evaporator where the heat was conducted across the film in the evaporator. They coupled this model with a film condensation model for the condenser in the rotating heat pipe. Song et al. (2003) noted that natural convection would likely occur in the evaporator of this rotating heat pipe at high speeds. Song et al. proposed a mixed convection model for the evaporator that was coupled with the film condensation model for the condenser section. They solved for the liquid flow and heat transfer in the rotating heat pipe for a range of cases, and noted that the thermal resistance of the evaporator was not small in many cases.

The effect of the working fluid charge in the heat pipe has an effect on the performance of the heat pipe because it affects the thickness of the working fluid on the

wall. For example, Ponnappan et al. (1997) measured the heat transfer rates of 25 mm diameter stainless steel heat pipes with 1^0 internal condensers taper for rotation rates of 10000 to 30000 RPM or accelerations of 1000 g to 9600 g. The thermal resistance of the condenser in these heat pipes was approximately 4 times that predicted using the standard Nusselt film condensation for rotating heat pipes. They speculated that this model did not apply to high speed case. Song et al. (2003) later noted that Ponnappan et al's. result could be reasonably predicted when the effect of working fluid charge was considered. In particular, Ponnappan et al. (1997) used approximately 10 times the minimum amount of fluid required for the heat pipe to operate. This fluid would tend to pool into the condenser when this amount of excess fluid is included.

Song et al. (2004) later performed an experimental study to characterize the effect of the working fluid charge on the performance of two cylindrical heat pipes and two tapered heat pipes with 2^0 internal condenser taper for rotational speeds of 2000 to 4000 RPM. They found that the fluid loading had a significant effect on the performance of the cylindrical heat pipes because the increase of fluid loading would increase the thickness of the liquid layer throughout the heat pipe. The performance of the tapered heat pipes was relatively unaffected where the fluid loading was increased by a factor of 2 to 3 because the addition of taper in the condenser section should reduce the amount of excess fluid in the condenser. In this case, the excess fluid would be contained in the adiabatic and evaporator sections. Song et al. (2004) found that the changes in the performance of the heat pipe with fluid loading and speed were in reasonable agreement with the predictions from the model proposed by Song et al. (2003). Song et al. (2004) found at

one operating point that the thermal resistance of the system increased rapidly when the heat flux was increased because the evaporator temperature increased. They suggested that this may be caused by some dry out in the evaporator section.

The presence of non-condensable gases inside the rotating heat pipe can be detrimental to the operation of the heat pipe. Marto (1976) reported that improper filling procedures that failed to remove all the non-condensable gas from the heat pipe before the working fluid was added have a marked effect on the performance of the system. In some cases, such as steel-methanol heat pipes, non-condensable gases can also form over time due to chemical reactions (Leland et al., 1999). Daniels and Williams (1978) conducted experiments to investigate the effects that non-condensable gases had on the performance of the condenser in the rotating heat pipe by introducing known amounts of nitrogen and carbon dioxide inside Acetone and Arcton 113 rotating heat pipes. The presence of non-condensable gases caused the condenser wall temperature to increase over the active part of the condenser and decrease over the end portion where the non-condensable gases were concentrated. The non-condensable gas hinder the condensation of the vapor by blocking part of the condenser and result in more heat transfer by conduction down the wall of the condenser causing a large variation in the wall temperature.

2.3 Effect of working fluid on the performance of rotating heat pipes

The working fluid used in the heat pipe has a significant effect on its performance in a large part because the heat must be conducted across the film in the condenser. Thus,

the conductivity of the fluid, the viscosity of the fluid, and the latent heat of the fluid that determines the mass flow rate for a given heat flux all have a significant affect on the performance of the heat pipe. The effect of the working fluid on the performance of the rotating heat pipe can be estimated from a Nusselt film condensation analysis of the condenser. In the simplest case, where the effect of the vapor, gravity, and excess fluid are ignored the heat flux through the condenser can be approximated by (Daniels and Al-Jumaily, 1975)

$$q_c^{\,4} = \frac{\omega^2 r \sin\alpha \Delta T^3{}_{fc}}{1.26 L_c}\left[\frac{\rho^2{}_l h_{fg} k^3{}_l}{\mu_l}\right] \tag{2.2}$$

where q_c is the average heat flux through the condenser section, ω is the angular velocity, r is the mean radius of the condenser section, α is the taper angle in the condenser, ΔT_{fc} is the temperature drop across the thin liquid film and L_c is the length of the condenser. Here, ρ_l is the density, h_{fg} is the latent heat of vaporization, k_l is the conductivity and μ_l is the dynamic viscosity of the working fluid. It follows that in this case the thermal resistance of the condenser is given by

$$R_{thc} = \left[\frac{1.26 L_c Q_c}{\omega^2 r \sin\alpha}\right]^{1/3}\left[\frac{1}{M}\right]^{1/3} \tag{2.3}$$

where, M is the liquid transport factor given by (Daniels and Al-Jumaily, 1975)

$$M = \frac{\rho^2{}_l h_{fg} k^3{}_l}{\mu_l} \tag{2.4}$$

Thus, fluids with high latent heat of vaporization are desirable in order to transfer large

amounts of heat with a minimum fluid flow. Similarly the working fluid should have a low viscosity to reduce flow resistance and the liquid thickness, and the thermal conductivity should be high to reduce the thermal resistance of the liquid film. This result suggests that changes in the thermal conductivity should have the most significant effect on the performance of the condenser region of the heat pipe, while the viscosity and latent heat should have weaker effect. This result also indicates that the thermal resistance of the condenser is non-linear, increasing with heat transfer rate.

For low temperature heat pipe applications in the range from 200 to 550 K, the working fluids commonly used in heat pipes are ammonia, acetone, the Freon compounds, ethanol, methanol and water. The melting and boiling points at atmospheric pressure and the useful ranges for the low temperature working fluids are summarized in Table 2.2. The change in the liquid transport factor as a function of the operating temperature for the fluids of interest here is shown in Figure 2.7. It is clear that water has the highest liquid transport factor in the temperature range of interest, and therefore heat pipes with water should have the best performance. Water will freeze at subzero temperatures and this could lead to the start-up problem in the current application. Apart from water, methanol has the highest liquid transport factor in the range of interest and should not freeze over the temperature range of interest. The liquid transport factor for both ammonia and acetone decrease in the temperature range of interest. Ethanol was also examined here as an alternative working fluid for this application.

Marto (Peterson, 1994) tested the performance of stainless steel heat pipes with 1^0 internal condenser taper with water, ethyl alcohol, and Freon-113 for two rotational

Working Fluid	Melting Point (^{0}C) at 1 atm	Boiling Point (^{0}C) at 1 atm	Useful Range (^{0}C)
Water	0	100	30 - 200
Methanol	-98	64	10 - 130
Ethanol	-112	78	0 - 130
Acetone	-95	57	0 - 120
Freon 11	-35	48	-40 - 120
Ammonia	-78	-33	-60 - 100

Table 2.2 Summary of the working fluids and temperature ranges for moderate temperature heat pipes.

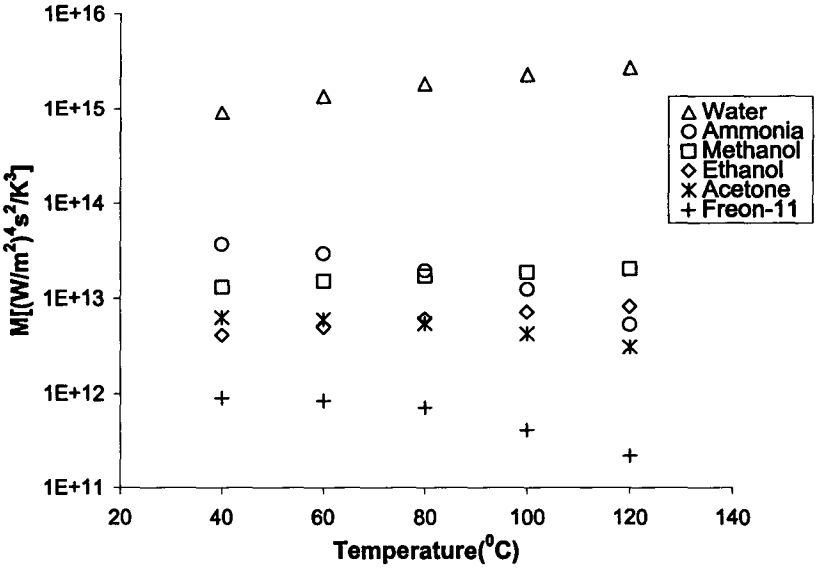

Figure 2.7 Liquid transport factor for the low temperature working fluids.

speeds of 700 and 2800 RPM. The experimental results showed that the rotating heat pipe with water as the working fluid had a heat transport capacity more than three times that of the heat pipes with ethyl alcohol and Freon-113. Daniels and Al-Jumaily (1975) found that the heat pipe with Arcton 21 had a better performance than the heat pipe with Arcton 113 because of its higher heat transport capacity. Ponnappan et al. (1998) found that heat pipe with water had a thermal resistance of half the heat pipe with methanol. Vasiliev and Khrolenok (1990) experimentally characterized the different heat transfer regimes in the evaporator of stepped heat pipes with water, ethanol and acetone as the working fluids. The measurements indicated that nucleate boiling only developed for water at higher heat fluxes. For the heat pipes with ethanol and acetone as the working fluid, the heat transfer seemed to be either natural convection or non-developed nucleate boiling. Vasiliev and Khrolenok found that the experimental data was in fair agreement with the prediction from the model for the condenser. It is not clear whether the existing analytical models are suitable to predict the performance of the rotating heat pipes with different working fluids. In particular, there has not been an investigation that compared performance of the rotating heat pipes with predictions from the analytical model for the entire rotating heat pipe.

Chapter 3 Experimental Methodology

The objective of this investigation was to characterize the effect of the working fluid on the performance of high speed rotating heat pipes. Tests were also performed to characterize the performance of heat pipes with lower fluid loading to examine the failure of the heat pipe when the fluid loading is too low. The experimental facility used in this investigation is presented first followed by a description of the rotating heat pipes tested. The calibration of the facility and the experimental procedure are also discussed in detail. Finally, an uncertainty analysis and energy balance is presented.

3.1 Experimental facility

The rotating heat pipe facility used in this investigation is shown in Figures 3.1 and 3.2. The rotating heat pipe is driven by a 2 HP Toshiba EQP3 motor with a VFS9S controller that is capable of rotational speeds up to 5000 RPM. The motor was mounted on a C-channel made of steel that had a series of holes so the location of the motor could be adjusted for different length heat pipes. The motor and heat pipe were connected using a 22.2 mm (0.875") diameter ODG Bowex coupling that reduced any effects of misalignment between the motor shaft and the heat pipe. The central section of the heat pipe was mounted into a 101.6 mm (4") long Teflon sleeve with an outer diameter 31.7 mm (1.25"). This was then pressed fit into a stainless steel sleeve with an outer diameter of 38.1mm (1.5") that was supported using two self-aligning steel bearings. The bearings

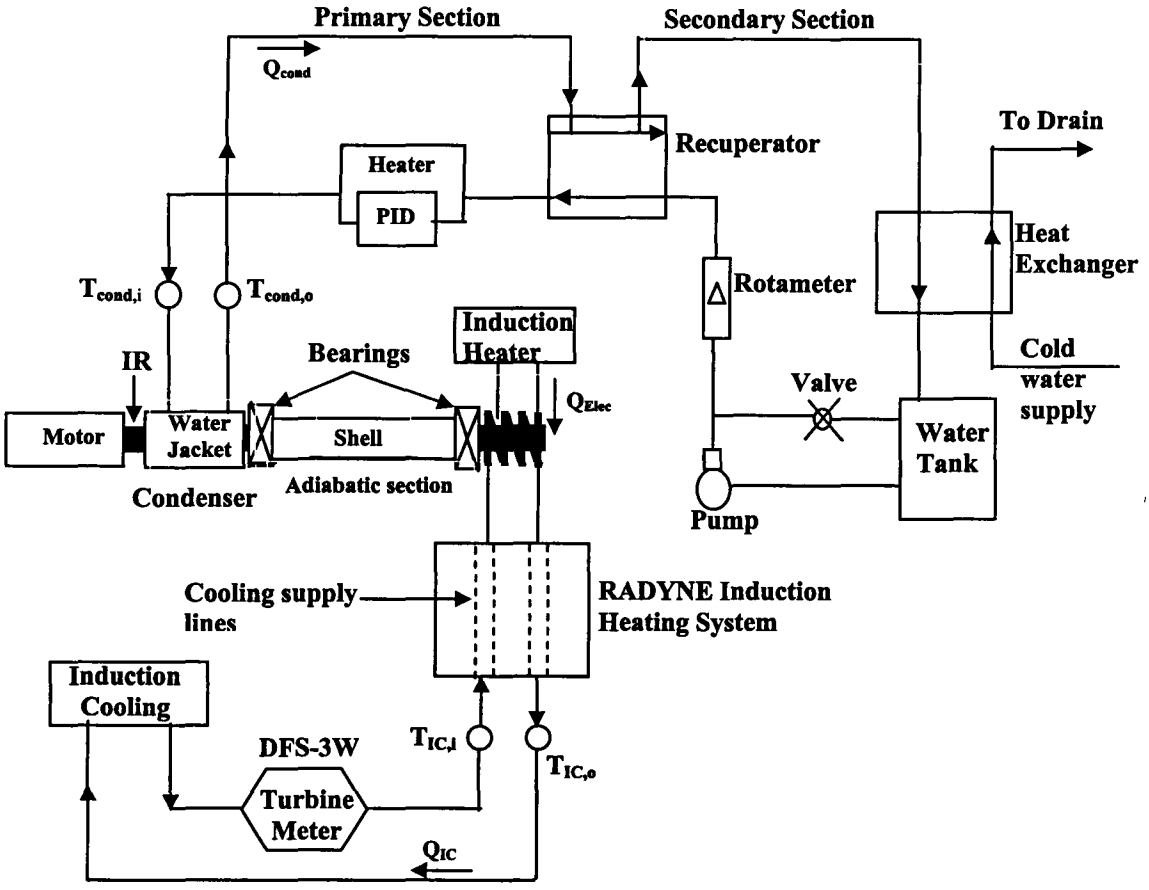

Figure 3.1 Schematic of the rotating heat pipe test facility.

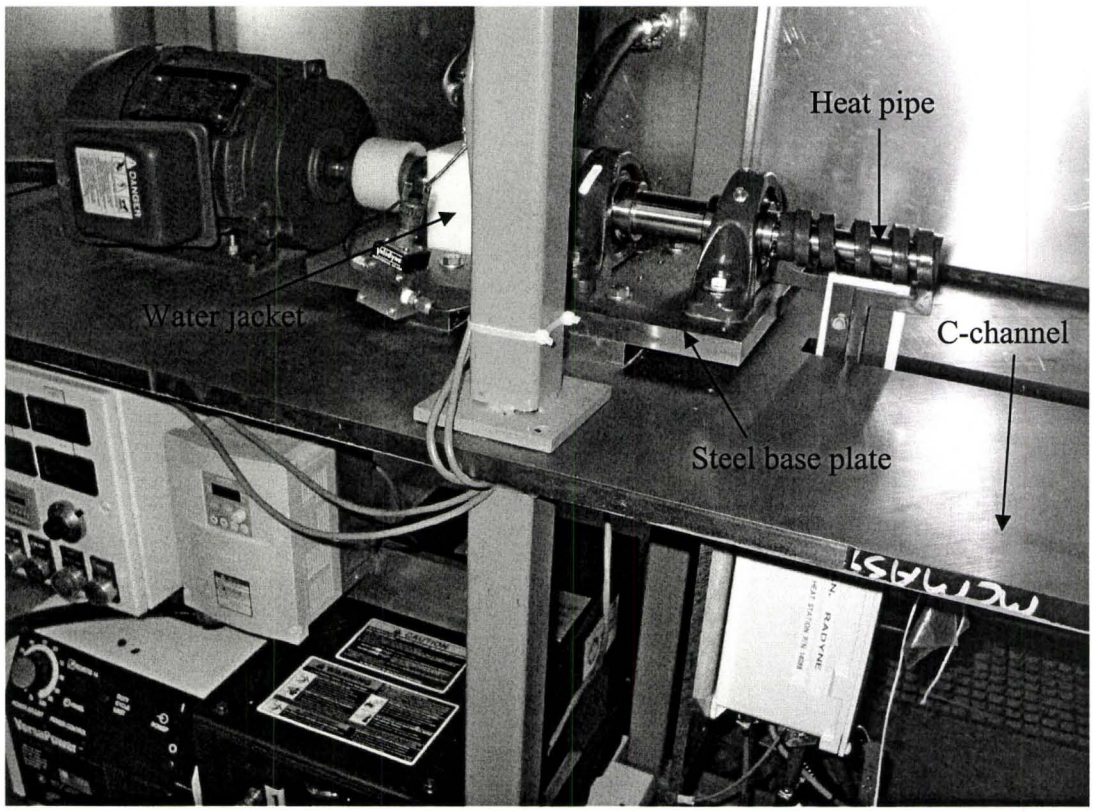

Figure 3.2 Photograph of the rotating heat pipe test facility.

were mounted 178 mm (7") apart on a small plate so that the height of the motor shaft was aligned with the axis of the bearings. The bearings were adjusted so they were aligned with the motor.

The power input at the evaporator end of the heat pipe was supplied by a RADYNE Versa Power induction heating coil designed to heat copper tubing. The system comprised of a 3 phase, 230 V-5 kW air cooled, solid state compact induction power source, an output matching transformer, an operators control, and a water to air cooling system for the induction coil assembly. The output power, voltage and current were measured using meters on the control panel. The RF induction coil assembly was cooled using a closed water loop that included an air cooling system. The water flow rate was measured using a DIGIFLOW DFS-3W turbine flow meter with a capacity of 0.41 L/s and an accuracy of ± 0.5% of actual flow reading. The turbine flow meter was connected to a DIGIFLOW 6100 D/A demodulator and the output was measured using a 16 channel NATIONAL INSTRUMENTS SCB-68 data acquisition board. The turbine flow meter was positioned approximately 40 cm downstream of the coolant tank. The temperatures of the coolant flow were measured using OMEGA T-type thermocouples with an accuracy of ± 0.5 ^{0}C that were connected to a 20-channel OMEGA temperature measuring board. The thermocouples were positioned at a vertical distance of approximately 15 cm from the cooling lines of the heat station.

The heat was removed from the condenser end of the heat pipe using a water jacket shown in Figures 3.3 and 3.4. The water jacket was made of Delrin that has a low conductivity to minimize the heat loss through the water jacket. The condenser was

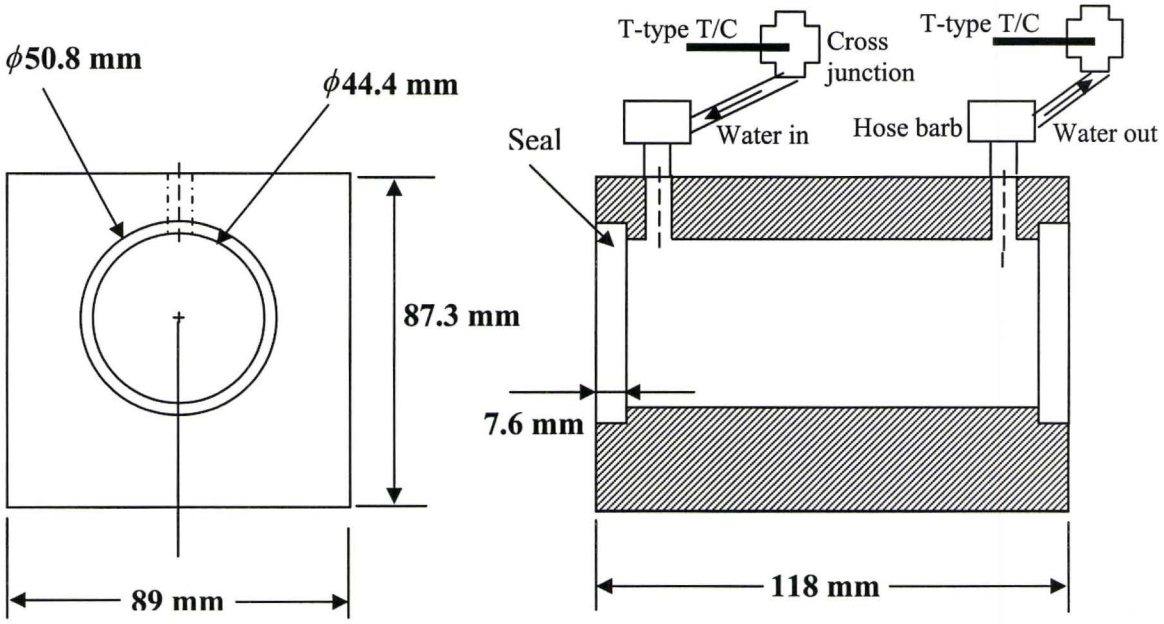

Figure 3.3 Schematic of the water jacket at the condenser.

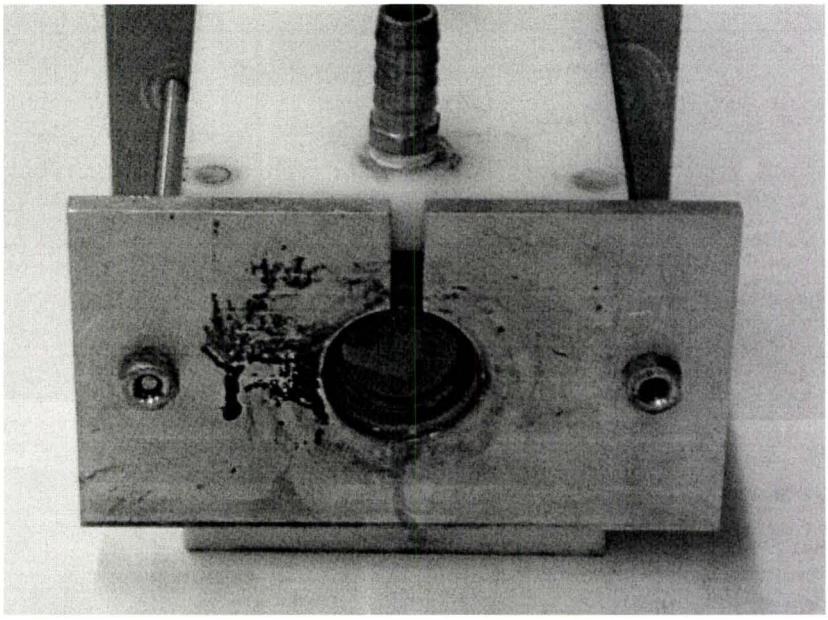

Figure 3.4 Photograph of the condenser water jacket.

sealed using CR10131 lip seals that were press fit into the water jacket using a thin layer of Epoxy adhesive (RTV 108). The seals were in direct contact with the heat pipe, and were rated for a linear speed up to 10.2 m/sec and pressure of 50 psi that were greater than the current requirements of 6.6 m/sec and approximately 5 psi. Aluminium end plates held in place by tie rods were added to the condenser to ensure that the seals remained in place during operation.

The cooling loop for the condenser section is shown in detail in Figure 3.5. The pipes in the loop were PVC tubing with a 12.7 mm (0.5") inner diameter. The flow in the tube was driven by a 0.25 HP OBERDORFER gear pump rated at 11.7 L/s of water at 40 psi. The mass flow rate of water to the condenser water jacket was controlled using a bypass that returned a portion of the flow back into the water tank. The cooling water flow to the condenser section initially passed through a recuperating heat exchanger that was used to preheat the water entering the condenser jacket. The flow then passed through a section of tube wrapped by a 1 m long tape heater that could provide up to 2 kW of heating. The heater was attached using an epoxy adhesive on a copper pipeline with an outer diameter of 22.2 mm (0.875"). The heater was controlled by a 16A2 LOVE PID controller. The input for the controller was a T-type thermocouple that was glued onto the tape heater.

The heated water exiting the pipe with the tape heater then passed through the water jacket. The flow in the water jacket was set up in a counter flow mode. The flow exiting the water jacket then passed through the recuperator and finally through a shell and tube heat exchanger used to cool the water before it entered the water tank. The PVC

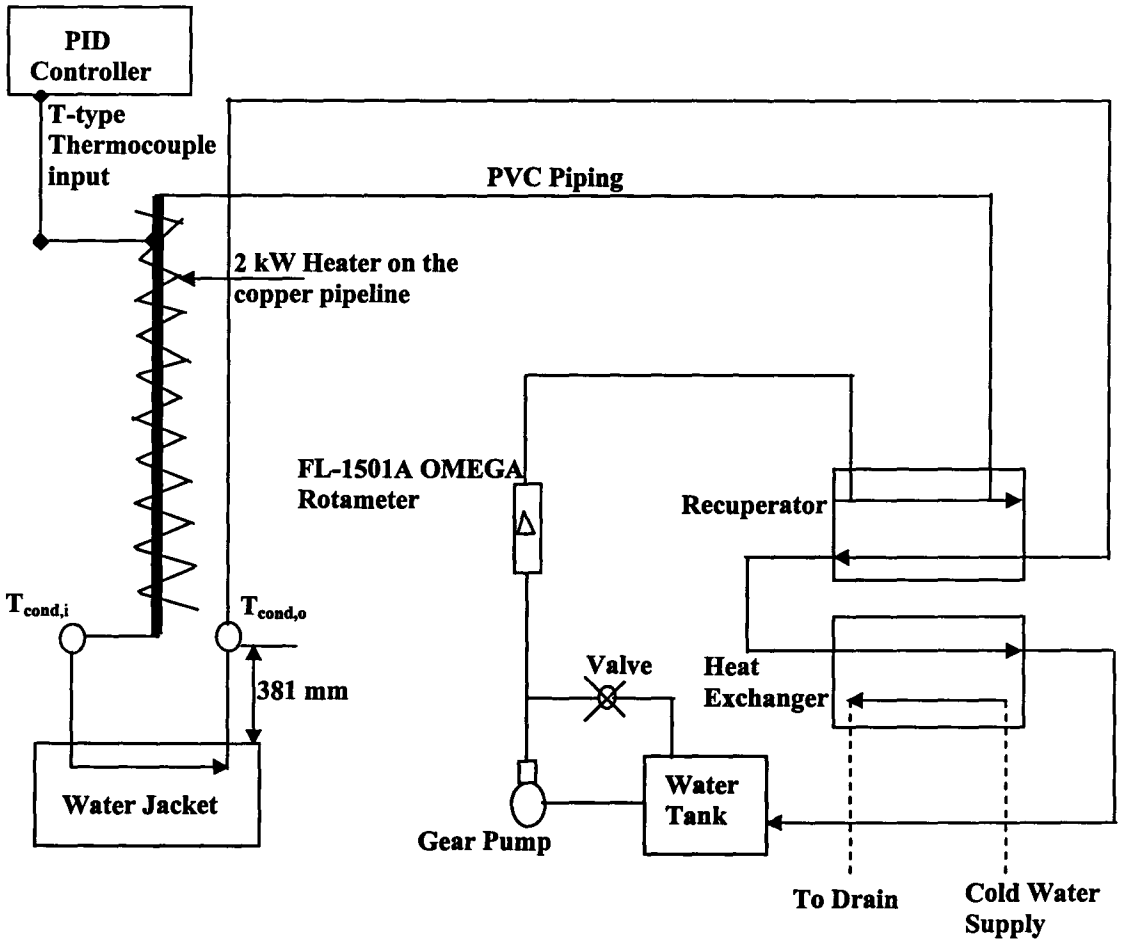

Figure 3.5 Detailed schematic of the condenser cooling section.

tubing and the copper pipe in this facility were insulated to prevent heat loss to the surrounding.

The wall temperature of the heat pipe was measured using a Raytek Thermalert GP series infrared (IR) temperature sensor connected to a Thermalert GP monitor that displays the temperature measured by the sensor. The output of the Thermalert GP monitor was measured using a NATIONAL INSTRUMENTS SCB-68 data acquisition board. The IR sensor had a spot size of 4.6 mm (0.18") at a distance of 203.2 mm (18"), with an accuracy of ± 1 ^{0}C. The infrared sensor was mounted on a traversing stage, at a vertical distance of 203.2 mm (18") from the surface of the heat pipe wall. The wall temperature measurements from the IR sensor were also compared to a high-speed infrared thermal imaging camera ThermCAM SC 3000.

The power removed from the condenser was estimated by

$$Q_{cond} = \dot{m}_{cond} c_p (T_{cond,o} - T_{cond,i}) \tag{3.1}$$

where $\dot{m}_{cond}$ is the mass flow rate of water through the condenser water jacket, and c_p is the specific heat of water, while $T_{cond,i}$ and $T_{cond,o}$ are the temperature of the water measured at the inlet and outlet of the water jacket. The inlet and outlet temperatures were measured using OMEGA T-type thermocouples mounted on cross-junctions that were located approximately 380 mm upstream and downstream of the water jacket. This was done to ensure the flow was well mixed before it was measured by the thermocouple. The T-type thermocouple had an accuracy of ± 0.5 ^{0}C. The thermocouples were connected to a 20-channel OMEGA temperature measuring board. The volumetric flow rate of the water was measured using a FL-1501A OMEGA rotameter mounted 76 cm

above the pump on the pipe leading to the recuperator. The maximum flow rate of this flow meter was 0.05 L/s, with an accuracy of $\pm\ 9.8\times10^{-4}$ L/s.

The power added to the heat pipe at the evaporator was estimated by subtracting the power removed by the coil cooling system and the losses from heat pipe to surroundings, from the electrical power to the induction coil, i.e.,

$$Q_{evap} = Q_{elec} - Q_{IC} - Q_{loss} \tag{3.2}$$

where Q_{elec} is the electrical power added to the induction coil. The electrical power was determined from the power meter on the remote controller for the induction coil. The power removed by the cooling water loop is given by

$$Q_{IC} = \dot{m}_{IC} c_p (T_{IC,o} - T_{IC,i}) \tag{3.3}$$

where $\dot{m}_{IC}$ is the mass flow rate of water in the cooling loop, c_p is the specific heat of water, and $T_{IC,i}$ and $T_{IC,o}$ are the temperatures of the cooling water loop measured at the inlet and outlet of the induction heating system.

The heat loss from the wall of the evaporator section of the rotating heat pipe, Q_{loss} is a combination of convection and radiation losses. The convection loss to the ambient from the rotating heat pipe was approximated by

$$Q_{conv} = Ah(T_{evap,w} - T_{\infty}) \tag{3.4}$$

Here $T_{evap,w}$ is the average evaporator wall temperature, T_{∞} is the ambient temperature in the enclosure of the test rig and A is the wall surface area of the evaporator. The heat transfer coefficient h was determined from a correlation for a rotating horizontal cylinder in ambient fluid given by (Anderson and Saunders, 1953)

$$Nu_D = \frac{hD}{k_{air}} = 0.11(0.5\,\mathrm{Re}_\omega{}^2 + Gr_D\,\mathrm{Pr})^{0.35} \tag{3.5}$$

Here Nu_D is the Nusselt number of the rotating horizontal cylinder in the air, h is the heat transfer coefficient, k_{air} is the thermal conductivity of air, Re_ω is the rotational Reynolds number, Gr_D is the rotating pipe Grashof number and Pr is the Prandtl number of air. The radiation loss from the rotating cylinder was approximated by

$$Q_{rad} = A\varepsilon\sigma(T_{evap,w}{}^4 - T_\infty{}^4) \tag{3.6}$$

Here, ε is the emissivity of TREMCLAD flat black paint that was coated on the heat pipe wall.

3.2 Rotating heat pipes

Tests were performed for the heat pipes shown in Figure 3.6. The heat pipe had a length of 431.8 mm (17") and an outer diameter of 25.4 mm (1"). The wall thickness of the heat pipe was 4.6 mm (0.18") in the evaporator and the adiabatic section. The heat pipes were designed with a 1^0 taper angle (half cone) in the condenser. The taper in the heat pipe started 305 mm (12") from the evaporator end cap. The length of the taper in the heat pipe was 101.6 mm (4"). The inner radius of the condenser section was 8.1 mm (0.32") at the straight end and 6.3 mm (0.25") where the taper ended. The rotating heat pipes were coupled to the drive motor by a copper plug that was press fit in to the condenser end. The copper plug had a diameter of 22.2 mm (0.875") and fit 12.7 mm (0.5") into the heat pipe.

The heat pipe was coupled to the stainless steel shell mounted in the bearing using

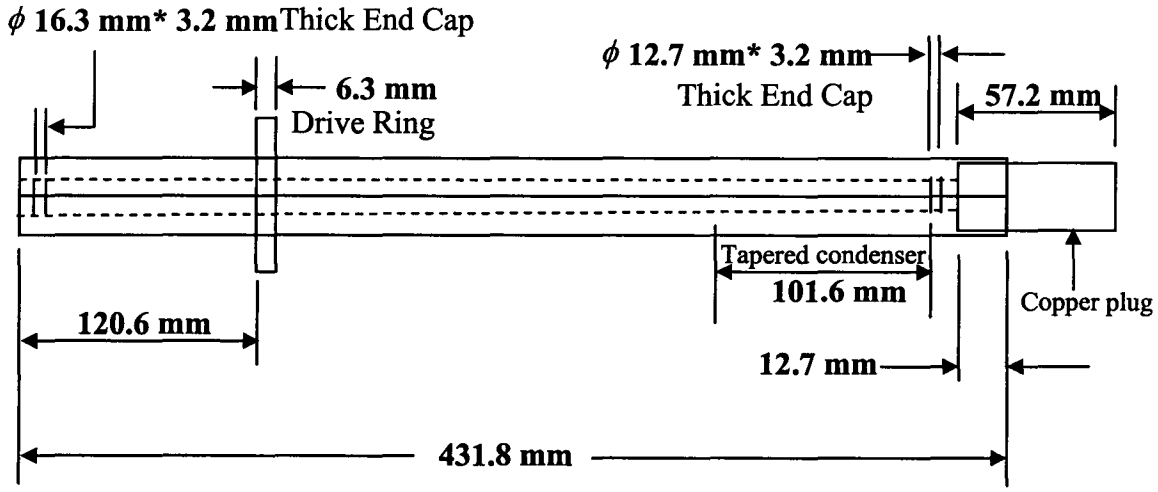

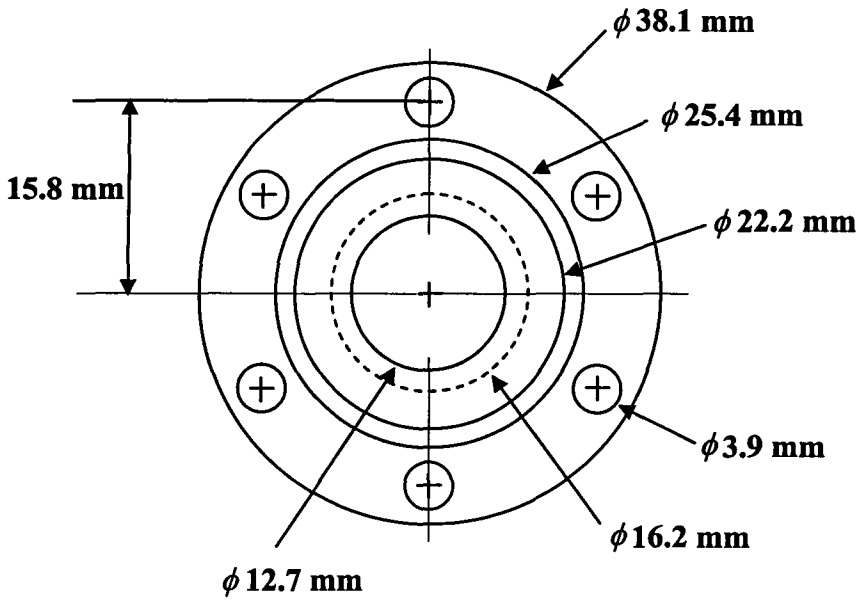

Figure 3.6 Schematic and section view of the rotating heat pipe used in this investigation.

Heat Pipes	Working fluid	Fluid charge(gm)	Volume fill ratio(%)
1	Methanol	11.6	18.6
2	Ethanol	11.73	18.6
3	Distilled water	14.64	18.6
4	Distilled water	5.5	6.9
5	Distilled water	4.88	6.2

Table 3.1 Summary of the fluid charge in the rotating heat pipes used in this investigation.

a copper ring brazed on the heat pipe. The drive ring had six equally spaced 3.9 mm diameter holes that were used to screw the drive ring to the stainless steel shell. This copper ring was used to align the heat pipe during start up and to transmit the drive torque from the rotating heat pipe to bearings.

The heat pipes tested were filled with different working fluids and fluid loadings. The fluid charges in the heat pipes to characterize the effect of working fluid were based on the same volume fill ratio. The properties of the fluid charge in the heat pipe are documented in Table 3.1.

3.3 Calibration of the facility

The motor controller was calibrated by measuring the speed of the rotating shaft using a LUTRON DT-2232C phototype digital tachometer that could measure speeds from 5 to 5000 RPM with an accuracy of ± 1 RPM. A 12 mm square piece of reflective adhesive tape was attached to the coupling for the measurement of the rotational speed using the tachometer. The change in the rotational speed with the motor setting is shown in Figure 3.7. It was found that the maximum speed of the motor was 4775 RPM that occurred when the controller setting was 80.2. The change in the rotational speed with the controller setting was found to be linear and repeatable.

The thermocouples used in the experiments were calibrated using a 100 ohm 4-wire platinum resistance thermometer (RTD), connected to an OMEGA DP251 Precision Digital Thermometer temperature display unit. The RTD and the DP251 had individual accuracy of ± 0.01 ^{0}C, and the combined system accuracy was ± 0.025 ^{0}C for the

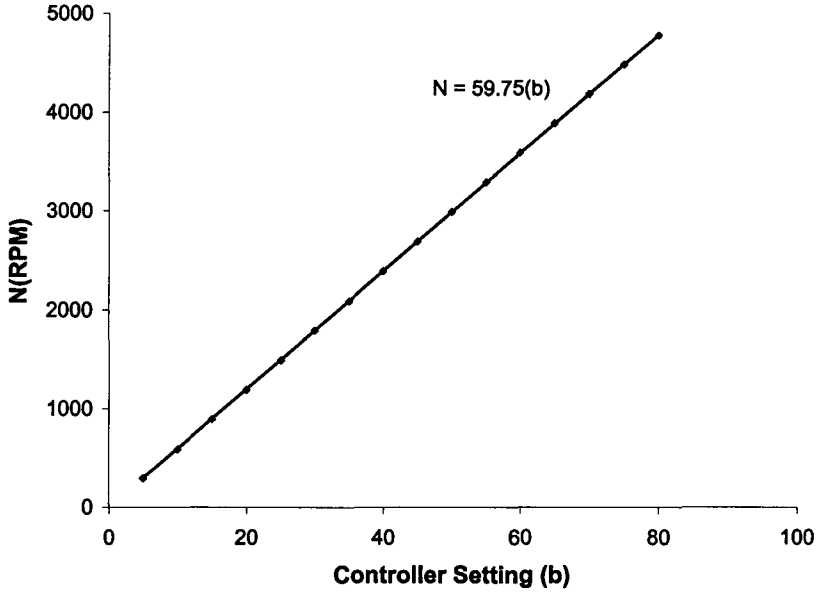

Figure 3.7 Change in the motor rotational speed with the controller setting.

temperature range -50 ^{0}C to +250 ^{0}C. The thermocouples were calibrated using an in-house temperature calibration facility where the RTD and thermocouples were mounted on a thermal copper block submerged in oil that was heated with a cartridge heater. The thermal block was surrounded by an acrylic block to prevent heat loss. The system was heated and allowed to reach steady state. The heater was switched off and the copper block was allowed to cool slowly to room temperature while the temperatures from the thermocouples and RTD were recorded every minute. A low temperature calibration was then performed by placing ice inside the wooden box that surrounded the acrylic block and repeating a similar procedure. The calibration curves for the four thermocouples are shown in Figures 3.8-3.11.

The emissivity of the black paint used on the heat pipe wall was determined previously by Gao (2000), and was 0.96 ± 0.01. The accuracy of the wall temperature measurements with the infrared sensor was examined by comparing to measurements with the ThermCAM SC 3000 IR camera. A representative thermal image of the evaporator section for the heat pipe with 11.6 gm of methanol is shown in Figure 3.12. A typical temperature distributions on the wall of the heat pipe with 11.6 gm of methanol measured using the IR camera at rotational speed of 2000 RPM are show in Figure 3.13. It is clear that the evaporator wall temperature is relatively uniform in all cases. The largest variation in the temperature was 7 ^{0}C along the evaporator length. The temperature on the evaporator wall was also measured at the two largest gaps using the IR sensor. Comparisons of the evaporator wall temperature measured with the IR sensor and from the IR camera images are shown in Figure 3.14. It is clear that the temperature

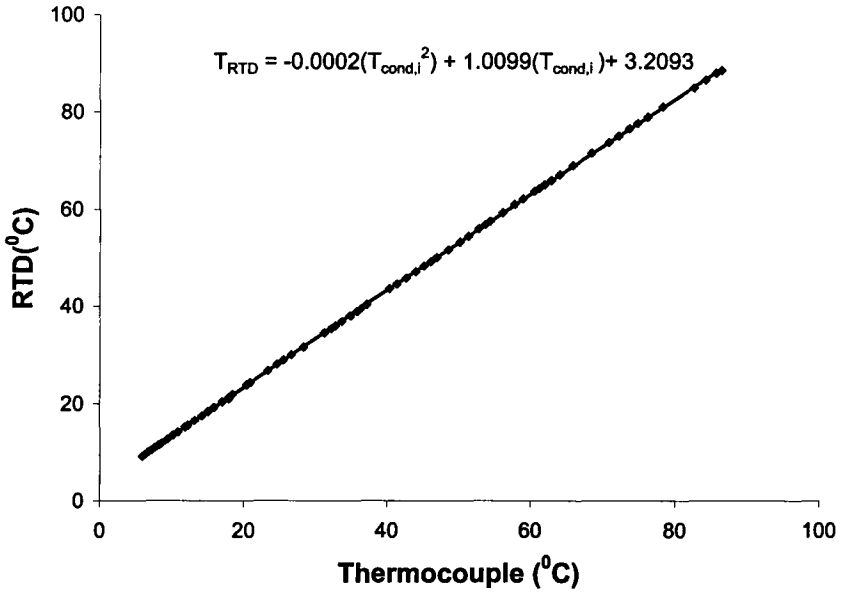

Figure 3.8 Calibration for the thermocouple used at the inlet of the condenser water jacket.

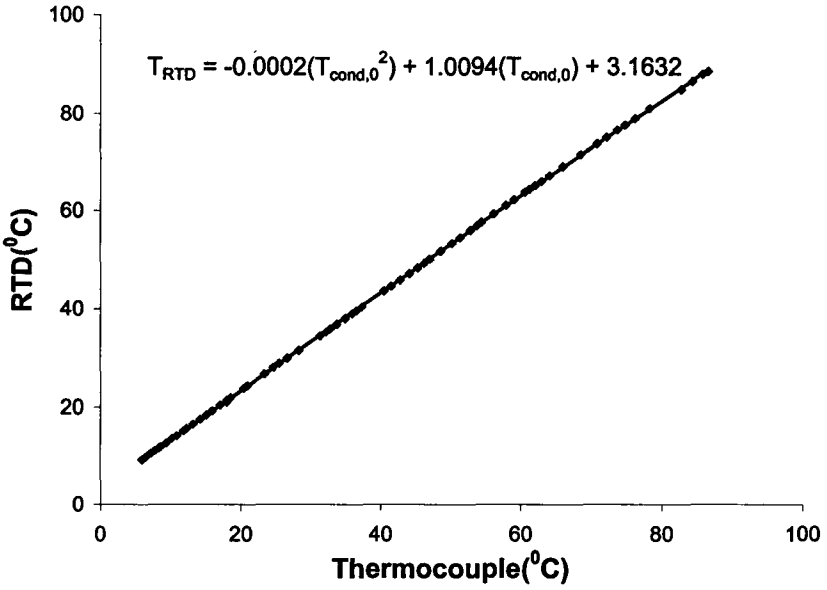

Figure 3.9 Calibration for the thermocouple used at the outlet of the condenser water jacket.

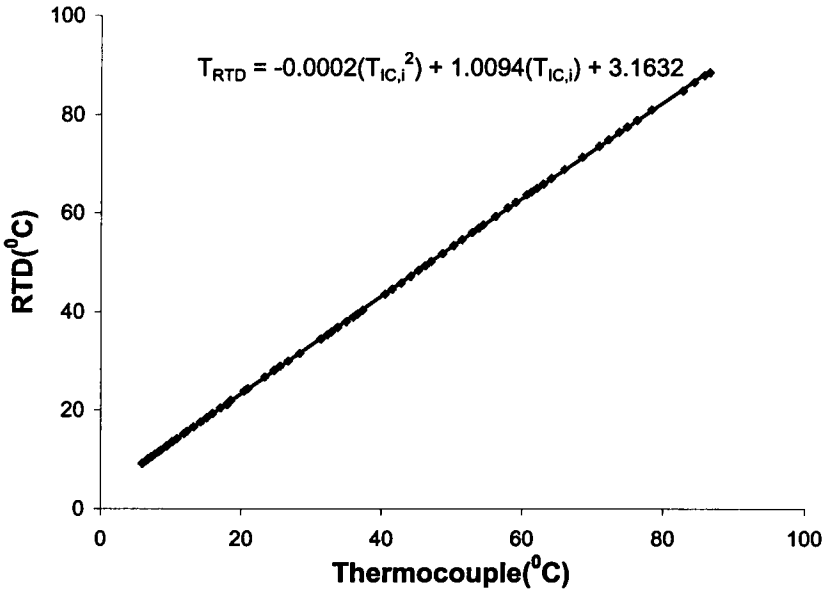

Figure 3.10 Calibration for the thermocouple used at the inlet of the induction heating station.

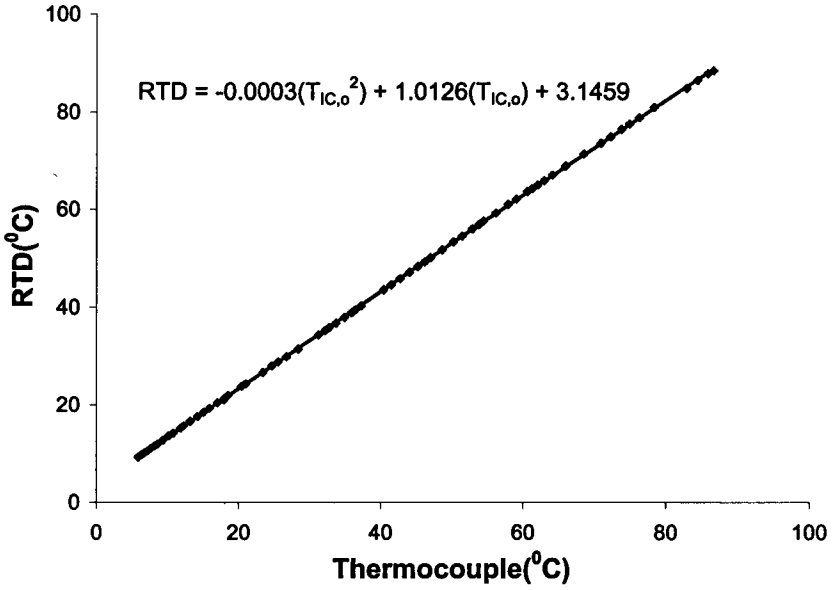

Figure 3.11 Calibration for the thermocouple used at the outlet of the induction heating station.

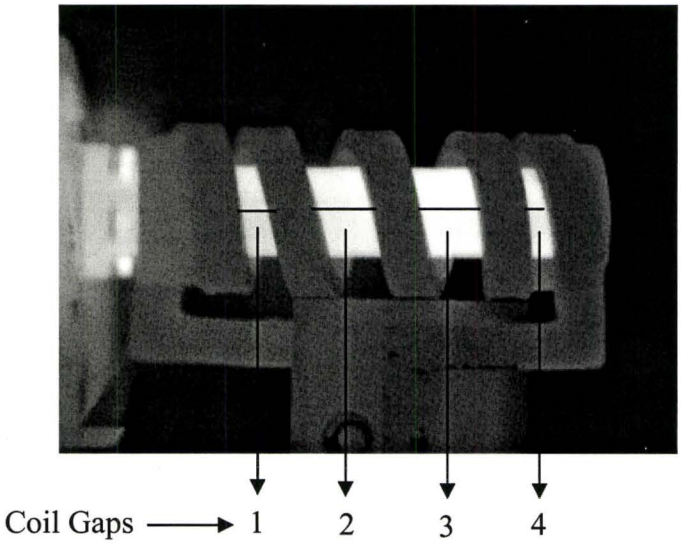

Figure 3.12 Thermal image of the evaporator section for the heat pipe with 11.6 gm of methanol at 2000 RPM and heat load of 0.325 kW.

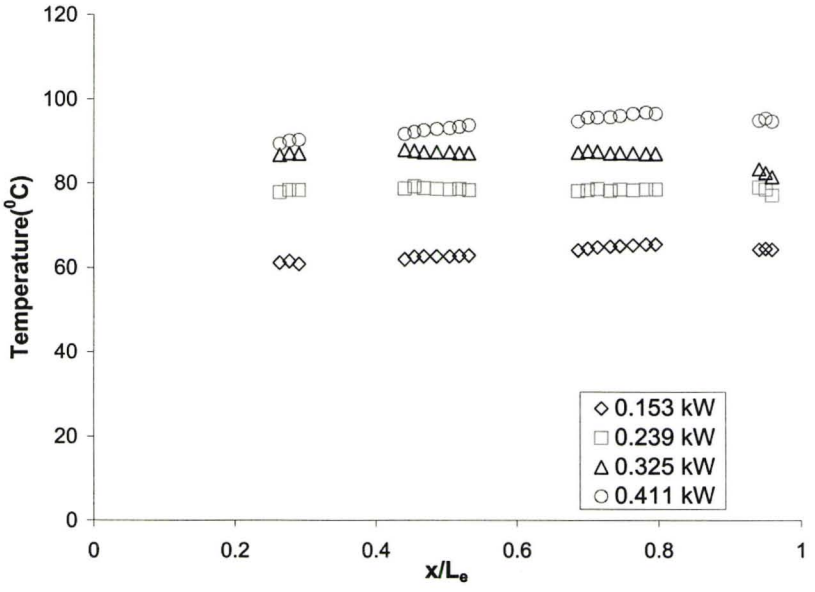

Figure 3.13 Evaporator wall temperature distribution at 2000 RPM for the heat pipe with 11.6 gm of methanol.

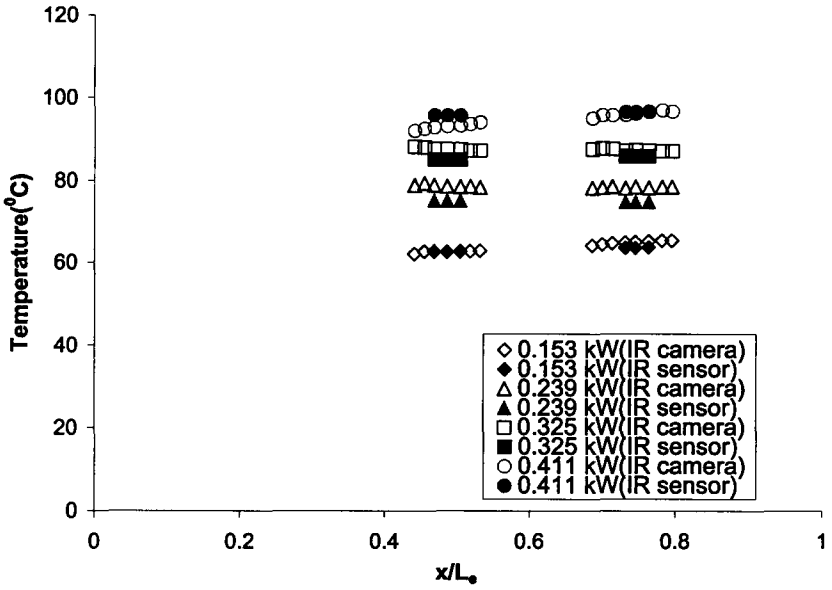

Figure 3.14 Comparison of the evaporator wall temperature at 2000 RPM for the heat pipe with 11.6 gm of methanol.

measurements with the IR camera and IR sensor are in good agreement, and within ± 4 ^{0}C. The thermal images of the condenser section between the water jacket and the motor, and the adiabatic section between the water jacket and the bearing for the heat pipe with 11.6 gm of methanol are shown in Figure 3.15. The average temperature measurements for the end cap of the condenser section and the adiabatic section beside the water jacket measured using the IR camera and IR sensor are shown in Figure 3.16. It is clear that the temperature measurements with the two sensors are in good agreement, and within ± 1 ^{0}C. The temperature of the wall measured on the two sides of condenser at different heat loads is shown in Figure 3.17. The results show that the temperature of the wall on the two sides of the water jacket are not the same. The average of the wall temperature on the two sides of the condenser water jacket are used here to represent the condenser wall temperature.

3.4 Experimental procedure

The tests on the heat pipe were carried out by initially purging any air from the condenser cooling loop system. The flow rate through the water jacket was then set to 2.95×10^{-2} L/s and the PID controller was set to control the inlet temperature of the cooling water. Following this, the heat pipe was brought to the desired rotational speed and operated for ten minutes before the heat was applied to the evaporator section. The power input to the induction coil unit was initially set at 0.5 kW. The heat pipe was allowed to reach steady state and the measurements were taken when the variation in the evaporator wall temperature was less than ± 0.1 ^{0}C for one hour. In most cases the heat

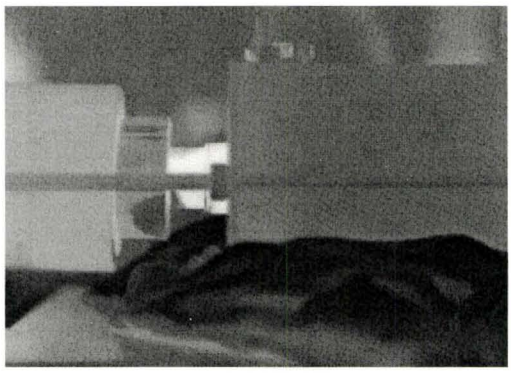

(a)

(b)

Figure 3.15 Thermal images of (a) condenser and (b) adiabatic sections for the heat pipe with 11.6 gm of methanol at 3000 RPM and heat load of 0.333 kW.

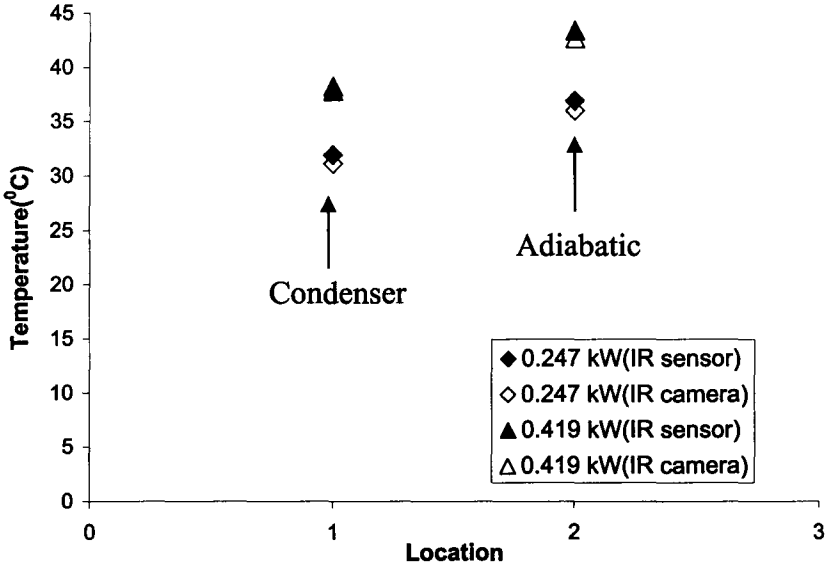

Figure 3.16 Comparison of the condenser and the adiabatic wall temperatures at 3000 RPM for the heat pipe with 11.6 gm of methanol.

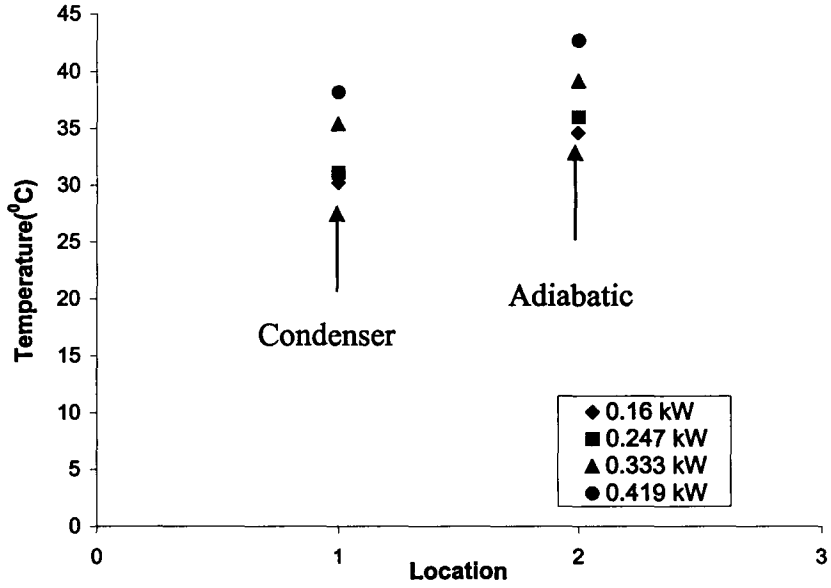

Figure 3.17 Wall temperature distribution from the condenser to the adiabatic section at 3000 RPM for the heat pipe with 11.6 gm of methanol using IR camera.

pipe reached steady state in 30 minutes. Once the heat pipe had reached steady state operation, the wall temperature at the evaporator end was measured using the IR sensor at 6 discrete points at the two largest gaps in the induction coil. Each gap was 18 mm wide and the temperature was measured at three locations spaced 2 mm apart in each gap. The wall temperature at the condenser end was measured on either side of the water jacket because it was not possible to directly measure the wall temperature inside the water jacket. Once the measurements were taken, the power input to the induction coil was increased in steps of 0.5 kW till the maximum of 3 kW was reached. This procedure was followed for all the rotational speeds.

3.5 Uncertainty analysis

The uncertainty in the measurements performed here was assessed using the approach outlined in Coleman and Steele (1999).The condenser heat transfer rate was given by

$$Q_{cond} = \dot{m}_{cond} c_p \Delta T_{cond} \tag{3.7}$$

where

$$\Delta T_{cond} = T_{cond,o} - T_{cond,i} \tag{3.8}$$

Since the measurements were independent, the random uncertainty in the condenser heat transfer rate can be approximated by

$$U_{Q_{cond}} = \pm \sqrt{\left(\frac{\partial Q_{cond}}{\partial \dot{m}_{cond}} \times U_{\dot{m}_{cond}}\right)^2 + \left(\frac{\partial Q_{cond}}{\partial c_p} \times U_{c_p}\right)^2 + \left(\frac{\partial Q_{cond}}{\partial \Delta T_{cond}} \times U_{\Delta T_{cond}}\right)^2} \tag{3.9}$$

where $U_{Q_{cond}}$, $U_{\dot{m}_{cond}}$, U_{c_p} and $U_{\Delta T_{cond}}$ are the uncertainties in the condenser heat transfer rate, mass flow rate, specific heat and temperature rise across the condenser water jacket. The specific heat of the water does not vary significantly over the temperature range so the uncertainty in the specific heat was neglected. The uncertainty in the temperature rise across the water jacket was given by

$$U_{\Delta T_{cond}} = \pm\sqrt{\left(U_{T_{cond,o}}\right)^2 + \left(U_{T_{cond,i}}\right)^2} \tag{3.10}$$

where $U_{T_{cond,i}}$ and $U_{T_{cond,o}}$ are the uncertainties in the temperature measurements for the condenser water jacket. The uncertainty of the temperature measurements after the calibration was estimated as ± 0.15 ^{0}C, so that the uncertainty in the temperature rise was ± 0.2 ^{0}C. The relative uncertainty in the mass flow rate measurement was ± 3.3%. As a result, the relative uncertainty in the condenser heat transfer rate varied from ± 15% to ± 5% for typical heat transfer rates between 0.165 kW and 0.57 kW.

A similar procedure was used to estimate the uncertainty in the power removed by the induction cooling loop. The uncertainties in the temperature measurement of the cooling loop were found to be ± 0.15 ^{0}C after the calibration test, so the uncertainty in the temperature rise was again ± 0.2 ^{0}C. The relative uncertainty in the mass flow rate measurement was ± 0.7%. As a result, the relative uncertainty for typical heat transfer rates between 0.399 kW and 1.965 kW varied between ± 11% to ± 2%.

3.6 Energy balance

A comparison of the estimate for the power added to the evaporator and the heat

transfer removed from the condenser for the rotating heat pipe with 11.6 gm of methanol at 4000 RPM is shown in Figure 3.18. There is a significant difference between the estimate of the power added at the evaporator and the power removed at the condenser that exceeds the experimental uncertainty. At the lower powers, the estimate of the power added to the evaporator was much less than the power removed from the condenser. At high powers, more power was added to the evaporator than removed at the condenser. Part of this is due to the estimate of the losses from the evaporator. The different components of the heat transfer involved are also shown as a reference in Figure 3.19. It is clear that approximately 70% of the electrical power added to the induction coil is removed by the cooling loop. The radiation loss was small compared to the convective loss from the evaporator surface. The estimate of heat losses from the evaporator surface are 13%-60% of the estimate of power added to the evaporator of the heat pipe. For example, when the power to the coil is 0.5 kW the loss is 60% of the net power. In these cases, the temperature of the adiabatic section is lower than the bearing temperature so that the heat from the bearing can be added to the heat pipe. Thus it was thought that the heat added at the evaporator was not reliable so the heat removed at the condenser was used to evaluate the heat transfer through the heat pipe.

The amount of the bearing heating was estimated by operating the heat pipe at different rotational speeds without heat being added at the evaporator. The temperature of cooling water in the condenser water jacket was changed so the bearing heating could be evaluated at different heat pipe temperatures. The heat transfer out of the condenser water jacket in these experiments provides a rough estimate of the bearing heating that is being

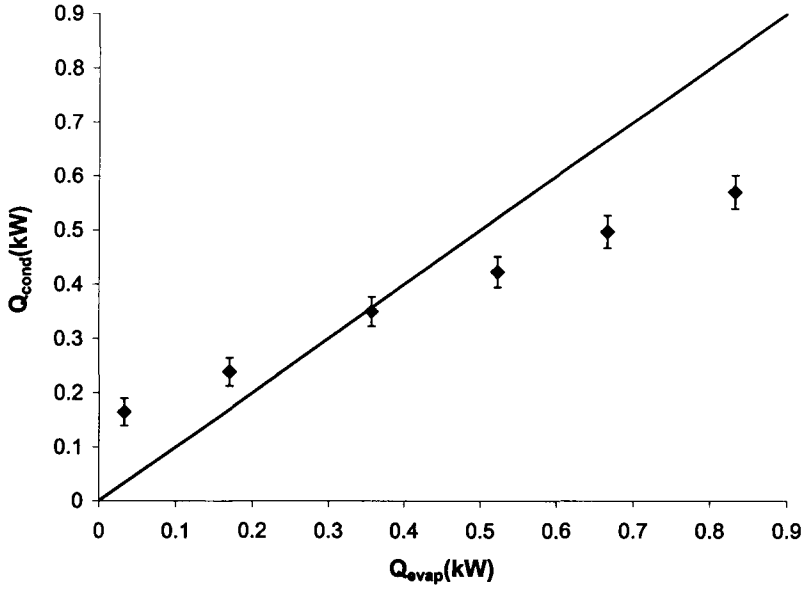

Figure 3.18 Comparison of the power added to the evaporator and heat transfer removed from the condenser at rotational speed of 4000 RPM for the heat pipe with 11.6 gm of methanol.

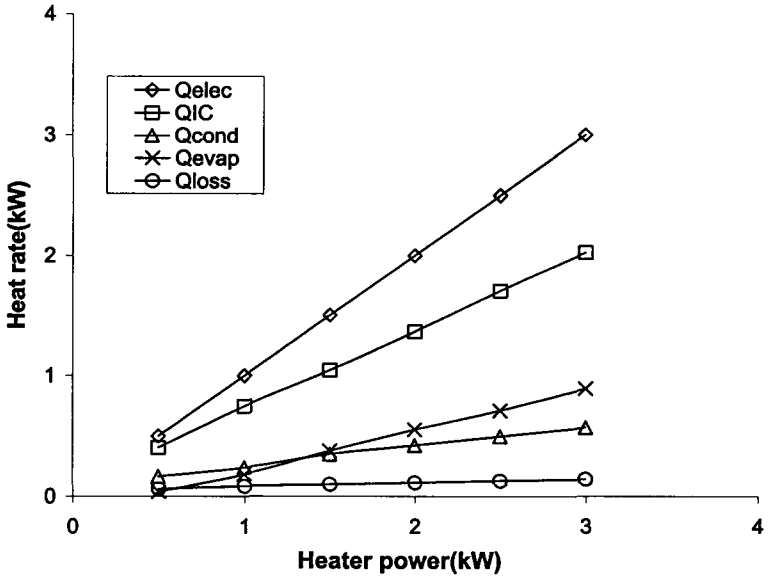

Figure 3.19 Energy balance at rotational speed of 4000 RPM for the heat pipe with 11.6 gm of methanol.

transferred to the heat pipe. These results are shown in Figure 3.20. It is clear that the bearing heating transferred into the heat pipe increases as the speed increases, and when wall temperature decreases, as expected. When the nominal adiabatic temperature was above 30 ^{0}C, the lowest temperature in most tests, the bearing heating varied from 40 W at 2000 RPM to 60 W at 4000 RPM. Thus, the bearing heat could introduce a significant uncertainty at the lowest heat fluxes. The bearing heat is smaller at the higher heat fluxes when the operating temperature of the heat pipe was higher. At higher heat fluxes, the induction heating of the surrounding surfaces becomes important. These losses are typically due to the end effects from the solenoid (Rudnev et al., 2003). Since these losses could not be quantified, the evaporator heat transfer can be significantly overestimated particularly because the steel base would induct heat better than the copper heat pipe.

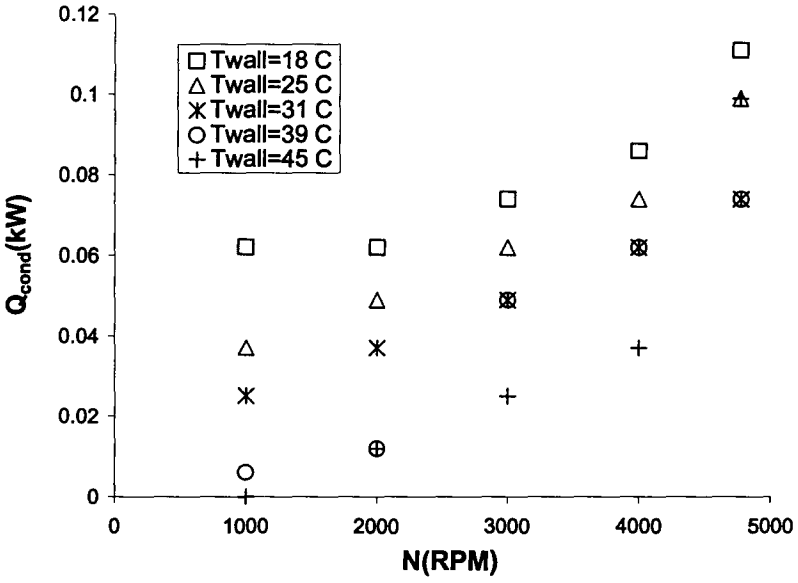

Figure 3.20 Estimate of bearing heating at rotational speed of 4000 RPM for the heat pipe with 11.6 gm of methanol.

Chapter 4 Results and Discussion

The results of the experimental investigation to characterize the steady state heat transfer performance of the 25.4 mm (1") diameter high-speed rotating heat pipes with a 1^0 taper in the condenser for different working fluids and rotational speed up to 4000 RPM are presented in this chapter. The experimental results are also compared to predictions from an existing model for the performance of high-speed rotating heat pipes.

4.1 Effect of working fluid

The effect of the working fluid was examined experimentally for three rotating heat pipes that were loaded with 11.6 gm of pure methanol, 11.73 gm of pure ethanol and 14.64 gm of distilled water respectively. The working fluid occupied approximately 19% of the pipe interior volume in each of these heat pipes. The performance of the individual heat pipes are presented first and then their performance are compared.

The temperature distribution on the wall of the heat pipe with 11.6 gm of methanol at rotational speeds of 2000, 3000 and 4000 RPM for different heat transfer rates are shown in Figures 4.1 to 4.3. The condenser wall temperature was again measured at points on either side of the water jacket while the temperature in the evaporator section was measured at the gaps in the induction coil with the infrared sensor. In all cases, the wall temperature at the evaporator end and at the condenser across the water jacket are relatively uniform, with the temperature difference along the

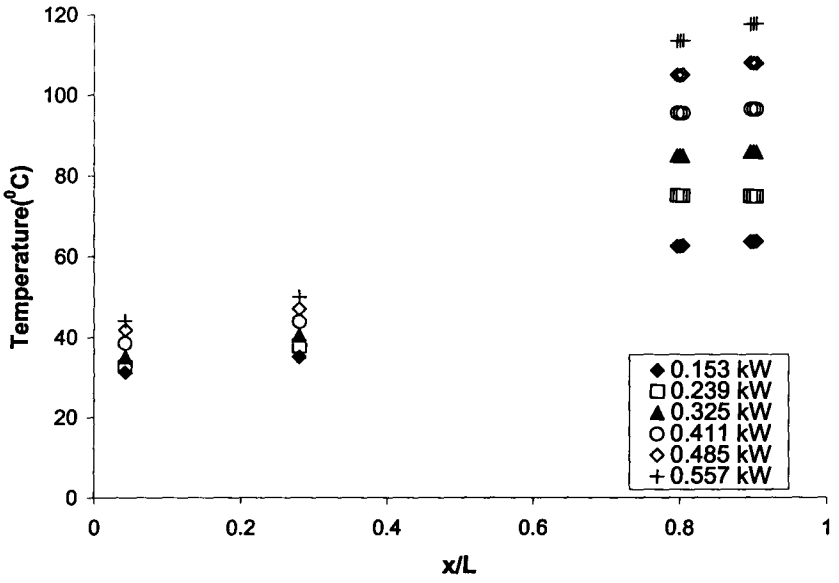

Figure 4.1 Wall temperature distribution at 2000 RPM for the heat pipe with 11.6 gm of methanol.

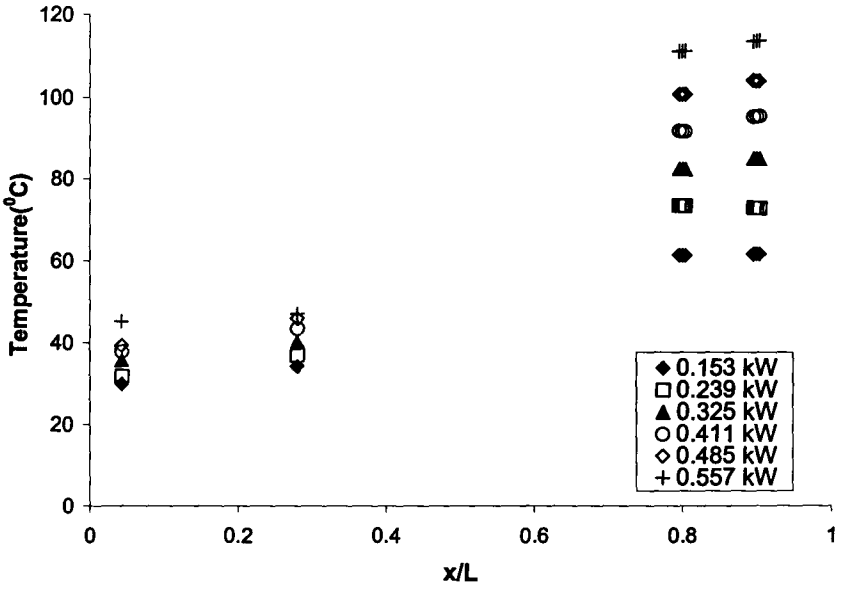

Figure 4.2 Wall temperature distribution at 3000 RPM for the heat pipe with 11.6 gm of methanol.

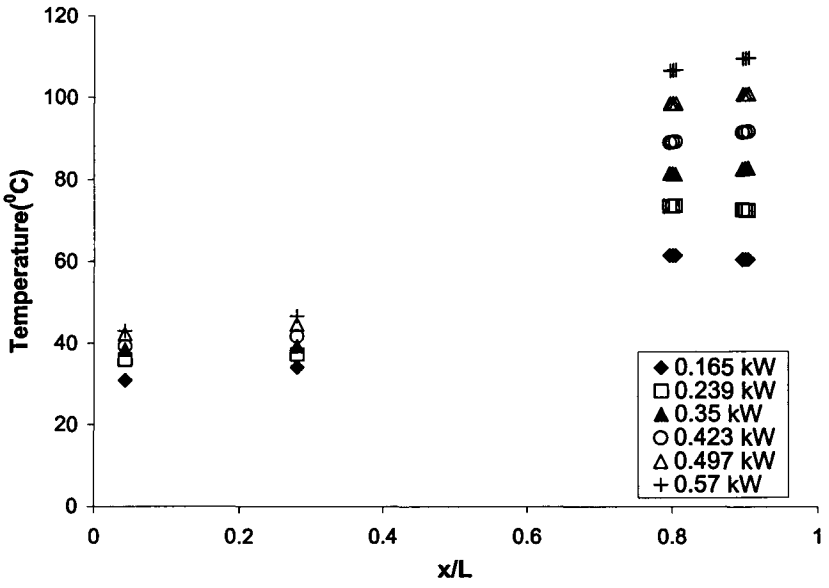

Figure 4.3 Wall temperature distribution at 4000 RPM for the heat pipe with 11.6 gm of methanol.

evaporator and across the condenser less than 5 ^{0}C and 7 ^{0}C respectively. The typical variation in the temperature difference along the evaporator section, and across the water jacket are approximately 4% and 10%, respectively, of the difference between the average evaporator and condenser temperatures.

The performance of the heat pipe was characterized by examining the change in the heat transfer from the condenser of the heat pipe with change in the temperature difference from the evaporator to the condenser as shown in Figure 4.4. The temperature difference here was the difference between the average of the temperatures measured along each of the sections. The heat transfer through the rotating heat pipe for a given temperature drop increased by approximately 20% when the rotational speed was increased from 2000 to 4000 RPM. This was expected because the increase of the rotational speed increases the component of the centrifugal force parallel to the flow direction in the condenser, and thus tends to thin the film in the condenser. The change in the thermal resistance of the heat pipe with heat transfer rate for the heat pipe with 11.6 gm of methanol is shown in Figure 4.5. It is clear that for all rotational speeds the thermal resistance is not constant. In all cases, the thermal resistance drops by approximately 25% when the heat transfer rate increases from 0.16 kW to 0.35 kW. For heat transfer rates greater than 0.4 kW the thermal resistance is more uniform. Thus, for the typical operating range of this heat pipe the thermal resistance can be approximated by a constant. The thermal resistance also decreased by 10% when rotational speed was increased from 2000 to 4000 RPM. Thus, the thermal performance improves as the speed increases.

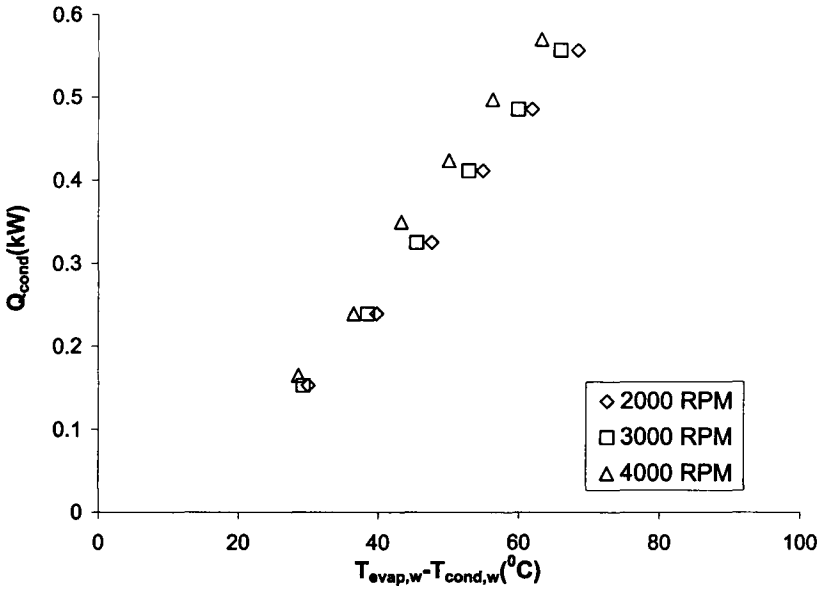

Figure 4.4 Change in the heat transfer with temperature difference for the heat pipe with 11.6 gm of methanol.

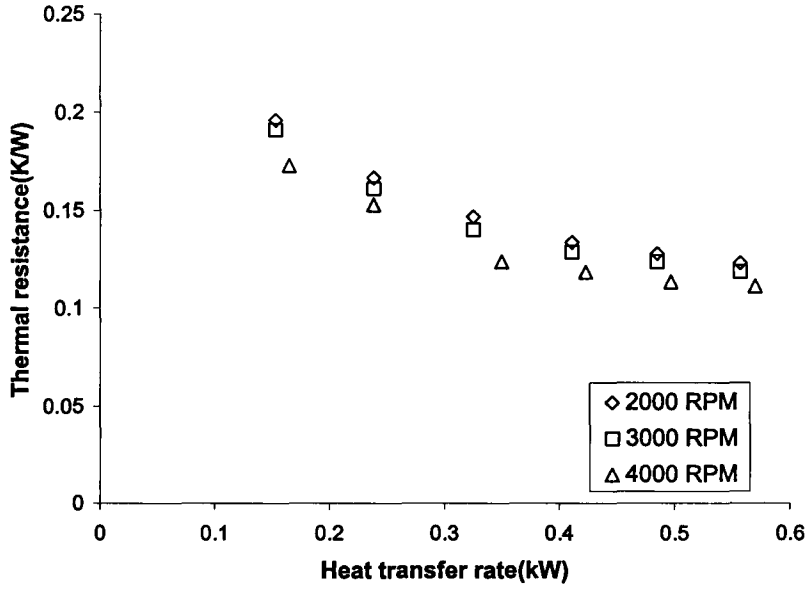

Figure 4.5 Change in the thermal resistance with heat transfer rate for the heat pipe with 11.6 gm of methanol.

The temperature distribution on the wall of the rotating heat pipe with 11.73 gm of ethanol for rotational speeds of 2000 and 4000 RPM are shown in Figure 4.6 to 4.7. The temperature measured at the evaporator section at all heat transfer rates varied less than 2 ^{0}C. The temperature from condenser to the adiabatic section is relatively uniform with the largest difference of 8 ^{0}C across the condenser length. In all the cases the temperature difference along the evaporator section and across the condenser length were less than 3% and 12%, respectively, of the difference in the averaged temperature of the evaporator and the condenser sections.

The change in the heat transfer rate through the heat pipe with temperature difference for the heat pipe with 11.73 gm of ethanol is shown in Figure 4.8. For a given temperature drop, the heat transfer rate through the heat pipe increased by more than 35% when the rotational speed was increased from 2000 to 4000 RPM. The change in the thermal resistance with heat transfer rate for the heat pipe with 11.73 gm of ethanol is shown in Figure 4.9. The thermal resistance decreases with the heat transfer rate in all cases and then appear to approaching a constant value. The thermal resistance in this case appears to be less non-linear than the methanol heat pipe. The thermal resistance drops by approximately 25% when the rotational speed is increased from 2000 to 4000 RPM that was more than the methanol heat pipe.

The temperature distribution on the wall of the rotating heat pipe with 14.64 gm of water at rotational speed of 2000 RPM is shown in Figure 4.10. The temperatures measured on the evaporator and across the condenser are uniform in this case. In particular, the maximum temperature difference along the evaporator was 2 ^{0}C while the

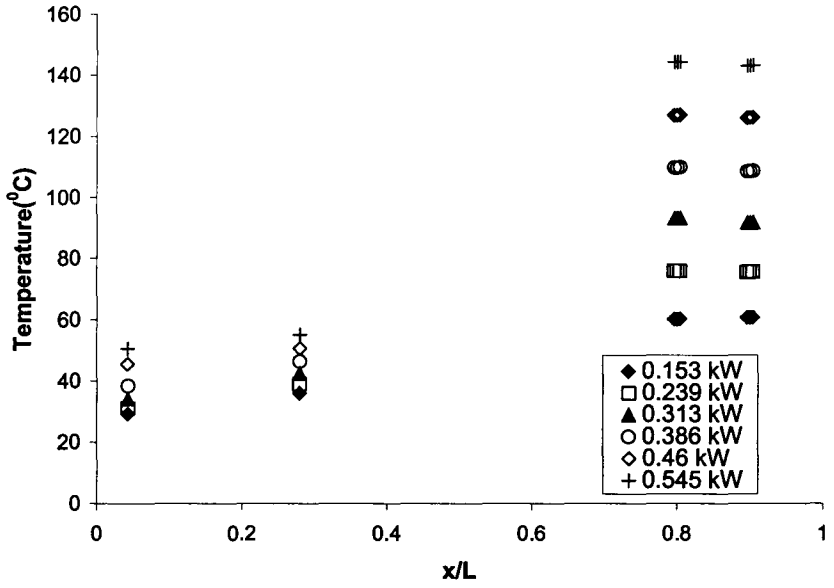

Figure 4.6 Wall temperature distribution at 2000 RPM for the heat pipe with 11.73 gm of ethanol.

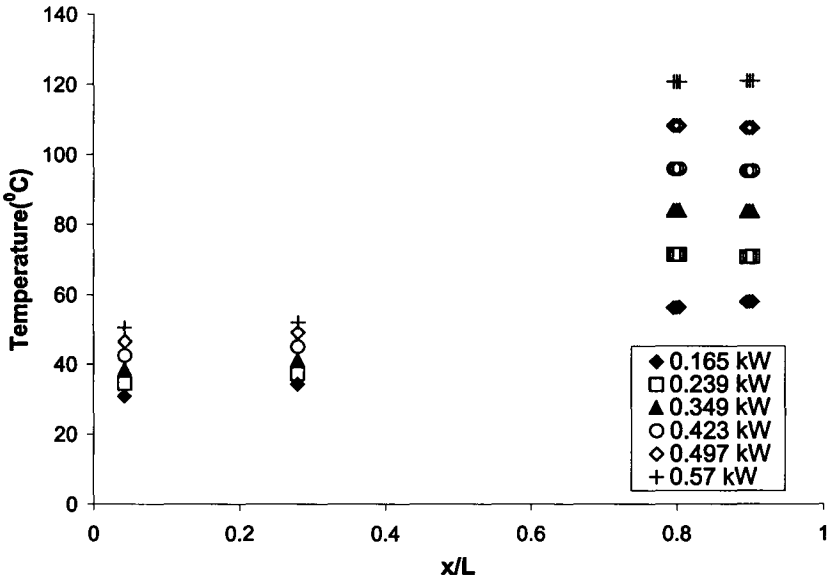

Figure 4.7 Wall temperature distribution at 4000 RPM for the heat pipe with 11.73 gm of ethanol.

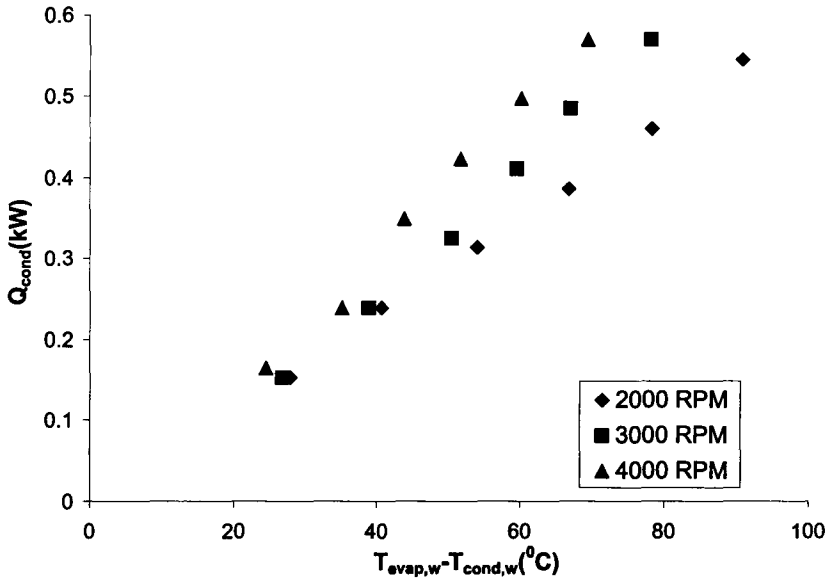

Figure 4.8 Change in the heat transfer with temperature difference for the heat pipe with 11.73 gm of ethanol.

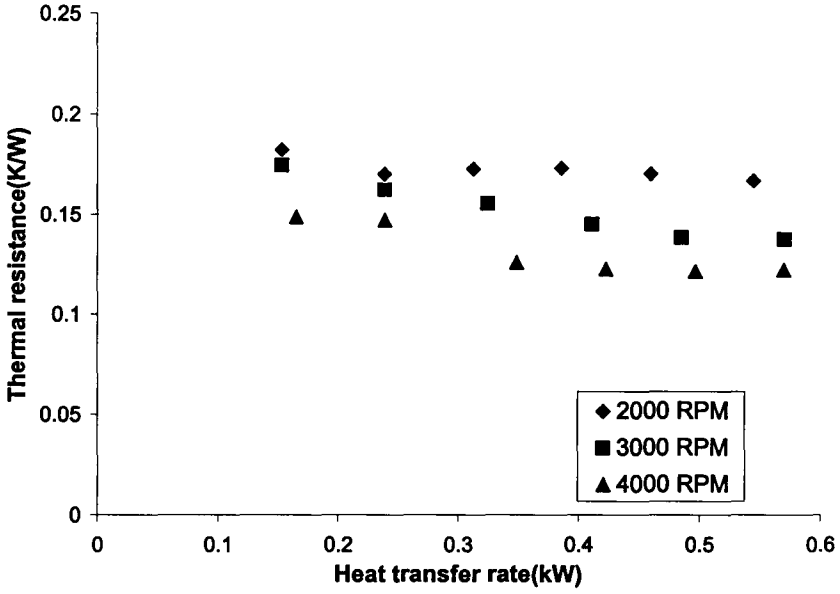

Figure 4.9 Change in the thermal resistance with heat transfer rate for the heat pipe with 11.73 gm of ethanol.

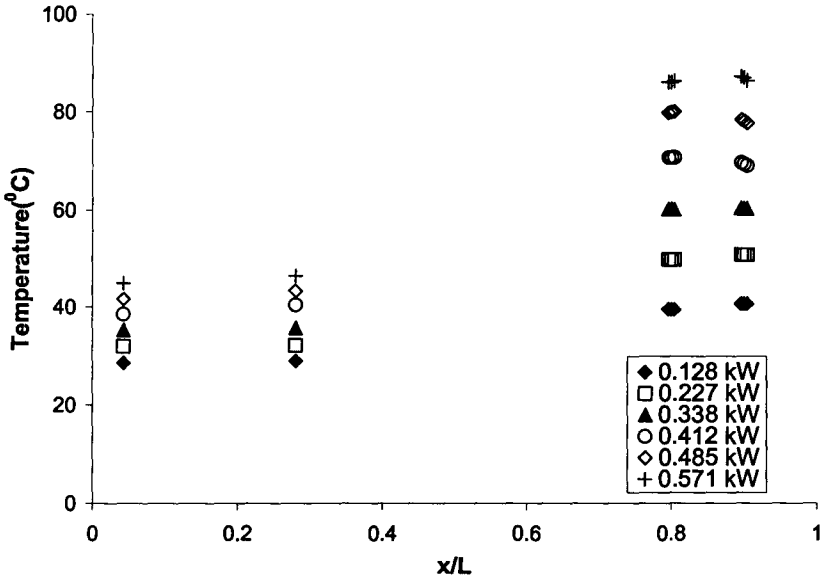

Figure 4.10 Wall temperature distribution at 2000 RPM for the heat pipe with 14.64 gm of water.

largest temperature difference across the condenser was 2^0 C as well. The variation in the temperature measured along the evaporator, and across the condenser was approximately 4% and 6%, of the difference in the average temperature at the evaporator and the condenser.

The change in the heat transfer rate through the heat pipe with 14.64 gm of water with the temperature difference between the average evaporator and condenser wall temperature is shown in Figure 4.11. It is clear that for a given temperature drop the heat transfer rate of the heat pipe increased by 25% as the rotational speed was increased from 2000 to 4000 RPM. The change in the thermal resistance of this heat pipe with heat transfer rate is shown in Figure 4.12. The thermal resistance of the heat pipe was non-linear, but in this case the thermal resistance increased with heat transfer rate for rotational speeds of 3000 and 4000 RPM. At the rotational speed of 2000 RPM, the thermal resistance decreases with heat transfer rate. The thermal resistance is approximately constant for heat transfer rates over 0.4 kW in all cases. The thermal resistance decreased by 25% at the higher heat transfer rates when the rotational speed increases from 2000 to 4000 RPM.

The change in the thermal resistance with heat transfer rate for 2^0 tapered heat pipes with 9.2 gm and 18.2 gm of water (Song et al., 2004) is shown in Figures 4.13 and 4.14 respectively. In this case the working fluid occupied approximately 9% and 18% of the pipe interior volume. The trends in the change in thermal resistance with heat transfer rate at different rotational speeds are not same as seen in Figures 4.12 to 4.14. The reason for the different trends in thermal resistance for the water heat pipes is not known at this

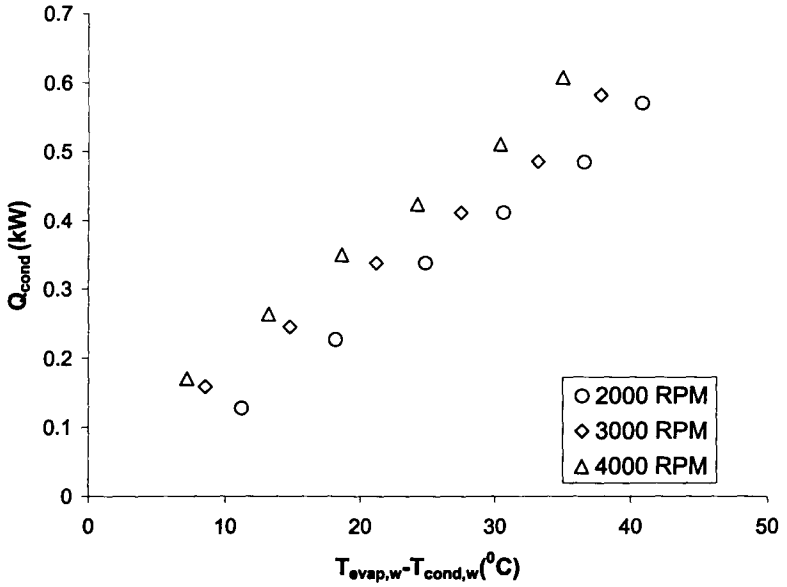

Figure 4.11 Change in the heat transfer with temperature difference for the heat pipe with 14.64 gm of water.

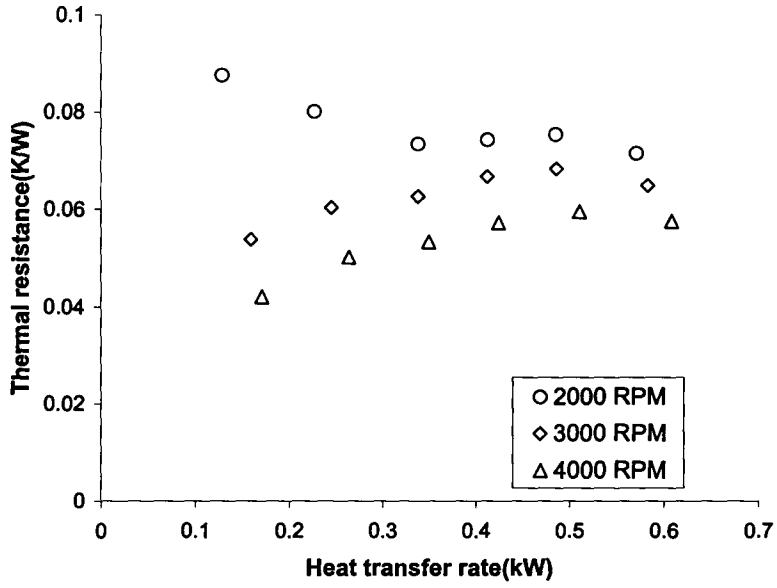

Figure 4.12 Change in the thermal resistance with heat transfer rate for the heat pipe with 14.64 gm of water.

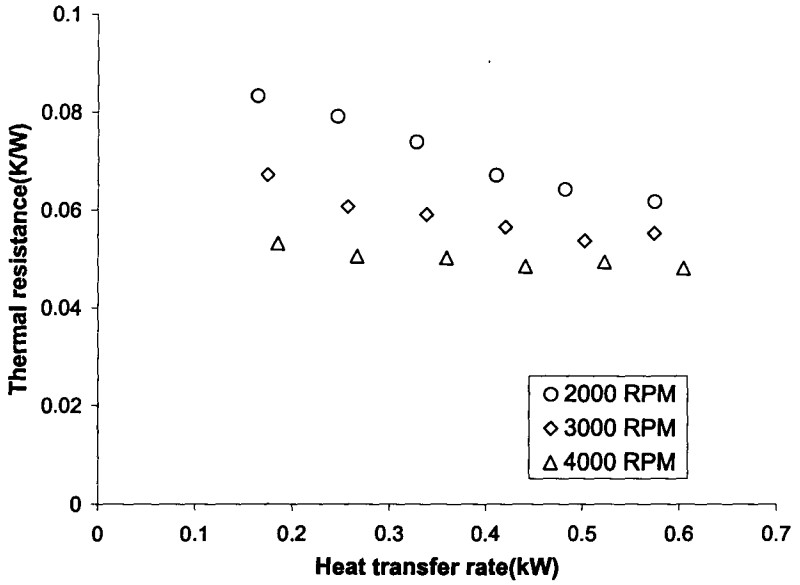

Figure 4.13 Change in the thermal resistance with heat transfer rate for the heat pipe with 9.2 gm of water (Song et al, 2004).

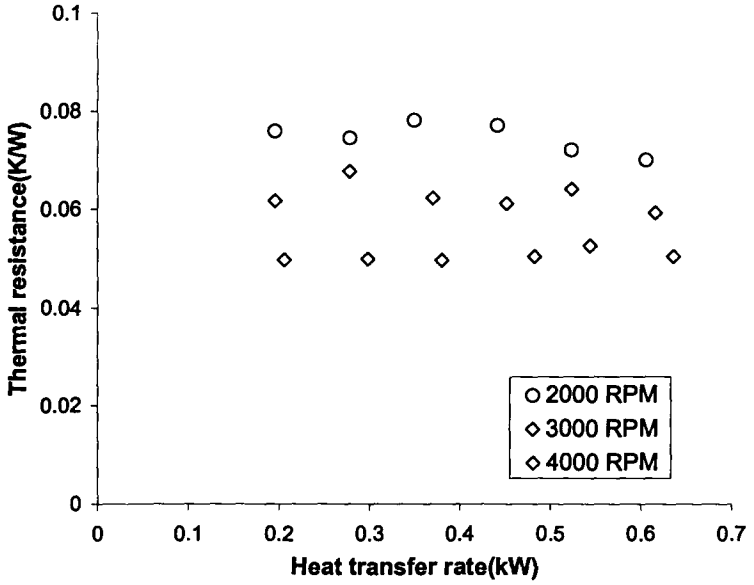

Figure 4.14 Change in the thermal resistance with heat transfer rate for the heat pipe with 18.2 gm of water (Song et al, 2004).

stage.

A comparison of the change in the thermal resistance with heat transfer rate for the heat pipes with water, methanol and ethanol as the working fluids is shown in Figure 4.15. The thermal resistances of heat pipes with ethanol and methanol as the working fluid were 50% to 80% larger than the heat pipe with water as the working fluid and thus, the heat pipe with water performed better as expected. In all cases, the change in thermal resistance with heat transfer rate was non linear. The large difference in the thermal resistance with speed for the ethanol heat pipe is apparent. The change in the thermal resistance with speed for the heat pipes is shown in Figure 4.16. The thermal resistance in this figure is the average of the thermal resistance for heat transfer rates above 0.4 kW. The thermal resistance of the heat pipe with methanol is lower than the heat pipe with ethanol at the low speeds. The thermal resistance of the heat pipe with ethanol changes more rapidly with speed though and it appears that it may have lower thermal resistance for heat pipes with speeds over 4000 RPM. The change in the thermal resistance for heat transfer rates greater than 0.4 kW with speed in the heat pipes can be approximated by $R_{th} = 6.6(N)^{-0.48}$ for the ethanol heat pipe, $R_{th} = 0.4(N)^{-0.16}$ for the methanol heat pipe and $R_{th} = 0.9(N)^{-0.34}$ for the water heat pipe.

4.1.1 Comparison to model predictions

The heat transfer measurements for the heat pipes were compared to the predictions of the model proposed by Song et al. (2003). The model results were computed for the case where a uniform wall temperature boundary condition was used

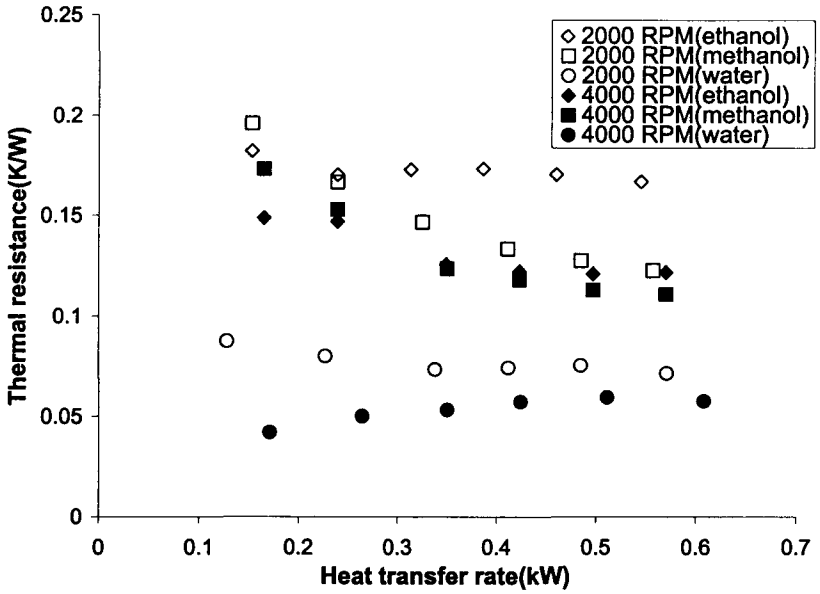

Figure 4.15 Change in the thermal resistance with heat transfer rate for the heat pipes with 11.73 gm of ethanol, 11.6 gm of methanol and 14.64 gm of water.

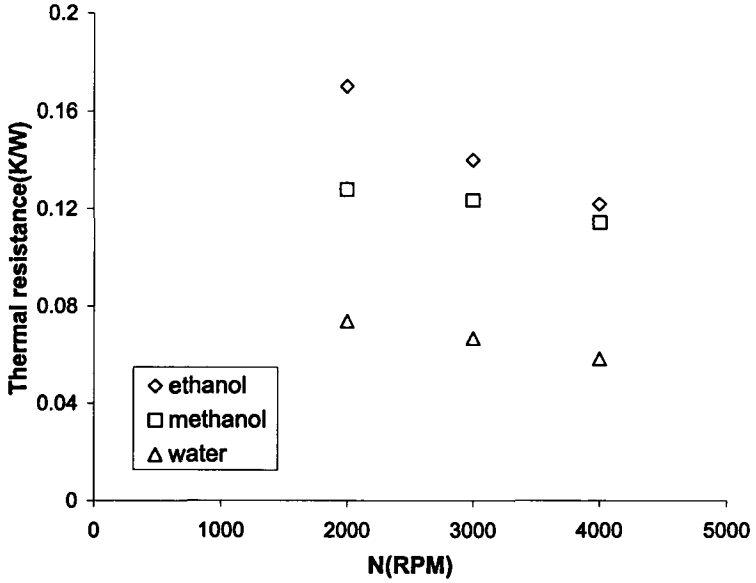

Figure 4.16 Change in the averaged thermal resistance for heat transfer rates above 0.4 kW with rotational speed for the heat pipes with 11.73 gm of ethanol, 11.6 gm of methanol and 14.64 gm of water.

for the evaporator and the condenser sections. The average of the temperature on the evaporator wall and the average of the temperatures on the two sides of the condenser water jacket were used as the boundary conditions. A comparison between the total thermal resistance predicted using the model of Song et al. (2003) and the measurements for the heat pipe with 11.6 gm of methanol and 11.73 gm of ethanol is shown in Figure 4.17 and 4.18 respectively. The predicted trends in the change in thermal resistance with heat transfer rate are not in agreement with the measurements. The model over predicted the thermal resistance by approximately 50% to 80%. The predicted change in the average thermal resistance with rotational speed for the ethanol and methanol heat pipes is shown in Figure 4.19. The model predicts the decrease in thermal resistance with increase in rotational speed. The predictions show that the thermal resistance of the methanol heat pipe is always lower than the ethanol heat pipe by approximately 30% at all low rotational speeds. However, the measurements show that rotational speed has a more profound effect on the thermal resistance of the ethanol heat pipe than the methanol heat pipe as seen in Figure 4.19. The disagreement between the model predictions and measurements is quite clear from Figure 4.19.

The contribution of the condenser and the evaporator thermal resistances to the overall thermal resistance for the methanol and ethanol heat pipes is shown in Figures 4.20 and 4.21 respectively. It is clear that the prediction for the thermal resistance of the condenser is higher than the thermal resistance of the evaporator. In particular, the condenser thermal resistance is larger than the evaporator by approximately 40% to 70% and 20% to 50% for the methanol and ethanol heat pipes respectively. The thermal

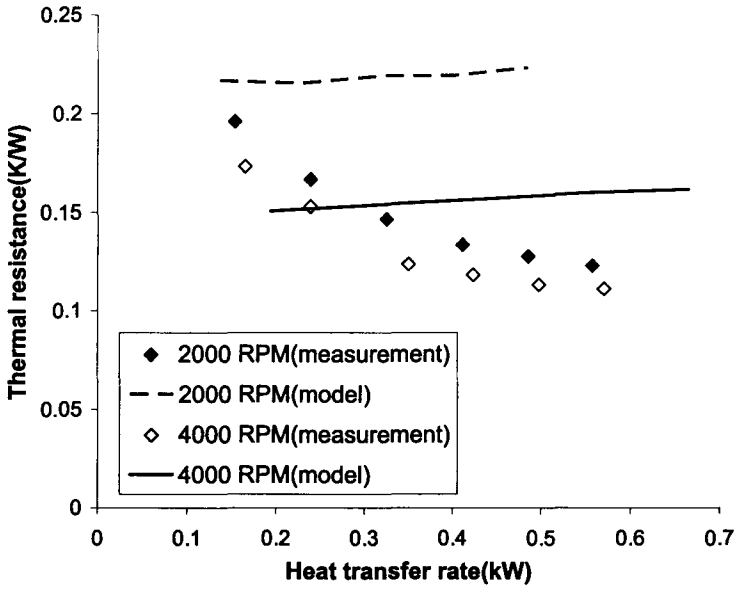

Figure 4.17 Comparison between the experimental and model predicted (Song et al., 2003) thermal resistance for the heat pipe with 11.6 gm of methanol.

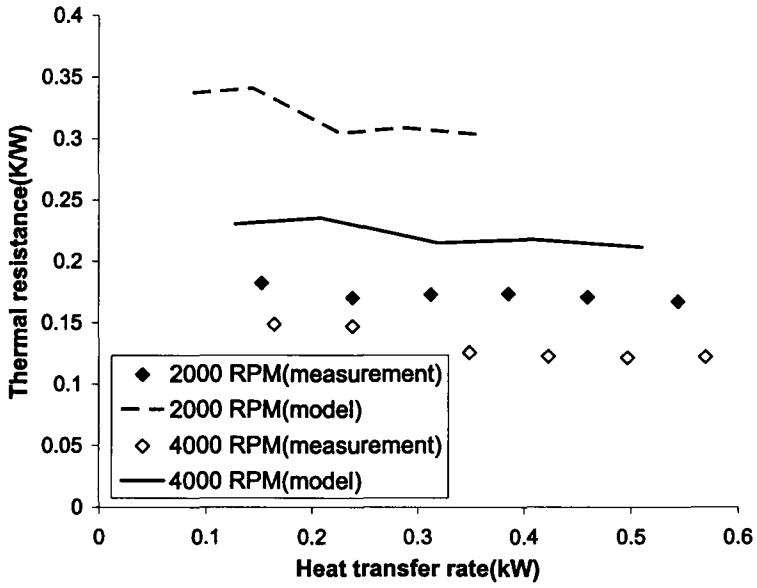

Figure 4.18 Comparison between the experimental and model predicted (Song et al., 2003) thermal resistance for the heat pipe with 11.73 gm of ethanol.

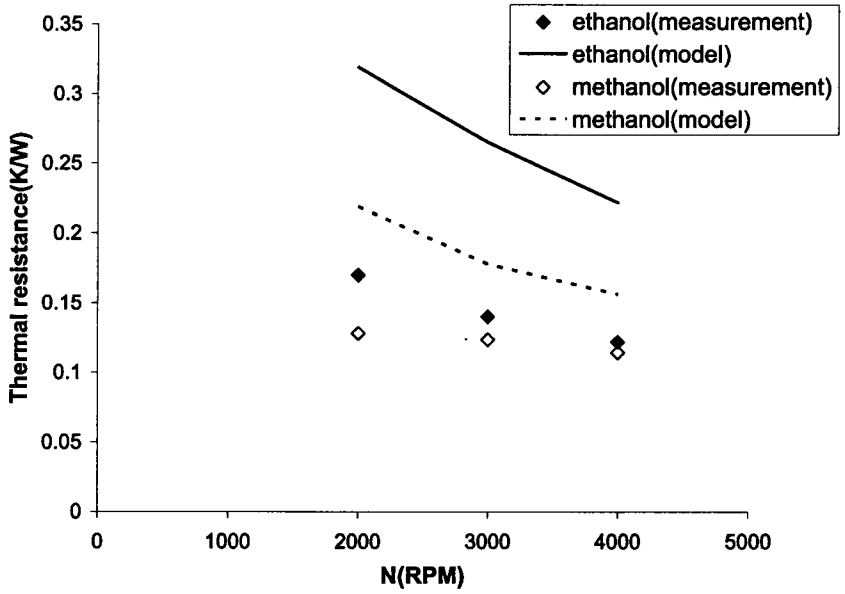

Figure 4.19 Comparison between the model predicted and measured change in the average thermal resistance with rotational speed for the heat pipes with 11.6 gm of methanol and 11.73 gm of ethanol.

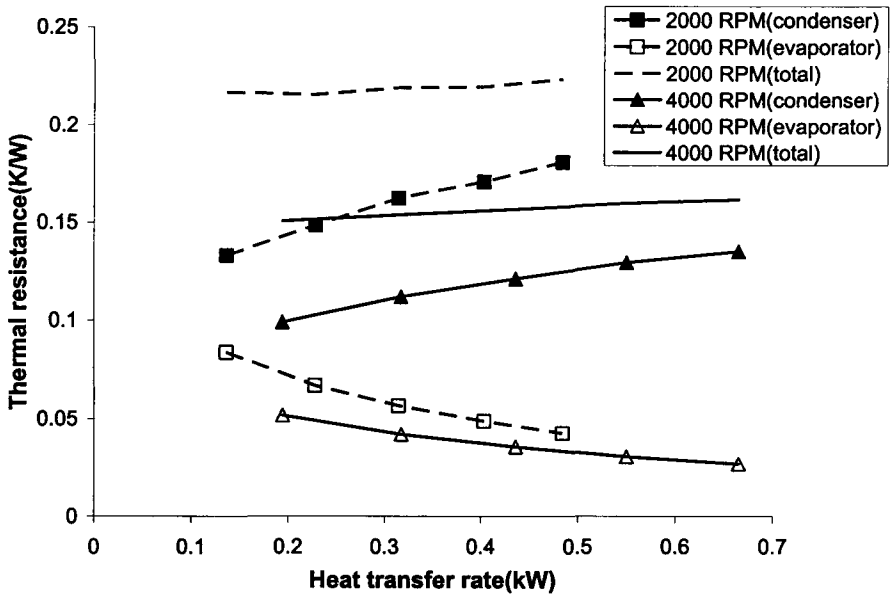

Figure 4.20 Contribution of the predicted condenser and the evaporator thermal resistance to the overall thermal resistance for the heat pipe with 11.6 gm of methanol.

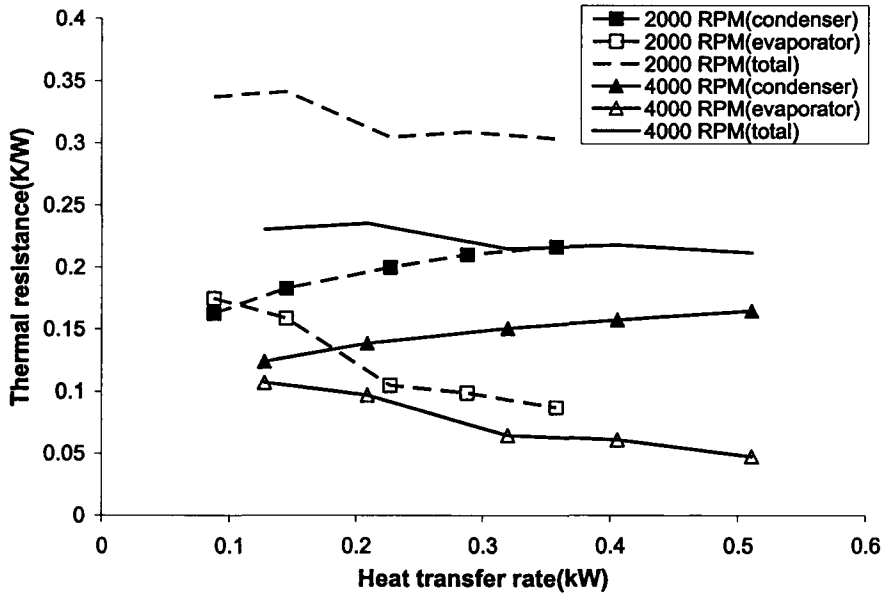

Figure 4.21 Contribution of the predicted condenser and the evaporator thermal resistance to the overall thermal resistance for the heat pipe with 11.73 gm of ethanol.

resistance of the condenser increases with the heat transfer rate while the overall thermal resistance decreases. This seems to be due to way the evaporator thermal resistance changes with the heat transfer rate.

The condenser is the dominant thermal resistance for the methanol and ethanol heat pipes, and it seems that the Nusselt-type film condensation model based on an annular flow regime may not be applicable for these heat pipes under the range of operating conditions investigated. Further work needs to be done to resolve the large discrepancy between the model predictions and the measurements.

4.2 Effect of fluid loading

The effect of fluid loading on the performance of rotating heat pipe was examined experimentally for heat pipes with an internal condenser taper of 1^0 that had lower fluid loadings of 4.88 gm and 5.5 gm of distilled water, respectively. The temperature distribution on the wall of the heat pipe with 4.88 gm of water measured with the IR sensor at rotational speed of 3000 RPM is shown in Figure 4.22. The wall temperature distributions for this heat pipe differed from the other heat pipes. In particular, the evaporator wall temperatures were high even at the very low heat loads. The evaporator wall temperature varied from 5 ^{0}C to 11 ^{0}C that was higher than the temperature variation for the other heat pipes. It was found, however, that the evaporator wall temperature was stable without any oscillation. In the tests, the maximum power removed from the condenser was 0.216 kW, so much of the heat transfer for this heat pipe could be due to bearing heating.

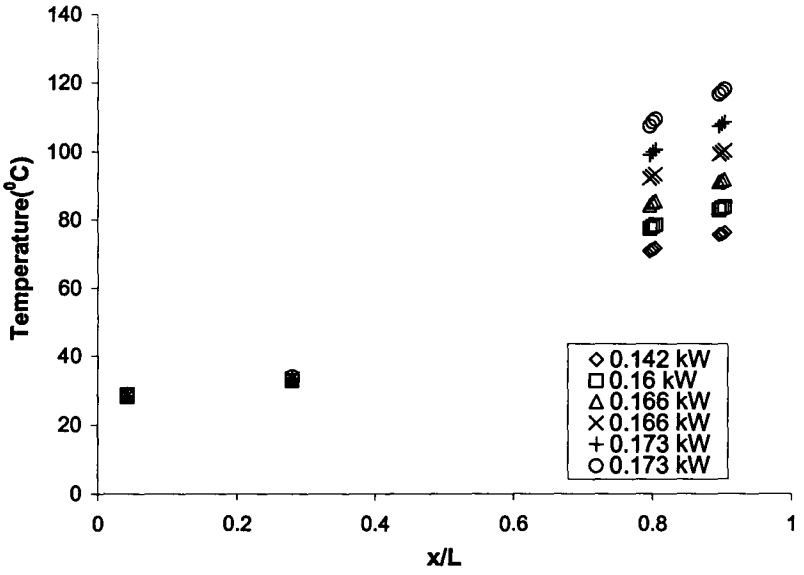

Figure 4.22 Wall temperature distribution at 3000 RPM for the heat pipe with 4.88 gm of water.

The change in the condenser heat transfer rate with the temperature drop for the heat pipe with 4.88 gm of water is shown in Figure 4.23. It is clear that the operation of this heat pipe is different from the other heat pipes. In particular, the heat transfer rate did not increase significantly when the temperature difference across the heat pipe increased. The change in the thermal resistance with heat transfer rate is shown in Figure 4.24. The thermal resistance increases rapidly with heat transfer rate over the range studied here and the thermal resistance was much higher than the other cases. It is thought that this heat pipe had insufficient working fluid to cover the entire inner wall of the heat pipe particularly in the evaporator section. As a result, the heat transfer process in the evaporator could be different. The evaporator wall temperature did not appear to oscillate over time suggesting their was some heat transfer process. The operation of this heat pipe is not similar to the two-phase heat transfer cycle in other heat pipes.

The change in the heat transfer from the condenser with the temperature difference for the heat pipe with 5.5 gm of water is shown in Figure 4.25. The heat transfer rate increased by approximately 50% for a given temperature drop when the rotational speed was increased from 2000 to 4000 RPM for this heat pipe. The change in the thermal resistance of the heat pipe with heat transfer rate at different rotational speeds is shown in Figure 4.26. The thermal resistance of the heat pipe increases with heat transfer rate at the higher rotational speed, similar to the heat pipe with 14.64 gm of water. The thermal resistance becomes approximately constant when the heat transfer rate increases above 0.4 kW. The thermal resistance in this range decreases by 40% when the speed increases from 2000 to 4000 RPM.

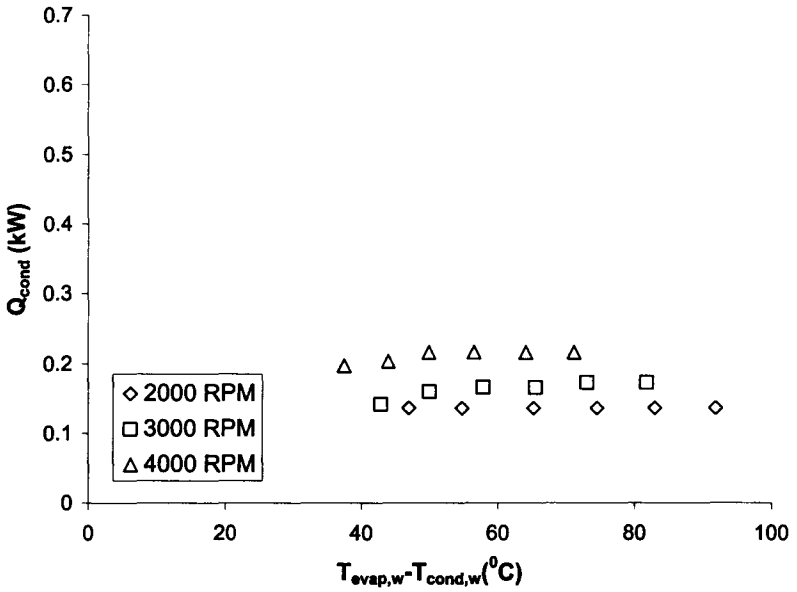

Figure 4.23 Change in the heat transfer with temperature difference for the heat pipe with 4.88 gm of water.

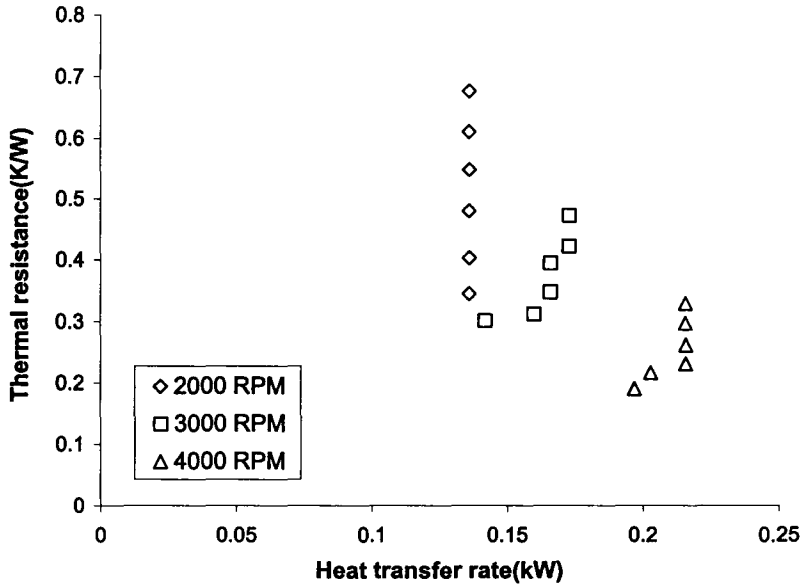

Figure 4.24 Change in the thermal resistance with heat transfer rate for the heat pipe with 4.88 gm of water.

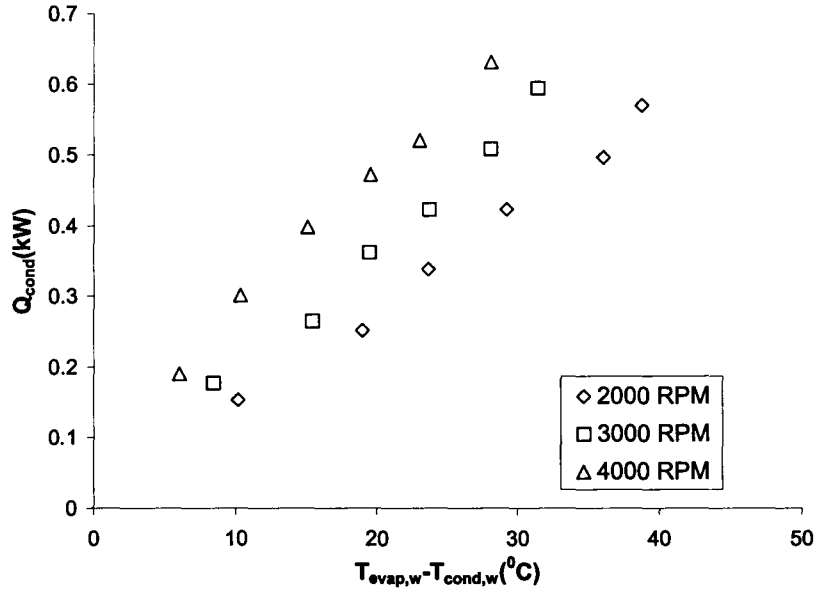

Figure 4.25 Change in the heat transfer with temperature difference for the heat pipe with 5.5 gm of water.

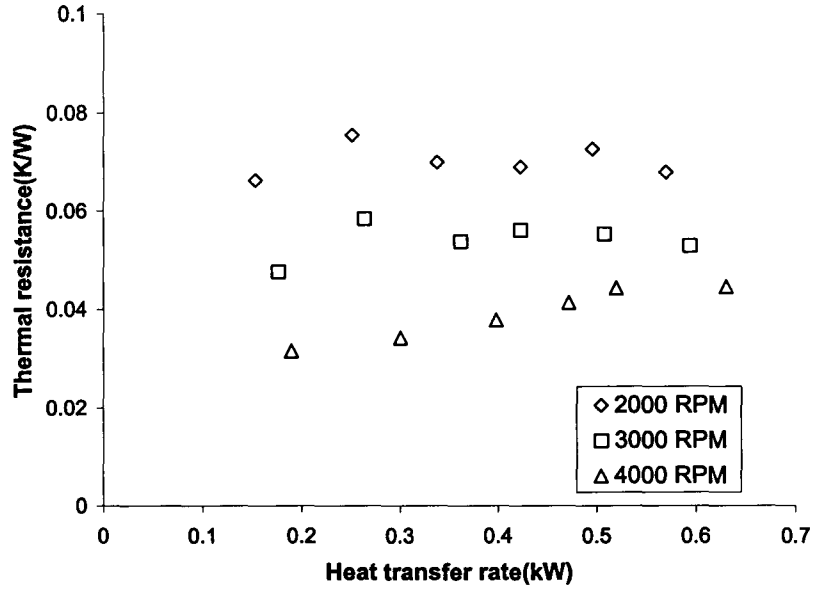

Figure 4.26 Change in the thermal resistance with heat transfer rate for the heat pipe with 5.5 gm of water.

A comparison of the thermal resistance between the heat pipes with 5.5 gm and 14.64 gm of water is shown in Figure 4.27. The thermal resistance of the heat pipe with 5.5 gm of water is approximately 20% lower than 14.64 gm. The difference in thermal resistance is large at the higher rotational speeds. In particular, the change in the thermal resistance with speed is shown in Figure 4.28. Here, again the thermal resistance shown is the average of the thermal resistance for heat transfer rates above 0.4 kW. The thermal resistance decreases with speed for both the heat pipes but it decreases more rapidly for the heat pipe with 5.5 gm of water.

4.2.1 Comparison with model predictions

A comparison of the predictions of the thermal resistance from the model of Song et al. (2003) and the measurements for the heat pipe with 5.5 gm and 14.64 gm of water is shown in Figure 4.29 and 4.30 respectively. The trends in the change in thermal resistance with heat transfer rate as predicted by the model are not consistent with the measurements. However, the model does predict that the thermal resistance is approximately constant at higher heat transfer rates. The agreement between the model prediction and the measurements is better at the higher heat transfer rates than at the lower heat transfer rates. The predicted change in the average thermal resistance with rotational speed for the heat pipes with 5.5 gm and 14.64 gm of water is shown in Figure 4.31. The model predicts an increase in thermal resistance with the increase in fluid loading which is consistent with the measurements. From Figure 4.31, it is clear that the agreement between the model predictions and measurements is good, with the model

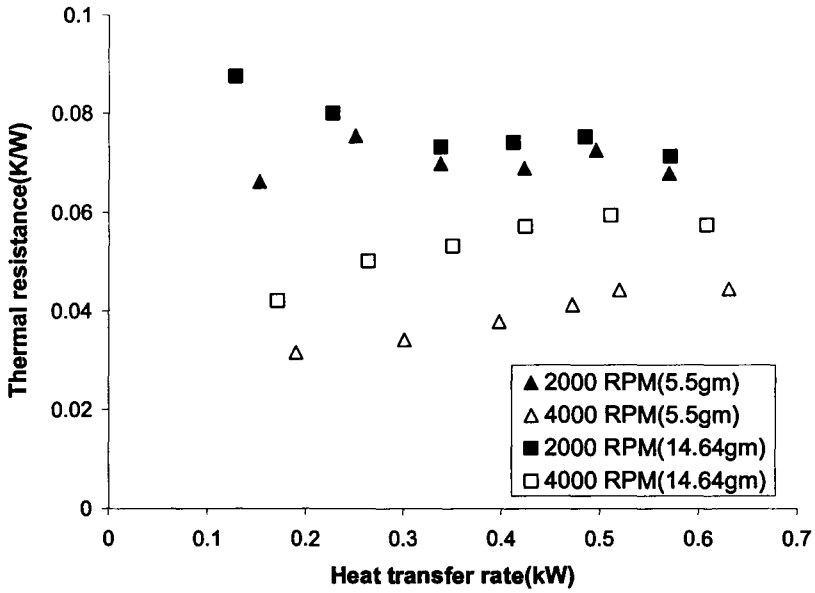

Figure 4.27 Change in the thermal resistance with heat transfer rate for the heat pipes with 5.5 gm and 14.64 gm of water.

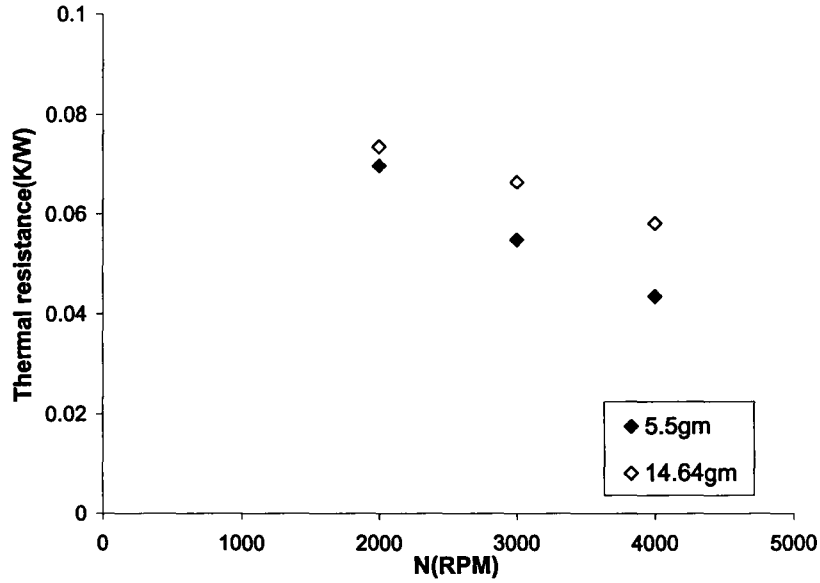

Figure 4.28 Change in the averaged thermal resistance for heat transfer rates above 0.4 kW with rotational speed for the heat pipes with 5.5 gm and 14.64 gm of water.

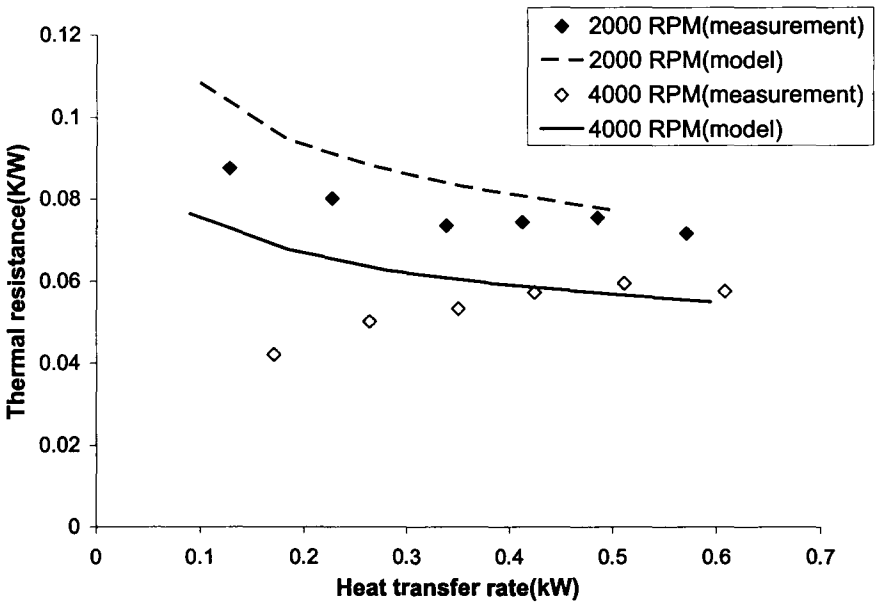

Figure 4.29 Comparison between the experimental and model predicted (Song et al., 2003) thermal resistance for the heat pipe with 5.5 gm of water.

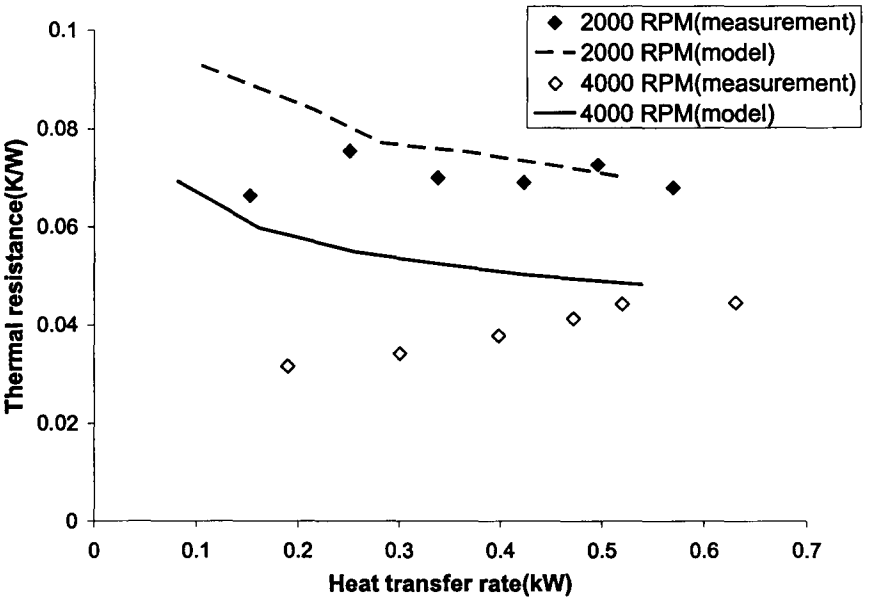

Figure 4.30 Comparison between the experimental and model predicted (Song et al., 2003) thermal resistance for the heat pipe with 14.64 gm of water.

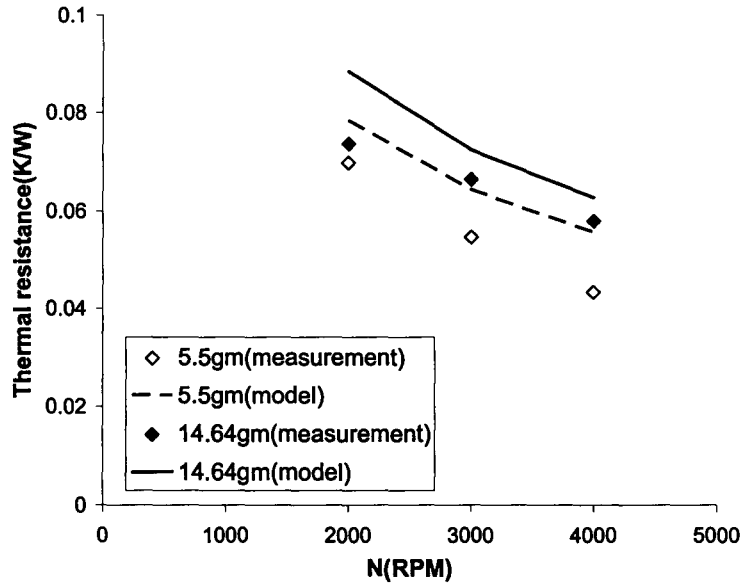

Figure 4.31 Comparison between the model predicted and measured change in the average thermal resistance with rotational speed for the heat pipes with 5.5 gm and 14.64 gm of water.

over predicting the thermal resistance by 10% to 20%.

The contribution of the condenser and the evaporator resistances to the overall thermal resistance for the heat pipes with 5.5 gm and 14.64 gm of water are shown in Figure 4.32 and 4.33 respectively. In both cases, the predicted condenser thermal resistance increases with heat transfer rate whereas the overall thermal resistance decreases. It is clear that the predicted thermal resistance of the condenser increases when the fluid loading is increased. The predicted condenser liquid film resistance increases approximately 50% when the fluid loading increases from 5.5 gm to 14.64 gm because of the excess liquid in the condenser section at the higher fluid loading.

The effect of the fluid loading on the thermal resistance of the heat pipe can be further understood by comparing the prediction of the liquid film distribution in the heat pipe. The liquid film thickness distribution from the condenser to the evaporator section for the heat pipes with 5.5 gm and 14.64 gm of water at rotational speed of 3000 RPM is shown in Figure 4.34. The centrifugal driving force $\rho_l \omega^2 r \sin\alpha$ due to the taper in the condenser section results in thin liquid film in the condenser, with the excess liquid pooling in the cylindrical adiabatic and evaporator sections. When the fluid loading is increased from 5.5 gm to 14.64 gm, the film thickness in the condenser section increases as more liquid pools in the adiabatic and the evaporator sections and eventually the liquid starts to pool in the condenser. The predicted thermal resistance of the evaporator is larger than the condenser because of the relatively thicker film in the evaporator than in the condenser section.

The evaporator liquid film resistance decreases with the increase in rotational

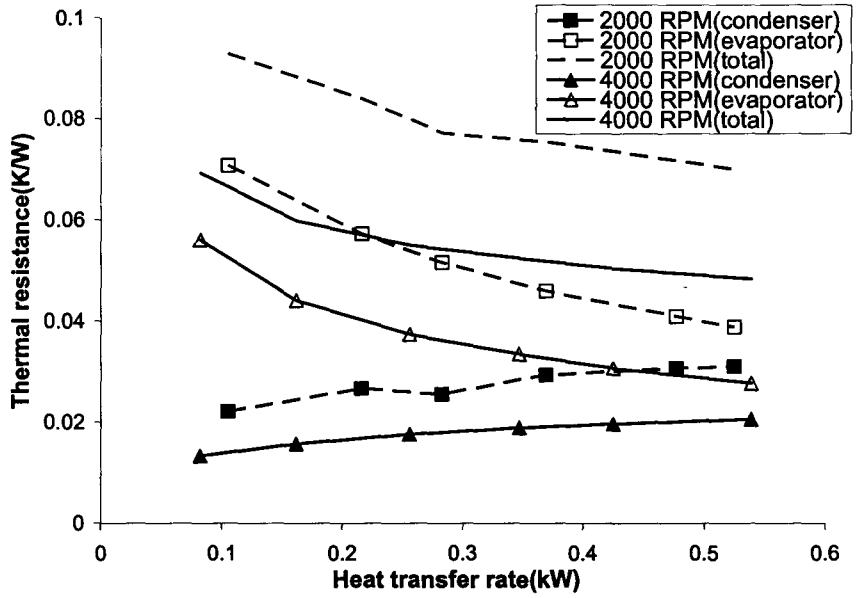

Figure 4.32 Contribution of the predicted condenser and the evaporator thermal resistance to the overall thermal resistance for the heat pipe with 5.5 gm of water.

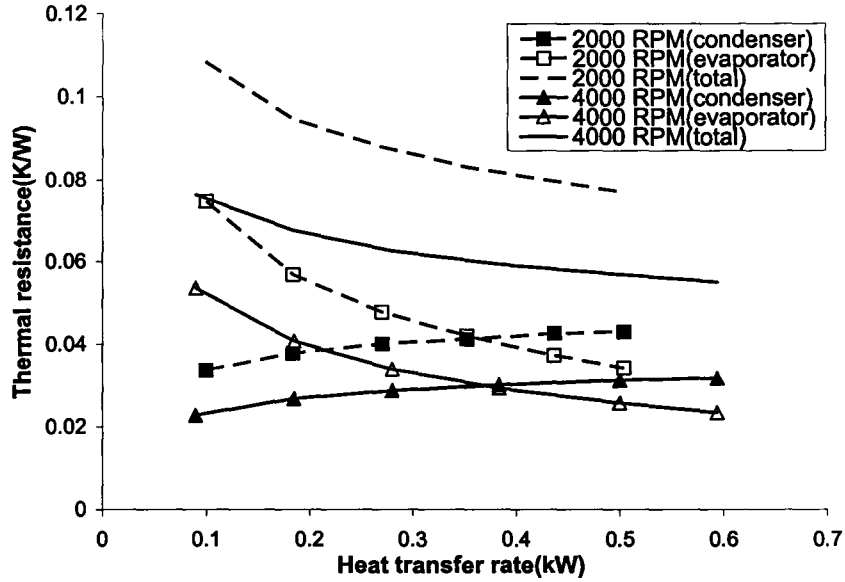

Figure 4.33 Contribution of the predicted condenser and the evaporator thermal resistance to the overall thermal resistance for the heat pipe with 14.64 gm of water.

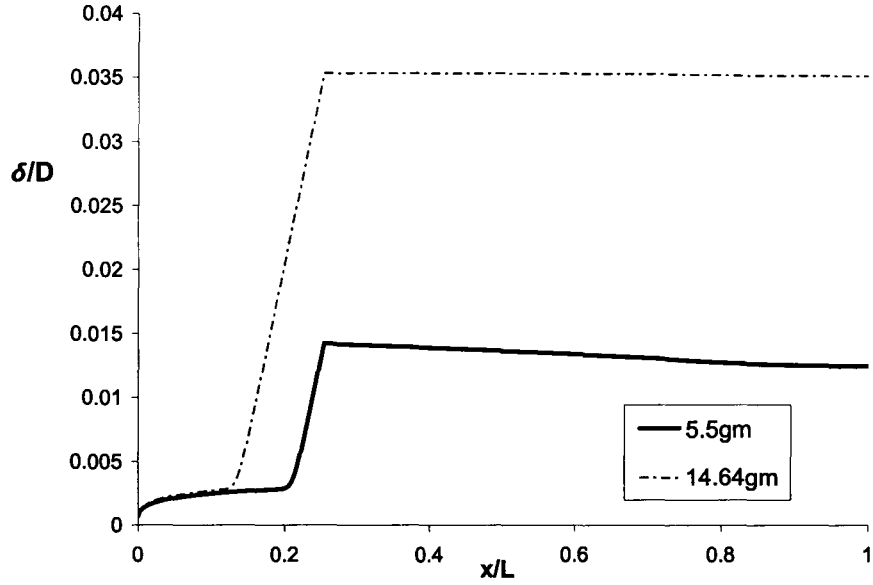

Figure 4.34 Comparison of liquid film thickness distribution for the heat pipes with 5.5 gm and 14.64 gm of water predicted using Song et al.'s (2003) model for a speed of 3000 RPM.

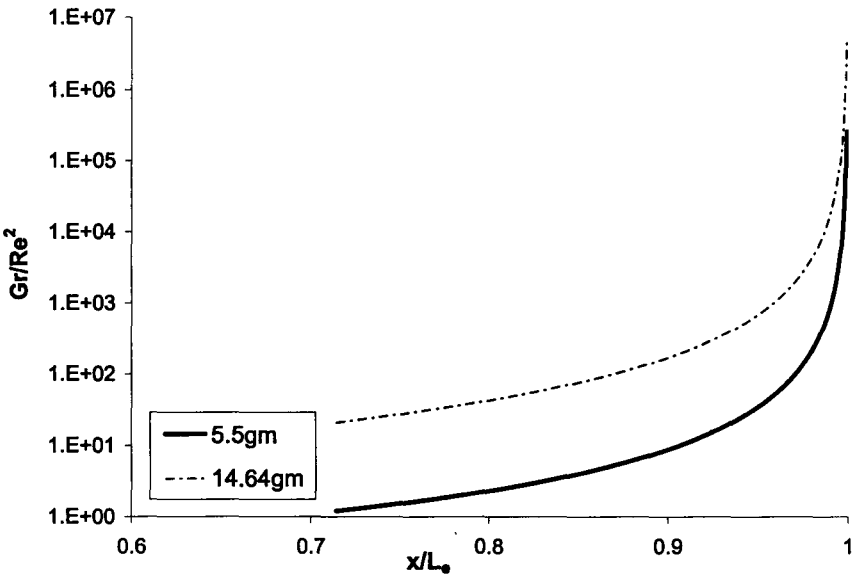

Figure 4.35 Variation of Gr/Re^2 in the evaporator for the heat pipes with 5.5 gm and 14.64 gm of water predicted using Song et al.'s (2003) model for a speed of 3000 RPM.

speed because of the enhancement of natural convection. The predicted evaporator thermal resistance decreases by approximately 6% when the fluid loading increases from 5.5 gm to 14.64 gm. When the fluid loading is increased there is more liquid in the evaporator section, however, this is offset by the enhancement of the natural convection in the thicker liquid film. The relative importance of natural convection in the evaporator can be estimated from the magnitude of the local value of Gr/Re^2 shown in Figure 4.35. The effect of natural convection is more significant for the 14.64 gm water heat pipe than the 5.5 gm water heat pipe, causing a lower predicted evaporator film thermal resistance for the 14.64 gm water heat pipe.

The change in the operation of the heat pipe with 4.88 gm of water is thought to be due to insufficient amount of working fluid in the heat pipe. This can be further examined by computing the minimum mass of the fluid that must be charged into the heat pipe to ensure that the entire evaporator surface is covered with liquid. The fluid loading ratio predicted from Song et al. (2003) model is given as

$$\gamma = \frac{actual\ mass\ of\ fluid}{\min imum\ mass\ of\ fluid} \tag{4.1}$$

The variation in the fluid loading ratio with the predicted heat transfer rate from the model proposed by Song et al. (2003) for the 4.88 gm water heat pipe at rotational speeds of 2000 and 3000 RPM is shown in Figure 4.36. For the heat transfer rates examined here, the fluid loading ratio is below 1. Thus, the model predicts that the heat pipe is under loaded. The heat pipe may have operated at heat fluxes below the heat fluxes encountered in the tests. The results also suggest that in the typical operating range for

this heat pipe, the ratio is approximately constant so that the model suggests the heat pipe will either function or not function.

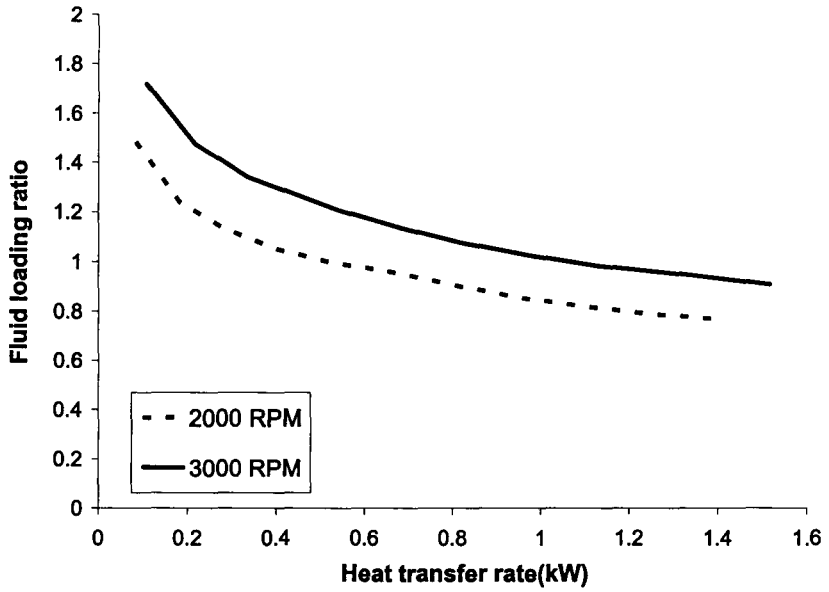

Figure 4.36 Change of fluid loading ratio with heat transfer rate predicted using the model proposed by Song et al. (2003) for the heat pipe with 4.88 gm of water.

Chapter 5 Conclusions

An experimental investigation was performed to characterize the effect of working fluid and fluid loading on the performance of high speed rotating heat pipes. The experiments were performed for rotating heat pipes with 1^0 tapered condenser section at rotational speeds of 2000, 3000 and 4000 RPM. The effect of working fluid was characterized by testing three heat pipes with 11.6 gm of methanol, 11.73 gm of ethanol and 14.64 gm of water. These working fluids occupied approximately 19% of the pipe inner volume. In all cases, it was found that the thermal resistance of the heat pipe change with heat flux for low heat fluxes. For the heat pipes using methanol and ethanol, the thermal resistance decreased with heat flux before approaching a constant value. For the heat pipe with water the thermal resistance differed at low and high speeds. The effective thermal resistance of the methanol and ethanol heat pipes were 50% to 80% larger than the water heat pipe. The performance of the methanol heat pipe was found to be better than the ethanol heat pipe particularly at the low rotational speeds. The thermal resistance decreased more rapidly with speed for the heat pipe with ethanol and may be lower than the heat pipe with methanol at higher speeds.

The effect of fluid loading was characterized by testing three heat pipes with fluid charges of 4.88 gm, 5.5 gm and 14.64 gm of water. The heat transfer performance of the heat pipe with 4.88 gm of water was significantly different than the other two heat pipes. The thermal resistance of this heat pipe increased dramatically with heat transfer at low heat fluxes. When the fluid loading was increased to 5.5 gm, the heat pipe operated

similar to the other heat pipes. When the fluid loading was increased from 5.5 gm to 14.64 gm the thermal resistance of the heat pipe increased by 5% to 25%. The thermal resistance decreased more rapidly with speed for the heat pipe with 5.5 gm of water.

The predictions from the model of Song et al. (2003) were in reasonably good agreement with the test results for the heat pipes with 5.5 gm and 14.64 gm of water. In particular, the model correctly predicts the general trends in the heat transfer performance with rotational speed and fluid loading. For the heat pipe with 4.88 gm of water, the fluid loading ratio predicted by the model of Song et al. (2003) indicated that this heat pipe failed throughout the range of operating conditions because it did not have fluid charge to completely wet the evaporator section. The predictions of the model were not in agreement for the case of heat pipes with methanol and ethanol as working fluids.

Chapter 6 Recommendations

In the future, it is recommended that the measurements should be extended to actually determine the evaporator and the condenser film thermal resistances in order to identify the major source of thermal resistance for the heat pipe. This would also shed light on to the type of heat transfer mechanism taking place in the evaporator. The measurements can be done by embedding temperature measuring sensor on the inner wall of the heat pipe at both the condenser and evaporator sections, and also by having it in the vapor core of the heat pipe. It would be also useful to test glass heat pipes where flow regime can be visualized in order to correctly know the type of flow regime inside the heat pipe.

Bibliography

Anderson, J.T., and Saunders, O.A., 1953, "Convection from an Isolated Heated Horizontal Cylinder Rotating about its Axis", Proc.R.Soc.London Ser.A, 217, pp. 555-562.

Ballback, L.J., 1969, "The Operation of a Rotating Wickless Heat Pipe", M.Sc. Thesis, U.S. Naval Post-Graduate School, Monterey California.

Chen, J., and Tu, C., 1987, "Condenser Heat Transfer in Inclined Rotating Heat Pipe", Proceedings of the 6th International Heat Pipe Conference, Grenoble, France.

Coleman, H.W., and Steele, W.G.JR., 1999, "Experimental and Uncertainty Analysis for Engineers", John Wiley & Sons, Inc., New York.

Daley, T.J., 1970, "The Experimental Design and Operation of a Rotating Wickless Heat Pipe", M.Sc. Thesis, U.S. Naval Post-Graduate School, Monterey California.

Daniels, T.C., and Al-Baharnah, N.S., 1978, "Temperature and Heat Load Distribution in Rotating Heat Pipes", Proceedings of the 3rd International Heat Pipe Conference, Palo Alto, California, pp. 202-207.

Daniels, T.C., and Al-Jumaily, F.K., 1975, "Investigations of the Factors Affecting the Performance of a Rotating Heat Pipe", International Journal of Heat and Mass Transfer, Vol. 18, pp. 961-973.

Daniels, T.C., and Williams, R.J., 1978, "Experimental Temperature Distribution and Heat Load Characteristics of Rotating Heat Pipes", International Journal of Heat and

Mass Transfer, Vol. 21, pp. 193-201.

Fries, P., 1970, "Experimentelle Ergebnisse Mit Einem Dochtfreien Zentrifugal-Warmerohr", International Journal of Heat and Mass Transfer, Vol. 13, pp. 1503-1504.

Gao, N., 2000, "Heat Transfer Enhancement in Impinging Round Jets", M.A.Sc Thesis, McMaster University, Hamilton.

Gray, V.H., 1969, "The Rotating Heat Pipe- A Wickless Hollow Shaft for Transferring High Heat Fluxes", ASME No.69-HT-19.

Groll, M., Krahling, H., and Munzel, W.D., 1978, "Heat Pipes for Cooling an Electric Motor", Proceedings of the 3rd International Heat Pipe Conference, Palo Alto, California, pp. 354-359.

Judd, R.L., and Merte Jr., H, 1972, "Evaluation of Nucleate Boiling Heat Flux Predictions at Varying Levels of Subcooling and Acceleration", International Journal of Heat and Mass Transfer, Vol. 15, pp. 1075-1096.

Katsuta, M., Kigami, N., Nagata, K., Sotani, J., and Koizumi, T., 1984, "Performance and Characteristics of Rotating Heat Pipes", Proceedings of the 5th International Heat Pipe Conference, Tsukuba, Tokyo, Japan, pp. 106-112.

Leland, Q.H., Ponnappan, R., and Brown, J.R., 1999, "Compatibility Test and Residual Gas Analysis on 4130 Steel and Methanol Thermosyphons", Journal of Thermophysics and Heat Transfer, Vol. 13, pp. 146-152.

Li, H.M., Liu, C.Y., and Damodaran, M., 1993, "Analytical Study of the Flow and Heat Transfer in a Rotating Heat Pipe", Heat Recovery Systems & CHP, Vol.13, pp. 115-122.

Lin, S., Sefiane, K., and Christy, J.R.E., 2002, "Prospects of Confined Flow Boiling in

Thermal Management of Microsystems", Journal of Applied Thermal Engineering, Vol. 22, pp. 825-837.

Ling, J., Cao, Y., and Lopez, A.P., 2001, "Experimental Investigations of Radially Rotating Miniature High-Temperature Heat Pipes", Journal of Heat Transfer, Vol. 123, pp. 113-119.

Maezawa, S., Suzuki, Y., and Tsuchida, A., 1981, "Heat Transfer Characteristics of Disk-Shaped Rotating, Wickless Heat Pipe", Proceedings of the 4th International Heat Pipe Conference, London, UK, pp. 725-733.

Marto, P.J., 1973, "Laminar Film Condensation on the Inside of Slender, Rotating Truncated Cones", Journal of Heat Transfer, Vol. 95, pp. 270-272.

Marto, P.J., 1976, "Performance Characteristics of Rotating, Wickless Heat Pipes", Proceedings of the 2nd International Heat Pipe Conference, Bologna, Italy, pp. 281-291.

Marto, P.J., 1984, "Rotating Heat Pipes", Heat and Mass Transfer in Rotating Machinery, Metzger, D.E., and Afgan, N.H., (Editors), Hemisphere Publishing Co., Washington, DC, pp. 600-632.

Marto, P.J., and Wagenseil, L.L., 1979, "Augmenting the Condenser-Heat Transfer Performance of Rotating Heat Pipes", AIAA Journal, Vol. 17, No. 6, pp. 647-652.

Marto, R., and Weigel, H., 1981, "The Development of Economical Rotating Heat Pipes", Proceedings of the Fourth International Heat Pipe Conference, London, UK, pp. 709-724.

Merte, H., and Clark, J.A., 1961, "Pool Boiling in an Accelerating System", Journal of Heat Transfer, Vol. 83, pp. 233-242.

Nakayama, W., Ohtsuka, Y., Itoh, H., and Yoshikawa, T., 1984, "Optimum Charge of Working Fluid in Horizontal Rotating Heat Pipes", Heat and Mass Transfer in Rotating Machinery, Metzger, D.E., and Afgan, N.H., (Editors), Hemisphere Publishing Co., Washington, DC, pp. 633-644.

Oslejsek, O., and Polasek, F., 1976, "Cooling of Electrical Machines by Heat Pipes", Proceedings of the 2nd International Heat Pipe Conference, Bologna, Italy, pp. 503-514.

Peterson, G.P., 1994, "An Introduction to Heat Pipes", John Wiley & Sons, Inc., New York.

Ponnappan, R., and Leland, J.E, 1998, "Rotating Heat Pipe for High Speed Motor/Generator Cooling", SAE 981287, pp. 257-262.

Ponnappan, R., and Leland, J.E., 1994, "Rotating Heat Pipe for Cooling of Rotors in Advanced Generators", AIAA 94-2033, 6th AIAA/ASME Joint Thermophysics and Heat Transfer Conference, Colorado Springs, CO.

Ponnappan, R., and Leland, J.E., 1995, "High Speed Rotating Heat Pipe for Aircraft Applications", SAE 951437, Aerospace Atlantic Conference, Dayton, OH.

Ponnappan, R., He, Q, and Leland, J.E., 1997, "Test Results of a High Speed Rotating Heat Pipe", AIAA Paper No. 97-2543, 32nd Thermophysics Conference, Atlanta, GA.

Ponnappan, R., He, Q., and Leland, J.E., 1998, "Test Results of Water and Methanol High-Speed Rotating Heat Pipes", Journal of Thermophysics and Heat Transfer, Vol. 12, pp. 391-397.

Rudnev, V., Loveless, D., Cook, R., and Black, M., 2003, "Handbook of Induction Heating", Marcel Dekker, Inc., New York.

Salinas, D., and Marto, P.J., 1991, "Analysis of an Internally Finned Rotating Heat Pipe", Numerical Heat Transfer, Vol. 19, pp. 255-275.

Song, F., Ching, C.Y., and Ewing, D., 2002, "Fluid Flow and Heat Transfer Modeling in Rotating Heat Pipes", 12th International Heat Transfer Conference, Grenoble, France.

Song, F., Ewing, D., and Ching, C.Y., 2003, "Fluid Flow and Heat Transfer Model for High-Speed Rotating Heat Pipes", International Journal of Heat and Mass Transfer, Vol. 46, pp. 4393-4401.

Song, F., Ewing, D., & Ching C.Y., 2004, "Experimental Investigation on the Heat Transfer Characteristics of Axial Rotating Heat Pipes", International Journal of Heat and Mass Transfer, Vol. 47, pp. 4721-4731.

Sparrow, E.M., and Hartnett, J.P., 1961, "Condensation on a Rotating Cone", Journal of Heat Transfer, Vol. 83, Series C, pp. 101-102.

Streby, M.A., Ponnappan, R., Leland, J.E., and Beam, J.E., 1996, "Design and Testing of a High Speed Rotating Heat Pipe", Paper No. 96301, IECEC-96, Washington, D.C.

Tien, C.L., and Chung, K.S., 1979, "Entrainment Limits in Heat Pipes", AIAA J., Vol. 17, No.6, pp. 643-646.

Ulucakli, M.E., and Merte Jr., H, 1990, "Nucleate Boiling With High Gravity and Large Subcooling", Journal of Heat Transfer, Vol. 112, pp. 451-457.

Vasiliev, L.L., and Khrolenok, V.V., 1990, "Heat Transfer in Rotating Heat Pipes", Proceedings of the 7th International Heat Pipe Conference, Minsk, USSR, pp. 285-294.

Appendix

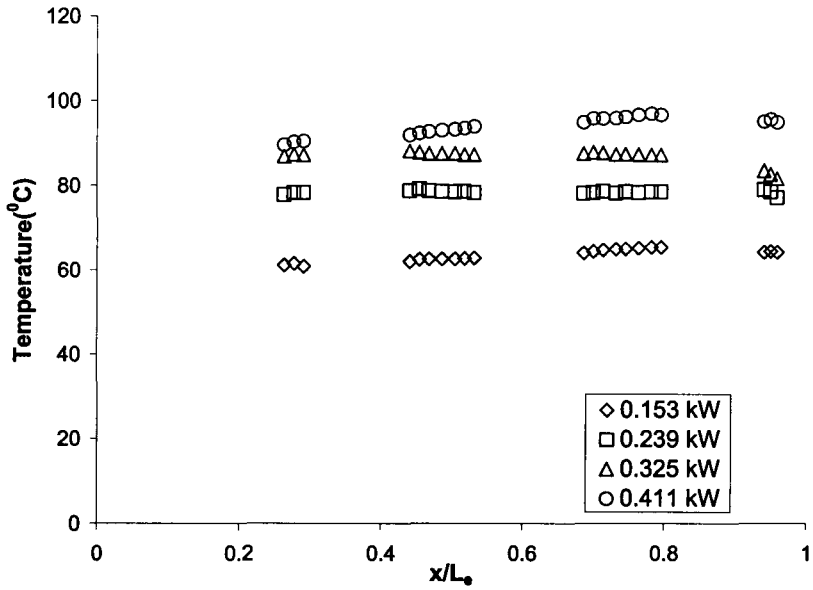

Figure A.1 Evaporator wall temperature distribution at 3000 RPM for the heat pipe with 11.6 gm of methanol using IR camera.

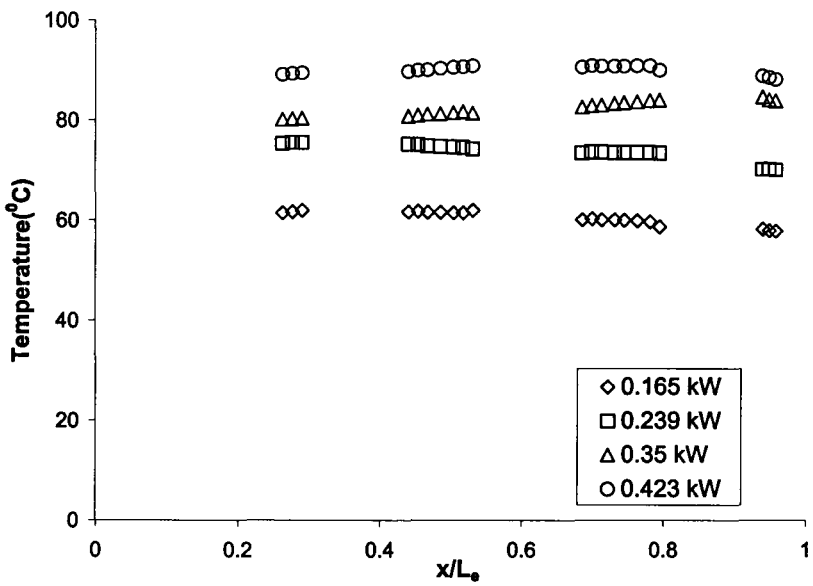

Figure A.2 Evaporator wall temperature distribution at 4000 RPM for the heat pipe with 11.6 gm of methanol using IR camera.

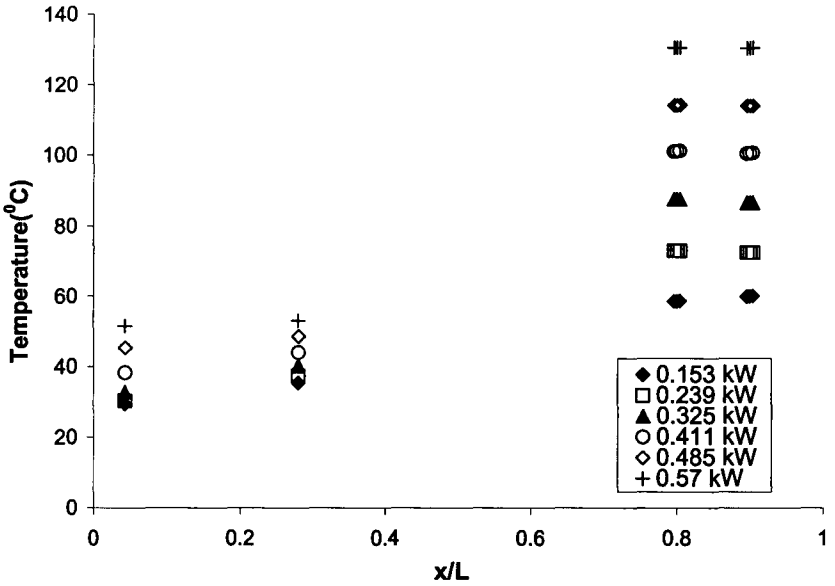

Figure A.3 Wall temperature distribution at 3000 RPM for the heat pipe with 11.73 gm of ethanol.

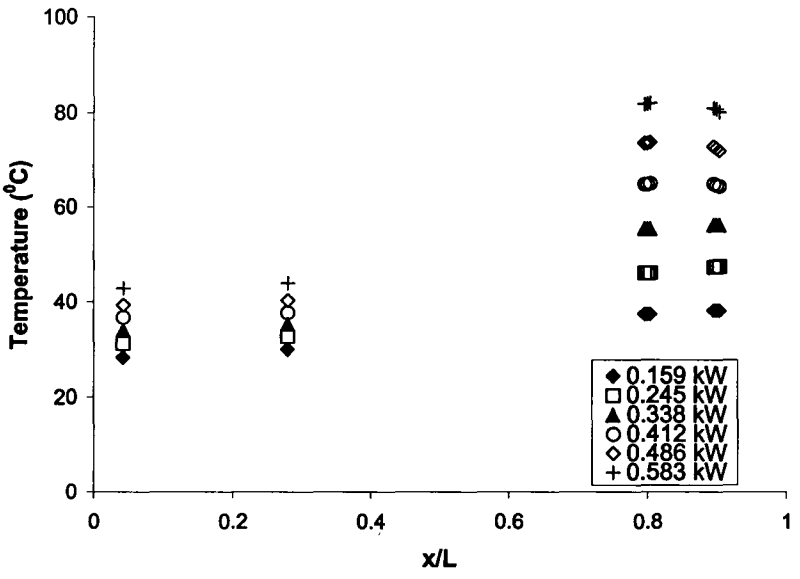

Figure A.4 Wall temperature distribution at 3000 RPM for the heat pipe with 14.64 gm of water.

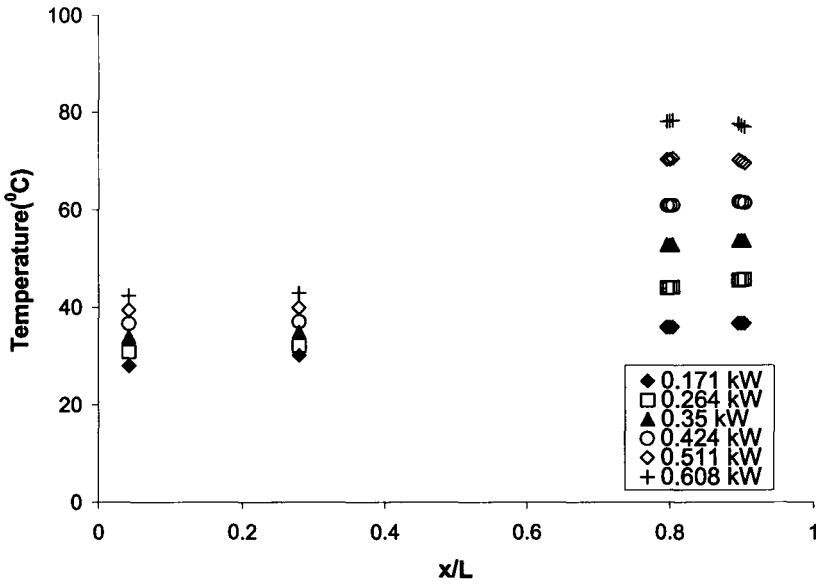

Figure A.5 Wall temperature distribution at 4000 RPM for the heat pipe with 14.64 gm of water.

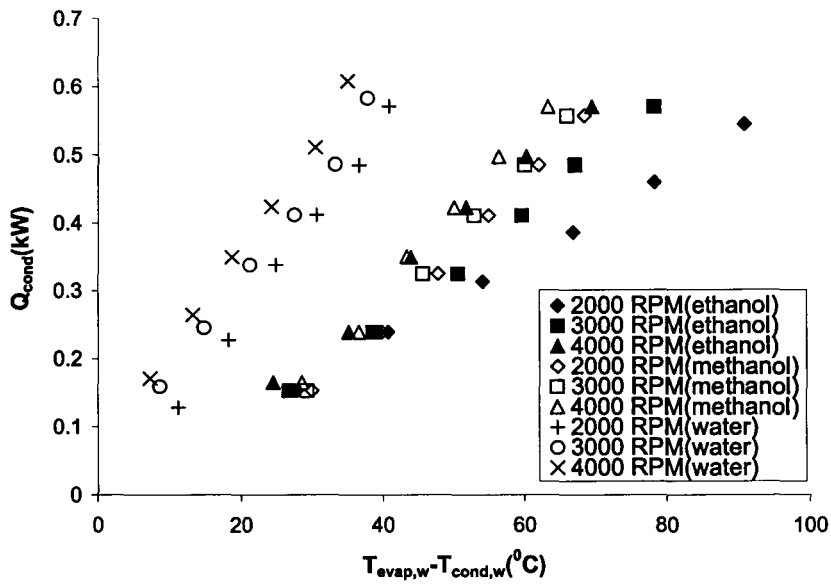

Figure A.6 Change in the heat transfer with temperature difference for the heat pipes with 11.6 gm of methanol, 11.73 gm of ethanol and 14.64 gm of water.

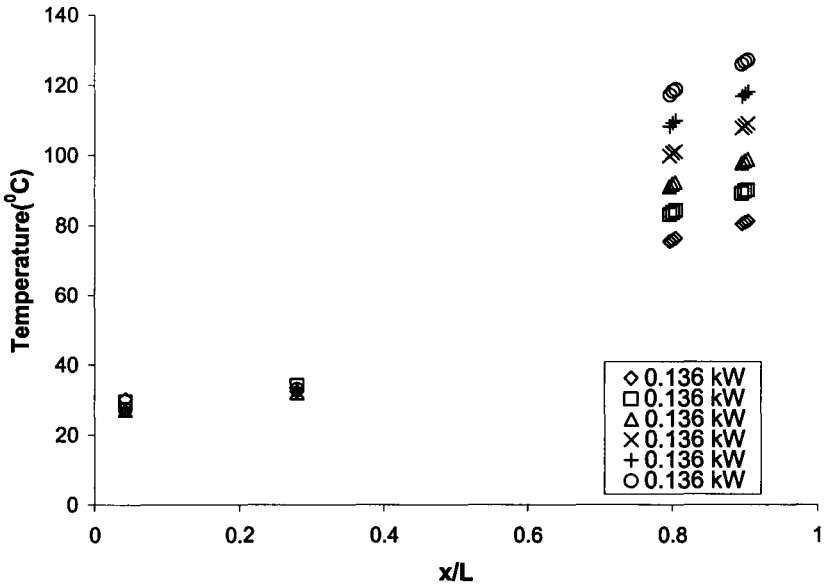

Figure A.7 Wall temperature distribution at 2000 RPM for the heat pipe with 4.88 gm of water.

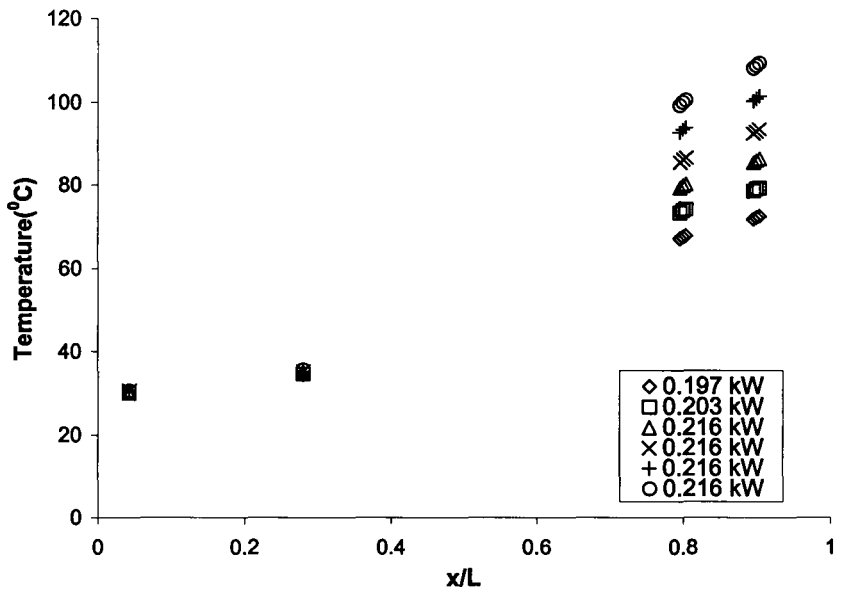

Figure A.8 Wall temperature distribution at 4000 RPM for the heat pipe with 4.88 gm of water.

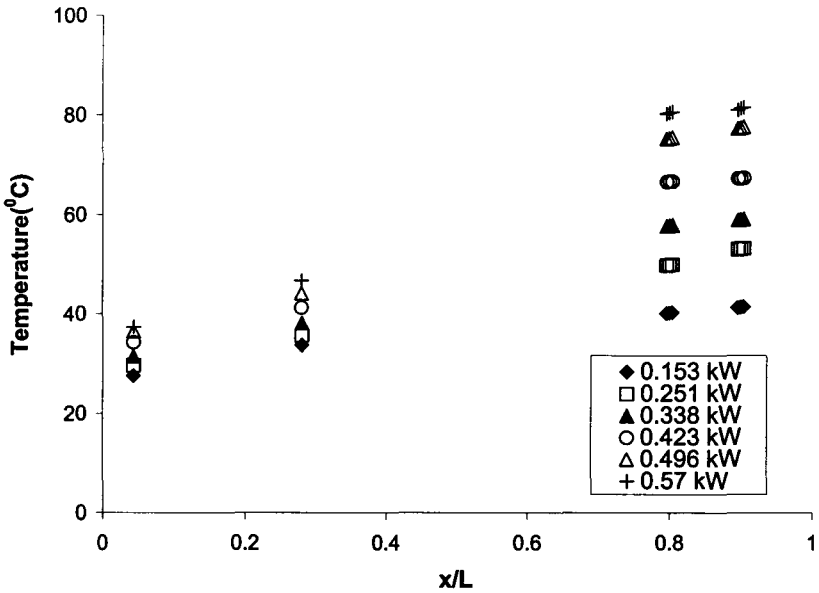

Figure A.9 Wall temperature distribution at 2000 RPM for the heat pipe with 5.5 gm of water.

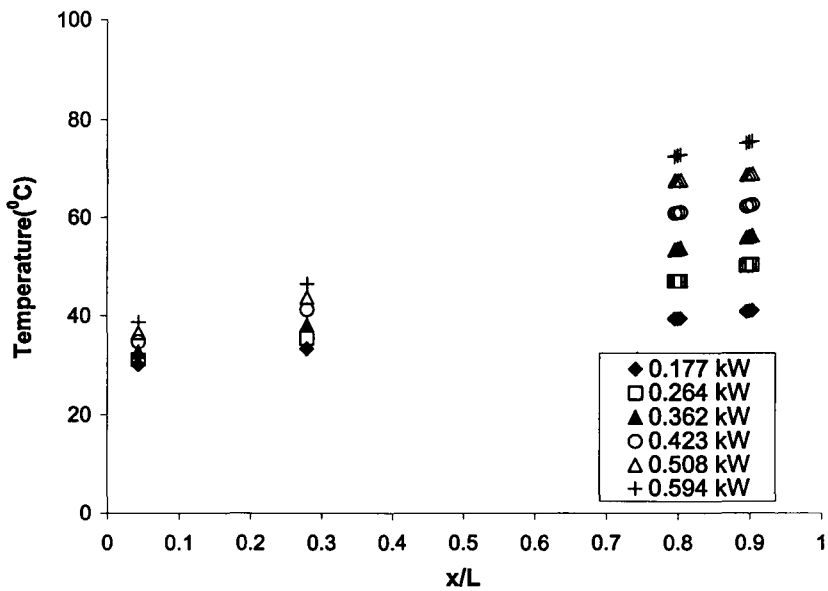

Figure A.10 Wall temperature distribution at 3000 RPM for the heat pipe with 5.5 gm of water.

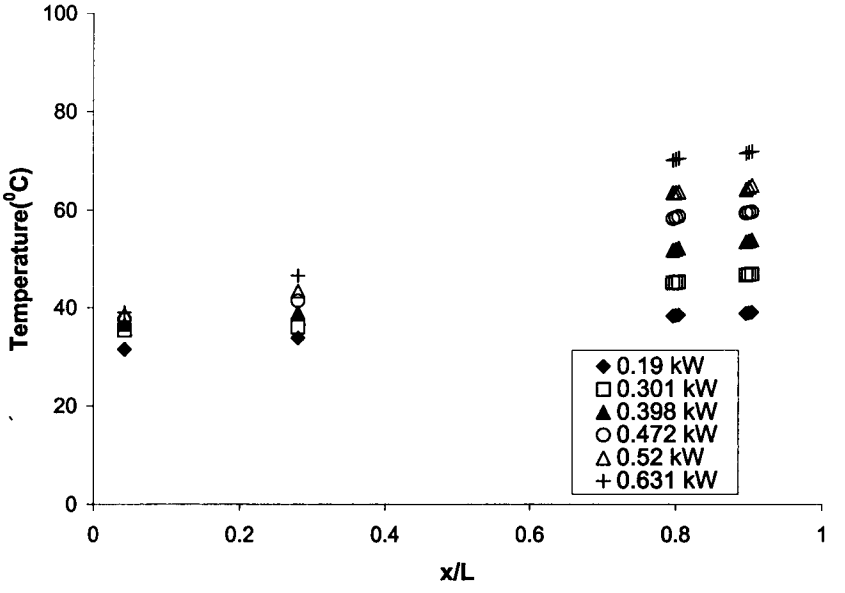

Figure A.11 Wall temperature distribution at 4000 RPM for the heat pipe with 5.5 gm of water.

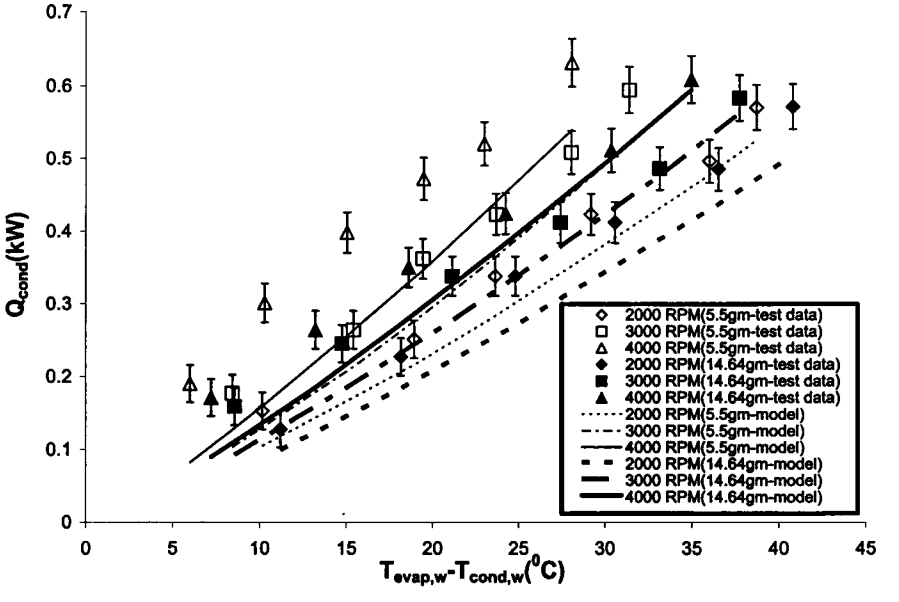

Figure A.12 Comparison between the measurements and model prediction of Song et al. (2003) for the change in heat transfer with temperature difference for the heat pipes with 5.5 gm and 14.64 gm of water.